MSc. Guang Mei Wu

Quantitative Assessment and Optimization of Flame Retardancy by the Shielding Effect in Epoxy Nanocomposites

BAM-Dissertationsreihe · Band 77
Berlin 2011

Die vorliegende Arbeit entstand an der BAM Bundesanstalt für Materialforschung und -prüfung.

Impressum

Quantitative Assessment and Optimization of Flame Retardancy by the Shielding Effect in Epoxy Nanocomposites

2011

Herausgeber:
BAM Bundesanstalt für Materialforschung und -prüfung
Unter den Eichen 87
12205 Berlin
Telefon: +49 30 8104-0
Telefax: +49 30 8112029
E-Mail: info@bam.de
Internet: www.bam.de

Layout: BAM-Arbeitsgruppe Z.64

ISSN 1613-4249
ISBN 978-3-9814281-7-9

Quantitative Assessment and Optimization of Flame Retardancy by the Shielding Effect in Epoxy Nanocomposites

vorgelegt von

MSc. Guang Mei Wu

aus Jiangsu China

Von der Fakultät III - Prozesswissenschaften

der Technische Universität Berlin

Zur Erlangung des akademischen Grades des

Doktor der Ingenieurwissenschaften (Dr.-Ing.)

genehmigte Dissertation

Promotionsausschuss:

Vorsitzender: Prof. Dr. rer. nat. Claudia Fleck

Berichter: Prof. Dr.-Ing. Manfred H. Wagner

Berichter: Dr. rer. nat. habil. Bernhard Schartel

Tag der wissenschaftlichen Aussprachen: 21. June 2011

Berlin 2011

D 83

This dissertation is dedicated to my family: my mother, brother and his loving family for their endless love and support. I am especially grateful for the spirit of my father whom I missed a lot. Also to my love for his continuous encouragement and trust. Without their love and supporting words that helped to sustain me in my faith during those dark days, this work would not have been possible, my dream would not have come true...

A journey of a thousand miles must begin with a single step.

.....Confucius

Contents

Zusammenfassung

Diese Arbeit trägt zum halogenfreien Flammschutz von Epoxidharzen durch Nanokomposite mit Phosphonium modifiziertem Schichtsilikat bei. Der Flammschutz resultiert aus der während der Pyrolyse entstehenden inorganisch-organischen Schutzschicht. Diese Brandrückstandsschicht wirkt als Hitzeschild für das darunterliegende Material. Ziel dieser Arbeit ist die experimentelle und quantitative Beschreibung dieses Effekts und die Optimierung der Flammschutzwirkung.

Die während der erzwungenen Verbrennung im Cone Calorimeter auftretenden Wärmeflüsse und Materialoberflächentemperaturen wurden in selbst konzipierten Experimenten bestimmt. Der durch die Schutzschicht zurückgestrahlte Wärmefluß und die daraus resultierte Reduktion des in der Pyrolysezone effektiv in Brennstofffreisetzung umgesetzten Wärmeflusses wurden erfolgreich quantifiziert. Mit diesem effektiven Wärmefluß nahmen wichtige Brandeigenschaften wie die Wärmefreisetzungsrate ab.

Zur Optimierung der Schutzschicht wurde drei Ansätze verfolgt: Variation der organischen Modifizierung, verbesserte Dispersion durch den Einsatz von interkaliertem Triphenylphosphat und die Optimierung der Morphologie der Schutzschicht durch die Kombination von Schichtsilikat mit niedrig schmelzenden Gläsern. Durch den Einsatz verschiedener organischer Kationen lässt sich die Verteilung der Nanopartikel, die Struktur der Schutzschicht und damit die Flammschutzwirkung optimieren. Obwohl die Interkalation von Triphenylphosphat eine deutliche Aufweitung der Schichtabstände im Schichtsilikat bewirkt, zeigen die entsprechenden Nanokomposite keine verbesserte Verteilung der Partikel, keine homogenere Schutzschicht und keine Erhöhung der Flammschutzwirkung im Vergleich zu analogen Mischsystemen, in denen additiv Triphenylphosphat zugegeben wurde. Die Kombination von organisch modifiziertem Schichtsilikat und niedrig schmelzenden Gläsern zeigen in den meisten der untersuchten Systeme antagonistische Effekte. Nur in wenigen Kombinationen ist, die Superposition bzw. sogar eine Synergie zwischen den Flammschutzeffekten beider Zusätze zu beobachten.

Die erstmalige experimentelle Quantifizierung des Hitzeschildes in Polymernanokompositen ist ein wertvoller Beitrag für ein grundlegendes Verständnis der Flammschutzmechanismen in Nanokompositen. Die Abhängigkeit der Flammschutzwirkung von der Struktur der Schutzschicht wurde nachgewiesen. Zur Optimierung der Schutzschichtstruktur und damit des Flammschutzes wurden drei Ansätze vorgeschlagen.

Abstract

The motivation of this study was to pursue effective eco-friendly and economical flame retarded polymer materials. With wide-ranging advantages such as improved fire and physical properties, halogen-free and relatively low cost, layered silicate / epoxy nanocomposite (EP_LS) was targeted for high efficiency of flame retardancy. One main goal of this study was to increase the understanding of the flame retardancy phenomenon in EP_LS by assessing the shielding effect of the protection layer experimentally and quantitatively. Another main goal of this study was to optimize the flame retardancy by the shielding effect in EP_LS.

To assess the shielding effect in EP_LS, a self-designed experiment was used to monitor the online heat flux and temperature at the burning surface during flaming combustion in the modified cone calorimeter. The shielding effect is quantified as $\dot{q}''_{rerad}$, which is determined by a hot surface temperature according to $\dot{q}''_{rerad} = \sigma\varepsilon T_S^4$. Based on the determination of the net heat flux to the pyrolysis zone during steady-state combustion by several important factors, as in equation $\dot{q}''_{net} = \dot{q}''_{ext} + \dot{q}''_{flame} - \dot{q}''_{rerad} - \dot{q}''_{loss}$, with a defined external heat flux $\dot{q}''_{ext}$ from cone heater, the online heat flux and temperature measurements were used to determine $\dot{q}''_{flame}$ and $\dot{q}''_{rerad}$. The heat loss $\dot{q}''_{loss}$ through conduction into specimen and surrounding was estimated to be negligible.

During flaming combustion of EP and EP_LS, $\dot{q}''_{flame}$ was measured online as a constant value of 20 kW m^{-2}, independent of the external heat flux defined for both materials. For EP the surface temperature equals the pyrolysis temperature ($T_{surface} = T_{pyrolysis}$), and remained constant independent of external heat flux. For EP_LS the surface temperature does not equal to the pyrolysis temperature ($T_{surface} \neq T_{pyrolysis}$) and varied depending on the external heat flux. A quantitative assessment of the shielding effect for flame retardancy was illuminated by a linear reduction in the fire parameters including burning velocities at the pyrolysis front, the steady-state heat release rate (HRR) and the peak HRR (PHRR) at the end of combustion as compared with the corresponding net heat flux on the burning surface.

To optimize the flame retardancy by the shielding effect in EP_LS, different approaches were proposed: improving thermal stability of LS by using different organic modifications; improving the dispersion of LS by preloading the organo-LS with a spacer of triphenylphosphate (TriPP), and enhancing the fire residue integrity by combining organic-LS with low-melting glass. The investigation methods used were differential scanning calorimetry (DSC), thermogravimetry (TG) and Fourier transform infrared spectrometry (FTIR) for identifying the material's pyrolysis behaviour; limiting oxygen index (LOI) and UL 94 test for flammability; cone calorimeter for fire behaviour; scanning electron microscopy (SEM) for characterizing the relationship between the integrity of fire residue structure and fire properties.

With the various additives (i.e., different organo-LSs and low-melting glasses), the general pyrolysis behaviour of EP composites was not changed significantly in comparison to EP in either aerobic or in anaerobic atmospheres. The additional pyrolysis residue of EP composites was related to the presence of inorganic additives with limited additional carbonaceous char. The different additives functioned mainly as inert fillers during pyrolysis of EP since no spectra of additional decomposition products were detected in the gas phase. With respect to flammability, the LOI value was improved slightly by most of the additives used except phenylsiloxane glass. All of the investigated materials achieved an HB rating in the UL 94 test. With respect to fire behaviour, the various inert additives did not cause any significant flame inhibition during combustion in the gas phase. The PHRR was reduced remarkably (Δ = 34 - 57 % for the use of different organo-LSs, Δ = 32 - 60 % for the use of different low-melting glasses). The reduction of PHRR in terms of flame retardancy was attributed mainly to the protective layers of the fire residue in the condensed phase.

When the EPs with different additives were compared systematically, the materials with higher thermal stability of LS showed higher efficiency of flame retardancy. The higher flame retardancy corresponded to higher fire residue integrity. A clear superposition effect on LOI value and reduction of PHRR was observed by the use of organo-LS and the spacer TriPP. The fire behaviour of EPs with the different organo-LSs indicated that although no improvement on the dispersion of LS was observed at room temperature, the exfoliation of LS can be affected considerably by several important factors, such as heating, decomposition, evaporation of decomposition products and accumulation during combustion.

Throughout the use of combinations of organo-LS and the different low-melting glasses, no improvement was found in flammability and ignitability in terms of reaction to a

small fire. Using the inorganic glasses (Ceepree and Sulphate glass) showed an antagonistic effect on reducing PHRR. The antagonism was attributed to a dominant columnar structure on the micro-scale resulting when LS was added, which also appeared as a less efficient fire residue structure on the macro-scale. Nevertheless, through the use of combination of LS and inorganic glasses, the characteristics of the fire residue surface demonstrated that the enhanced fire residue integrity on the micro-scale contributes to the efficiency of flame retardancy. For the combination of organic-LS and phenylsiloxane glass used a clear superposition / pseudosynergism in reducing PHRR, which is not a common effect found when only two inert fillers are used, was quantitatively described by mathematical models. This promising effect on flame retardancy was attributed to the enhanced integrity of fire residue structure.

In conclusion, on the approach of understanding the flame retardancy mechanism in EP_LS, first time the shielding effect was assessed quantitatively and experimentally by the self-designed online heat flux and temperature measurements. It was demonstrated that the shielding effect exerted by the inorganic-carbonaceous fire residue surface protection layer is the only main flame retardancy effect in the polymer nanocomposites based on non-charring or hardly charring polymers with inert nanometric additives. On the approaches of optimizing the flame retardancy by shielding effect, it was proved that the intercalated and exfoliated structure of LS dispersion by organic modification is prerequisite for high efficiency of EP composites. Although the combination of LS and low-melting glass was not universally effective for all the glass selections, a promising effect was possible and available when the fire residue integrity was enhanced. A new route was discovered that the fire residue integrity on the macro and the micro-scales is critical for flame retardancy efficiency.

Chapter 1. Motivation and Issues

1.1 Introduction

Flame retarded polymeric materials are vital and crucial for industrial applications. The development of flame retarded polymeric materials aims at reducing the potential fire hazards, including ignitability, flammability, ease of extinction, rate of heat release, total amount of heat evolved, smoke and toxicity [1-2]. This can be achieved by modification of the polymer chemistry, such as inserting flame retardant moieties in the polymer backbone or network, increasing aromatic contents or increasing cross-linking density (more challenging work, and expensive) [3-6], or by incorporating flame retardant additives such as conventional halogenated, nitrogen, phosphorous-based compounds or inorganic compounds and minerals (easy to process and relatively low cost) [7-11]. In general, such conventional flame retardants for polymers tend to provide high efficiency of flame retardancy. However, the use of some of them is limited because of environmental and toxicity issues (e.g., halogen content), some confirm that the efficiency of flame retardancy depends on the given polymeric materials and additives (e.g., phosphorus compounds are not effective in styrenic resins and polyolefins), and some require high loading for sufficient flame retardancy, resulting in a deterioration of physical properties (e.g., inorganic hydroxides). Most of the recent developments are based on the optimization of established approaches, such as synthesising new derivates to improve thermal stability or compatibility with the polymer, adjusting the combinations of flame retardants to work as synergists or adjuvants, and proposing new combinations of additives to reduce the load or costs without diminishing the efficiency of flame retardancy [12-15]. In developing a suitable flame retarded polymer product, attention must be paid to the material's cost, its properties and processing capabilities, and to health and safety issues. Effective eco-friendly and economical flame retarded polymer materials with minimized trade-offs are thus always sought for commercial demands.

For more than a decade and a half, a great deal of research has focused on the use of nanofillers such as layered silicates, nanofibres or nanotubes, with dimensions on the nanometer scale, for halogen-free flame retarded polymer nanocomposites [16-21]. According to the literature, the nano-fillers are usually dispersed in polymer matrix on the nanometer scale. In many cases, due to the unique character of nanofillers, which exhibit high strengths, high surface areas and high aspect ratios, not only flame retardancy of the polymer nanocomposites are improved, but also their physical properties (e.g., mechanical and barrier properties) [22-27]. Such wide-ranging advantages (i.e., improved physical

properties, improved flame retardancy, halogen-free flame retardant alternatives and relatively low cost) are seldom found in other traditional flame retardants.

1.2 Impacts on the flame retardancy of layered silicate / polymer nanocomposite

The flame retardancy of layered silicate / polymer nanocomposite (LS/PN) has been the subject of many publications since the mid-1990s. Various phenomena have been observed during the pyrolysis of LS/PN depending on the nature of polymer matrix and LS. For instance, some systems show a minor influence of LS on the decomposition pathway [28-29], some show a slight enhancement of the onset decomposition behaviour [30], and others induce a change in decomposition products [31-34]. For fire behaviour of LS/PN, it is generally true that the peak of heat release rate (PHRR) and peak of mass loss rate are reduced in LS/PN in comparison to the non-filled reference polymer, which is one of the most significant fire properties monitored by cone calorimeter and gasification testing [35-39]. The reduction of PHRR in terms of flame retardancy corresponds well with the structural integrity of fire residue. A homogeneous residue with structural integrity is believed to be crucial in providing the most effective barrier [40-44]. Unfortunately a fully closed structure without fracture cracks on the surface of layer formation is hard to achieve in most LS/PNs [45-47]. The approach to improving of the integrity of LS/PN's fire residue is thus a promising way to achieve high efficiency of flame retardancy.

Further, because LS works mainly as inert filler during combustion, the overall flame retardancy achieved by using LS alone is generally not sufficient [48-51]. Apart from limited effects on carbonaceous charring, the total heat evolved (THE) in terms of fire load is not affected significantly in LS/PN. No flame inhibition occurs in the gas phase during combustion [49,51]. Further it has been reported that the flame retardancy decreases with decreasing external heat flux [49]. In addition, ignitability (time to ignition) and flammability (reaction to a small flame: LOI, UL 94) usually reveal only little or no improvement [48-51]. Thereby, the issue of reducing the fire hazards, such as reducing the fire load and improving the ignitability / flammability, must be addressed.

1.3 The influence of layered silicate dispersion on flame retardancy

The natural crystal structure of LS consists of two-dimensional layers with galleries occupied by intercalated exchangeable ions (i.e., d-spacing is ~0.9 nm for cationic clays and ~0.5 nm for anionic clays) [52-53]. Placing the long molecule chains of a surfactant in such a confined space leads to an expansion of the d-spacing to form organically modified

LS [54-57]. The quality of LS exfoliation is governed by the components used in the nanocomposite and their intrinsic properties, including the molecular weight of the polymer, the polarity of the polymer, the kind of clay modification and the ion-exchange capacity [58-60]. Furthermore, processing parameters like shear stress, temperature and resident time are important to achieve good nanoscale dispersion of organo-LS—depending on the polymer type, mainly via extrusion and injection moulding for thermoplastics and in situ polymerization for thermosets [60-63].

The morphology of composites is often characterized by means of X-ray diffraction (XRD), scanning electron microscopy (SEM) and transmission electron microscopy (TEM) [56-63]. Three types of dispersion morphology are commonly termed in the literature as immiscible, intercalation and exfoliation. For the case designated immiscible, because aluminosilicate platelets of the LS do not delaminate, particles comprised of tactoids or agglomerates exist in the polymer matrix as a form of microcomposite. If long molecular chains are diffused into the galleries, it results in an increased d-spacing of platelets, and thus a form of intercalation. The intercalated platelets can be separated further apart until an exfoliated state is reached during processing, and thus another form of nanocomposite [22,64-65]. In many cases, complete or ideal exfoliation is rarely achieved on the macro scale, while a mixture of intercalation and exfoliation is often observed.

The nanoscaled dispersion morphology is crucial for the structure-property relationship and their respective fire retardancy mechanisms [50,66]. In principle, at room temperature nanocomposite morphology does not act itself or directly contribute to flame retardancy [50,67]. During combustion of LS/PN, some further movement of LS can be facilitated by the heating and decomposition of the polymeric network, entailing a series of activities such as migration, bubbling, convection and agglomeration and thus resulting in the formation of a protective surface layer [68-74]. Nevertheless it is still proposed that polymer nanocomposites with a nano-scaled dispersion morphology, such as an exfoliated or intercalated structure, is a mandatory prerequisite for a flame retardancy effect in LS [75]. Different studies on LS/PN show the strong influence of nano-filler dispersion morphology on fire behaviour. It has been observed that LS/PN with a nano-scale dispersion exhibits an extraordinary reduction in PHRR, while microcomposites show no significant change in the PHRR. Several authors have demonstrated that better polymer nanocomposite morphology, with greater nanofiller dispersion, provides higher efficiency of flame retardancy [50,76-78]. For every system, the preparation and optimization of the materials, the choice of a suitable organic modifier for the LS and need to increase nano-dispersion are crucial to obtain an advantageous LS/PN for flame retardancy.

1.4 The flame retardancy mechanism of LS/PN

Different flame retardancy mechanisms have been proposed in polymer nanocomposites [79-82]. It is generally accepted that the main flame retardancy effect is a shielding effect of an inorganic-carbonaceous layer on heat and mass transport during combustion [83-84]. Different mechanisms like ablation, migration, bubbling, accumulation and precipitation are believed to play important roles in specific systems, resulting in distinct fire residue formations [73-78]. It is also proposed that the catalytic effects on crosslinking / charring occur during the decomposition of nanocomposites [85]. However, detailed description or full understanding of the physical and chemical processes occurring in the condensed phase is still limited. At least a quantitative assessment of these mechanisms is entirely lacking.

Quantitative and analytical approaches to flame retardancy by the formation of the protection layer have been recently discussed by B. Schartel et al. [86-87]. The reradiation emitted by a hot surface with the consequent shielding effect has been identified as the most important factor in the fire residue protection layer. A similar conclusion has been drawn by Delichatsios et al., who simulated the burning of nanocomposites in the cone calorimeter [88-89]. Since the flame retardancy in LS/PN decreases with decreasing irradiation, it is thus necessary to assess the shielding effect as it depends on irradiation, experimentally and quantitatively.

1.5 Overview

To sum up, the motivation of this study was to pursue effective eco-friendly and economical flame retarded polymeric materials. With wide-ranging advantages such as improved physical and fire properties, no halogen content and relatively low cost, LS/PN was targeted for high efficiency of flame retardancy. The issues tackled by this work to increase the understanding and optimization of flame retardancy by the shielding effect were:

- providing an experimental and quantitative assessment of the shielding effect on flame retardancy;
- improving the thermal stability of LS and also increasing LS dispersion;
- enhancing the integrity of fire residue.

Chapter 2. Approaches and Main Focuses

2.1 Approaches

In addressing the issues outlined above, the approaches for high efficient flame retardancy of LS/PN in this study aimed to

- quantify the net heat flux in the pyrolysis zone during combustion;
- use different organic modifications for LS;
- further modify organic-modified LS using a compound containing phosphorus as a spacer;
- combine LS and low-melting glasses.

2.1.1 Quantitative assessment of the shielding effect

The model used for discussion and quantitative assessment consists of one-dimensional burning of a solid material with integrated thermocouples as illustrated in Fig 2.1. During the combustion of a solid material HRR is determined by the net heat flux at the pyrolysis front as defined in the Eq. (1) [98-101]:

$$\mathrm{HRR} = \chi h_c^{o} \dot{m}_g'' = \chi(1-\mu)\frac{h_c^{o}}{h_g}\dot{q}_{net}'' \qquad (1),$$

where χ is the combustion efficiency in the gas phase, $\dot{m}_g''$ the mass loss rate per unit area, μ the char yield, h_c^{o} the effective heat of combustion of the volatiles, h_g the heat of gasification and $\dot{q}_{net}''$ the net heat flux per unit area transformed into gasification. In this model h_g and $\dot{q}_{net}''$ include all contributions necessary for gasification, including heating the material from room temperature to up pyrolysis temperature, phase transitions, decomposition, and vaporization. The net heat flux is simply quantified as the difference between the major important heat fluxes imposed on the surface during burning as defined in the Eq (2) [98-101]:

$$\dot{q}_{net}'' = \dot{q}_{ext}'' + \dot{q}_{flame}'' - \dot{q}_{rerad}'' - \dot{q}_{loss}'' \qquad (2),$$

with $\dot{q}''_{ext}$ the irradiation and $\dot{q}''_{flame}$ the total (radiative + convective) heat flux from the flame to the surface. $\dot{q}''_{rerad}$ is the reradiative heat flux of the hot surface. $\dot{q}''_{loss}$ represents the loss due to conduction through the specimen into the surroundings and is approximated to $\dot{q}''_{loss}$ = 0 kW m^{-2} for the cone calorimeter tests performed in the following discussion. Due to the thermal insulation realized by the cone calorimeter set-up this approximation is reasonable. The determination of the heat fluxes $\dot{q}''_{ext}$, $\dot{q}''_{flame}$ and $\dot{q}''_{rerad}$ is key for the quantitative experimental assessment of the net heat flux transformed into pyrolysis of the solid material, and thus the impact of the shielding effect.

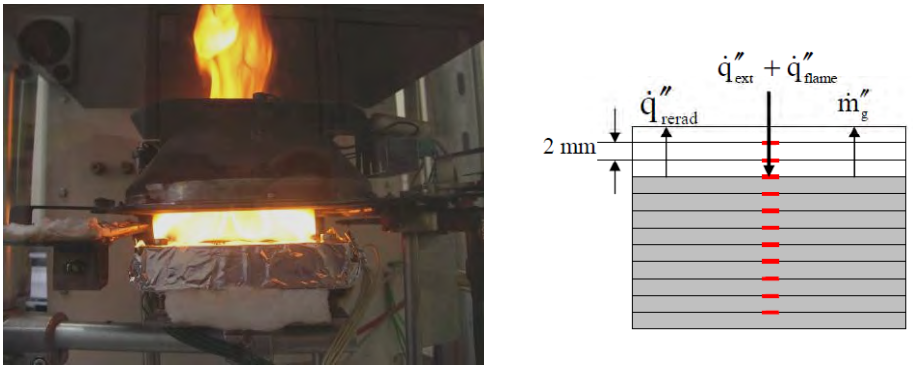

Fig 2.1. *One-dimensional burning model used for the discussion of the shielding effect impact during flaming combustion in the cone calorimeter*

2.1.2 Using different organic modification for LS

As mentioned above in section 1.3, a suitable modification for LS with nano-dispersion is a prerequisite for the effective flame retardancy of nanocomposites. In the literature, alkylammonium-modified LS has been reported as the most common organoclay to prepare nanocomposites from a variety of polymers [52]. However, the thermal stability of the alkylammonium-modified LS is limited [55-56]. As reported, the thermal stability of phosphonium, pyridinium and imidazolium salts is higher than that of ammonium salts [55-57]. According to previous studies on different organo-LS from IFAM [28], natural sodium montmorillonite (Na_MMT) was modified by different organic salts in order to increase the thermal stability of organo-LS (as illustrated in Fig 2.2). In TG measurements in air with a heat rate of 5 K min^{-1}, both MMTs treated by tetraphenylphosphonium (TPP_MMT) and 2-phenylimidazolium salts (2PI_MMT) showed a higher thermal oxidative

stability than octadecylammonium-treated MMT (ODA_MMT). The onset decomposition with 5 wt% mass loss occurred at about 673 K for TPPMMT and 2PIMMT, while at only 513 K for ODA_MMT. For the issues addressed our efforts focused on the use of new thermally stable TPP-MMT and 2PI_MMT for the preparation of nanocomposites.

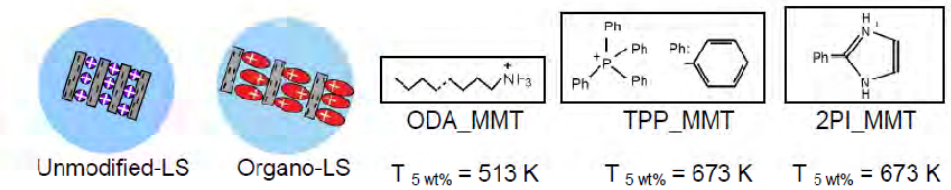

Fig 2.2. *Structural scheme of unmodified layered silicates and different salts for organo-LS. ODA_MMT: octadecylammonium-treated montmorillnite, TPP_MMT: tetraphenylphosphonium-treated montmorillnite, and 2PI_MMT: 2-phenylimidazolium-treated montmorillnite (Source: picture adopted from Dr. M. Kleemeier, IFAM, Bremen, in cooperation for joint project (SCHA 730/8-1, 8-2, HA 2420/6-1 and 6-2))*

2.1.3 Further modification of organo-LS with triphenylphosphate as a spacer

As reported before, the dispersion of LS modified by adding ammonium and phosphonium salts in epoxy resin is limited to the micrometer range and by the intercalation morphology [28-29]. In order to increase the d-spacing of organo-LS to yield greater exfoliation, the organo-LS was further modified by preloading with the phosphorous flame retardant triphenylphosphate (TriPP) as a spacer (illustrated in Fig 2.3). On the other hand, due to some limited benefit of using LS alone, it becomes clear that the combination of LS with conventional effective flame retardants is essential to achieve high efficiency for a synergistic or adjuvant effect in flame retardancy, not to mention an acceptable environmental impact [8]. Among the traditional flame retardants, the phosphorus-based compounds have been successfully promoted as halogen-free alternatives for various flame retarded polymeric materials. Phosphorus-based compounds contribute to flame retardancy mainly in the condensed phase by enhancing charring, by yielding intumescences or through inorganic glass formation, as well as through flame inhibition in the gas phase [90]. Combinations of LS with conventional phosphorus-based flame retardants with resultant synergistic effects have been published in the literature [91]. Thereby the pre-treatment of TriPP might function not only as a spacer to increase the dispersion of organic modified LS, but also work as the second additive to generate an adjuvant or synergistic effect on flame retardancy.

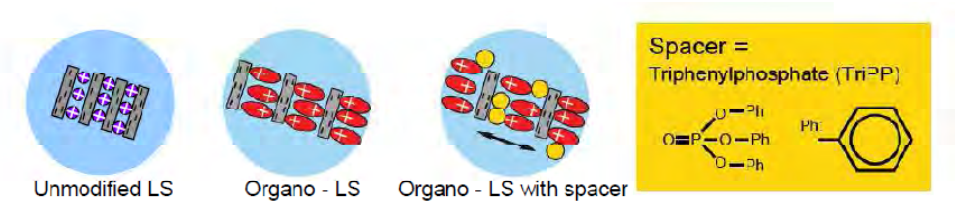

Fig 2.3. *Scheme structure of unmodified, organic modified layered silicates and organic modified layered silicate with a conventional flame retardant triphenylphosphate (TriPP) as a spacer (Source: picture adopted from Dr. M. Kleemeier, IFAM, Bremen, in cooperation for joint project (SCHA 730/8-1, 8-2, HA 2420/6-1 and 6-2))*

2.1.4 Combining LS with low-melting glass

Among the halogen-free flame retardant additives available for polymers, low-melting inorganic glass also has been promoted as a flame retardant / smoke suppressant for organic polymers [92-96]. The flame retardancy effect is due to the glass forming a protective layer at a sufficiently low temperature during combustion. Such low-melting glasses for flame retardancy have been reported for various common thermoplastic polymers such as PVC, PP, PA, PMMA, etc., but rarely for thermosets [97]. In addition, LOI and UL 94 performance can be improved by incorporating low-melting glass in polymer materials. However, relatively high loading is required for significantly efficient flame retardancy, which is detrimental to other physical properties [97].

Therefore, organo-LS was combined with conventional low-melting glasses such as silicate and sulphate glass, and synthesised low-melting glass phenylsilixoane glass for polymer composites in order to optimize the protection layer. Both additives should promote the physical barrier formation mechanism for flame retardancy. The aim is to provide a more integral layer, so that the low-melting glass may act as a kind of glue to bind and strengthen the mixture of layered silicate and polymer/char during combustion. The combination of organo-LS and low-melting glass may lead to synergistic effects. Such a combination is also appropriate to the purpose of producing halogen-free flame retarded and easily processable polymer composites.

2.2 Main Focuses

Generally flame retardancy can be achieved either physically or chemically, taking place in the gas phase or the condensed phase during polymer combustion [7-10]. Fire properties including ignitability, flammability, flame spread, heat release and fire penetration

are not intrinsic material properties, but depend strongly on different fire scenarios [102]. Fig 2.4 illustrates the assessments and methods used most frequently to identify of flame retardancy during pyrolysis and fire behaviour in various fire scenarios. All the experimental methods are described in the following Appendix. The main focuses in this study were:

- identifying the pyrolysis behaviour of materials by differential scanning calorimetry (DSC) and thermogravimetry connected with Fourier transform infrared spectrometry (TG-FTIR);
- identifying the flammability of materials through the standard tests of limiting oxygen index (LOI) and UL 94;
- identifying the fire behaviour of materials by a benchscale fire test in the cone calorimeter, and characterizing the morphology of fire residue by scanning electron microscopy (SEM);
- monitoring the online heat flux and temperature inside of specimen during flaming combustion by modified cone calorimeter tests.

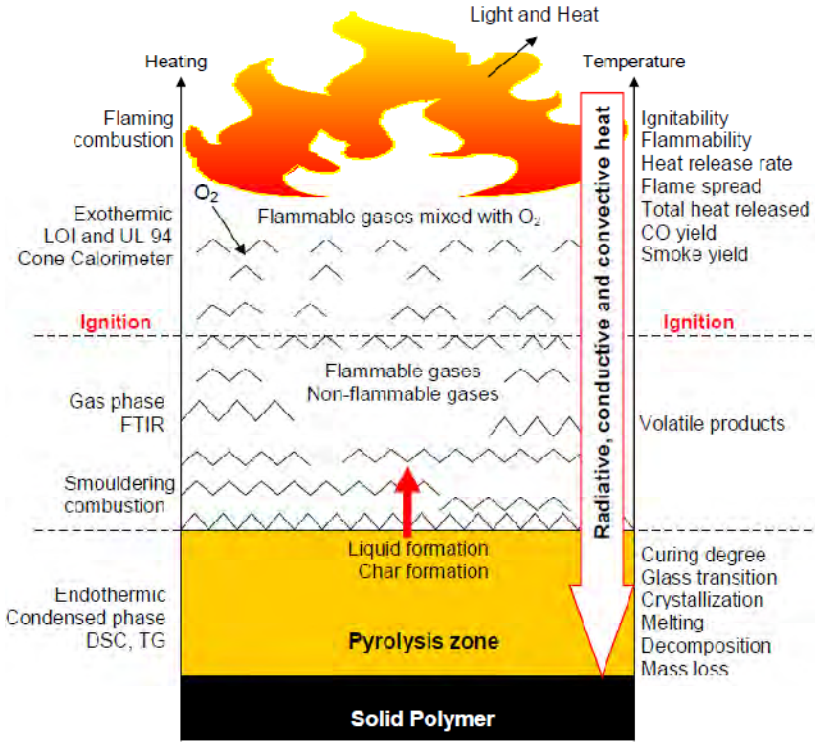

Fig 2.4. *Schematic combustion of solid materials at different stages during temperature development with their predominant characteristics by different assessments*

2.2.1 Pyrolysis behaviour

On heating a polymeric material up to decomposition temperature, depending on the nature of the material, the changes that occur may be physical rather than chemical (e.g., cross-linking and glass transition for thermosets, crystallization and melting for thermoplastics) [103]. For LS/PN, the incorporation of nanofillers influences material properties, related to various effects on the polymerization, crystallization or cross-linking behaviour of the polymers [104-105]. In addition, the thermal history during curing plays an important role in affecting the degree of polymerization and/or cross-linking of the polymer network. A plasticizing effect or reduced cross-link density may decrease the thermal stability of polymer nanocomposites [52]. DSC was thus used to identify the influence of additives on the curing degree of the polymer matrix and the glass transition temperature of the materials.

When sufficient heat is applied, the material starts decomposing into flammable or inflammable fragments to support a fire until the fuel is consumed. Decomposition reactions under heat are attributed to chemical bond breakage, rearrangement and cross-linking / charring [103]. The decomposition mechanism and decomposition products can be affected by the atmosphere applied, such as a vacuum, an inert or an oxidizing atmosphere [103]. Although it is controversial whether or not oxygen plays an important role during the pyrolysis of materials in flaming combustion, analytical studies in the micro-scale do give important information about the pyrolysis behaviour of materials that applies directly application to their fire behaviour. The analysis of evolved gaseous decomposition products, especially, provides useful hints for identifying flame inhibition in the gas phase. TG-FTIR was thus used to investigate thermal stability, thermal oxidative stability and the evolved gaseous decomposition products of materials.

2.2.2 Flammability and ignitability

The fire behaviour of materials differs from one fire test to the other depending on the different fire conditions with respect to various applications [102,106]. The flammability of a material is defined by its reaction to small flame and extinction behaviour under ambient conditions after removing an ignition source. A great number of small ignition tests have been developed, based on many factors such as specimen type, heat source, specimen orientation, flame direction and specimen substrate [12,107]. The standard flammability tests used most are the LOI and UL 94. LOI measures the minimum oxygen

concentration that will support a downward flaming combustion from the top in a flowing mixture of oxygen and nitrogen. This method is used to screen and compare the flammability of different materials. The higher the LOI, the better the flame retardancy [12]. The UL 94 methods, using an upward burning from the bottom (UL 94: V) and a horizontal burning from the side (UL 94: HB) classify materials based on a simple pass/fail system [107]. There is no clear correlation between LOI and UL 94 results, since the tests rely crucially on every parameter of the set-up, such as burning orientation, flame temperature, air flow rate, sample size and sample precondition [12,102].

The ignitability of a material refers to time to ignition (t_{ig}), which is determined by the thermal inertia $k\rho c$, the critical mass loss rate or heat flux for ignition ($\dot{q}''_{cr}$) and the ignition temperature (T_{ig}) [102,108]. A material with a lower $k\rho c$ will ignite more quickly than a material with a higher $k\rho c$ [108]. Ignition occurs when a critical temperature is reached at the surface. $\dot{q}''_{cr}$ designates the minimum heat flux is sufficient to heat the material surface to the T_{ig} over a very long exposure time (theoretically ∞) [108]. Different approaches have been developed to determine ignition properties by measuring these factors [107]. Ignitability is often evaluated by simple visual observation of t_{ig} in cone calorimeter under a defined fire scenario. It is worth noting that t_{ig} in cone calorimeter will be affected by the set-up of the cone calorimeter, such as the use of a pilot flame rather than spark ignition, or a change in the distance between the cone heater and the sample surface [12].

2.2.3 Fire behaviour

The cone calorimeter is the most commonly used benchscale fire test, which simulates a developing fire scenario with a small-scale specimen size (surface area of 100 cm^2) under a well-defined flaming conditions. Specific fire parameters including mass loss rate (MLR), heat release rate (HRR), peak of HRR (PHRR), total heat released (THR), char yield, smoke and CO production, are measured as a function of burning time during testing [12,101]. The HRR is determined by the oxygen consumption technique [109]. Different types of typical burning behaviour such as that of thermally thick or thin materials, non-charring or residue-forming materials, give rise to different characteristic curves of HRR over time [101]. The whole HRR curve over the full duration can adequately represent the fire behaviour, which is influenced by the material's specific properties (i.e., char yield, effective heat of combustion), the influences from the specimen (i.e., thickness,

deformation), and the physical and chemical mechanisms active during burning (i.e., increasing and cracking residue layer, endothermic reactions, release of different pyrolysis products, afterglow) [12].

Both PHRR and THE are two of the most important fire parameters for assessing fire hazards. The fire hazard is reduced by the flame retardants by lowering either the PHRR or the THE [12]. The reduction of PHRR depends on the fire scenario (or test set-up) [101]. THE depends strongly on the total mass loss, char yield, the effective heat of combustion of the volatiles and combustion efficiency in the flame zone. It is also influenced slightly by the applied irradiation, since more char oxidizes under higher irradiation [12, 101]. For the use of inert flame retardant additives, the PHRR is reduced physically by exerting a shielding effect through residue formation, while the THE is hardly changed. For the use of reactive flame retardants, both PHRR and THE can be reduced by flame inhibition reducing the effective heat of combustion in the gas phase, and chemically increasing the char yield in the condensed phase [101].

Other important fire properties include the production of CO and smoke resulting from incomplete combustion. CO and smoke production are strongly influenced by the nature of material (aromatic compounds tend to generate more soot than aliphatic compounds) and fire conditions (irradiation, ventilation, temperature and quenching effects) [101]. In general, flame retardants working through flame inhibition result in significantly increased CO and smoke yields under forced-flaming combustion, while flame retardants working as inert fillers result in hardly any change in CO and smoke yields [12].

For most solid material combustion in the cone calorimeter, the HRR is a function of the mass loss rate resulting from pyrolysis, which is determined by the net heat flux at the pyrolysis front, the decomposition temperature, heat transfer and kinetics [99-100]. As discussed above, the net heat flux for a flaming combustion is determined by many important factors such as the heat supplied by the cone heater and flame, heat loss by reradiation emitted by the hot surface, conduction and convection (through the inside / outside of specimen). Determination of the online heat flux and temperature during flaming combustion is a prerequisite for determining the net heat flux at pyrolysis front, and thus for a characteristic HRR.

Chapter 3. Results and Discussion

3.1 Experimental and quantitative assessment of the shielding effect

As mentioned in sections 1.2 and 1.4, the formation and role of the protective layer are universal for layered silicate/epoxy nanocomposites (EP_LS). The flame retardancy mechanism is attributed mainly to the shielding effect caused by the inorganic-carbonaceous residue layer in the condensed phase, working as a barrier to heat and mass transport. The aim of this chapter is to assess the shielding effect in EP_LS experimentally and quantitatively.

The approach to quantitative assessment of the shielding effect by determining each factor for the net heat flux in pyrolysis zone is introduced in section 2.1.1. During combustion of a solid material, the HRR is determined by the net heat flux at the pyrolysis front as in [99-100]:

$$\mathrm{HRR} = \chi h_c^{o} \dot{m}_g'' = \chi(1-\mu)\frac{h_c^{o}}{h_g}\dot{q}_{net}'' \qquad (1),$$

The net heat flux is quantified simply as the difference between the major important heat fluxes imposed on the surface during burning, defined in equation [101]:

$$\dot{q}_{net}'' = \dot{q}_{ext}'' + \dot{q}_{flame}'' - \dot{q}_{rerad}'' - \dot{q}_{loss}'' \qquad (2).$$

The model used for determination of the $\dot{q}_{flame}''$ and $\dot{q}_{rerad}''$ consists of one-dimensional burning of a solid material with integrated thermocouples. Experimental work is described in Appendix: Experimental (online heat flux and temperature measurements). The investigated materials were based on epoxy resin (EP) and EP nanocomposites (EP_LS) with 5 wt% tetraphenylphosphonium modified montmorillnite (TPPMMT). The details of sample preparation are described in Appendix: Experimental (materials). The morphology of layered silicate dispersion (refer to EP_TPPMMT5) is discussed in section 3.2.

3.1.1 Quantifying the $\dot{q}''_{flame}$, $\dot{q}''_{rerad}$ and $\dot{q}''_{loss}$

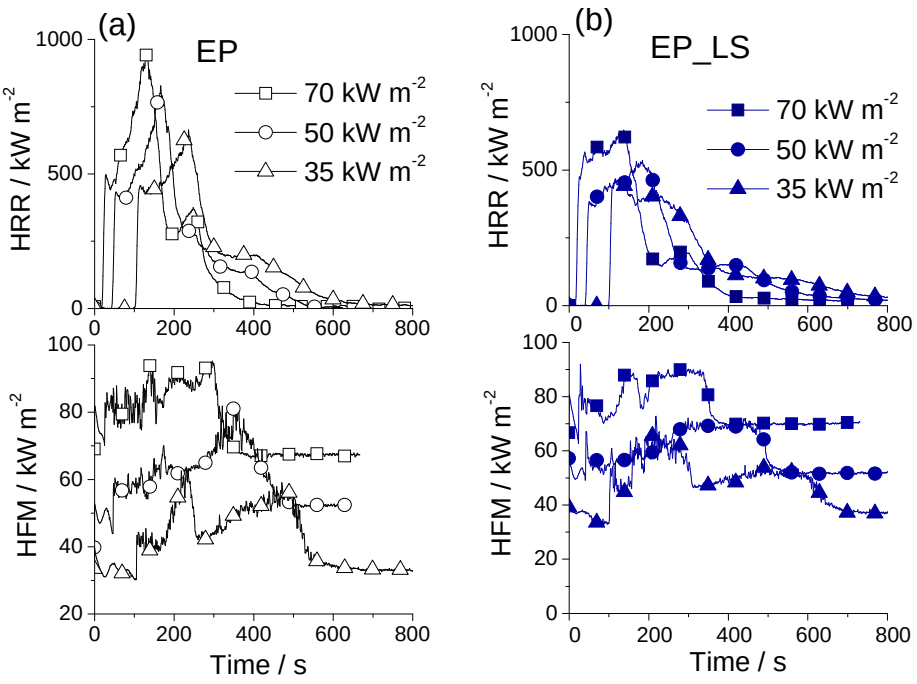

Fig 3.1.1. *HRR curves and online heat flux measurement at the burning surface under various external heat fluxes of 35, 50 and 70 kW m^{-2} applied; (a) EP and (b) EP_LS*

The flame heat flux $\dot{q}''_{flame}$ is one of the major contributors to the $\dot{q}''_{net}$ and thus to the burning rate of a material. In principle, the $\dot{q}''_{flame}$ is governed mainly by the emissivity of the flame, flame height and the flame temperature [124-126]. Fig 3.1.1 shows the HRR with the corresponding heat flux measured on the surface of the burning specimen under various external heat fluxes in the cone calorimeter. It was observed that the flame height increases along with the HRR. In practice it was difficult to measure the actual incident $\dot{q}''_{flame}$ during flaming combustion as in previous cases [125]. The fact that the surface of the heat flux meter was often coated by the condensation of the decomposition products resulted in a large systematic degree of error in the flame heat flux measurements. Nevertheless, apart from the defined irradiation of 35 - 70 kW m^{-2} applied, and assuming that the irradiation by the cone heater penetrated the flame and reached the surface, an

additional heat flux defined as $\dot{q}''_{flame}$ was observed in approximately the range from 7 - 20 kW m^{-2} and changed hardly at all of the heat flux measurements. Overall the higher values were believed to be the more accurate results, since the influence of the obvious condensation problem diminishes the measured value. Also, the constant value $\dot{q}''_{flame} \approx$ 20 kW m^{-2} was in good agreement with reliable data in the literature [126-127]. Comparing EP and EP_LS, the measured $\dot{q}''_{flame}$ was the same and independent of the external heat flux. Such a rather invariable heat flux from the flame to the surface of the burning material is typical for the cone calorimeter set-up [126]. Because of the significant flame, radiation to the surface comes mainly from the bottom area of the flame regardless of the flame height above the top of the cone heater, so that the upper parts of the flame above the cone heater do not influence the feedback of the flame to the surface. Although the flame height increases along with increasing burning rates, a similar and limited volume of the flame contributes to $\dot{q}''_{flame}$ [87].

When the specimen with integrated thermocouples was exposure to heat until ignition, a sequence of events took place at the position of each thermocouple, including preheating, pyrolysis and shifts across phase boundaries (such as solid-mesophase/liquid-gas for EP and solid-pyrolysing mesophase/liquid-solid for EP_LS) when the material was consumed from the top to the back of material. Fig 3.1.2 shows the temperature development monitored by the thermocouples as a function of the burning time in the cone calorimeter. The initial temperature rise from room temperature was a function of the rate of heat conduction into the material and boundary condition. No chemical reaction occurred during this preheating period. When the surface temperature increased to a sufficiently high temperature, pyrolysis began to occur, followed by the shift across phase boundaries. After a transition period accompanying the decomposition and vaporization of the decomposition products, the pyrolysis zone passed through each thermocouple, resulting in a leveling of temperature until flame-out. This temperature profile of heating polymeric material until gasification is in agreement with the literature [128-129]. During flame-out, the temperature profiles exhibited differences between EP and EP_LS, which correlated to the different fire residue characteristics (discussed below).

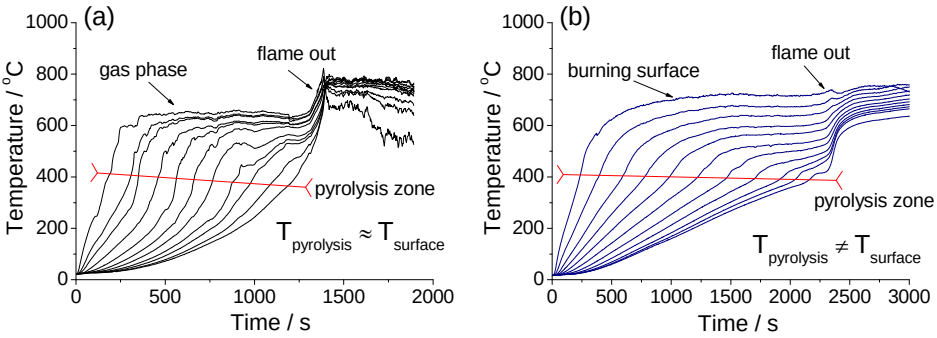

Fig 3.1.2. *Temperature profiles inside of burning material as a function of burning time in the cone calorimeter with an external heat flux of 50 kW m^{-2}; (a) EP and (b) EP _LS*

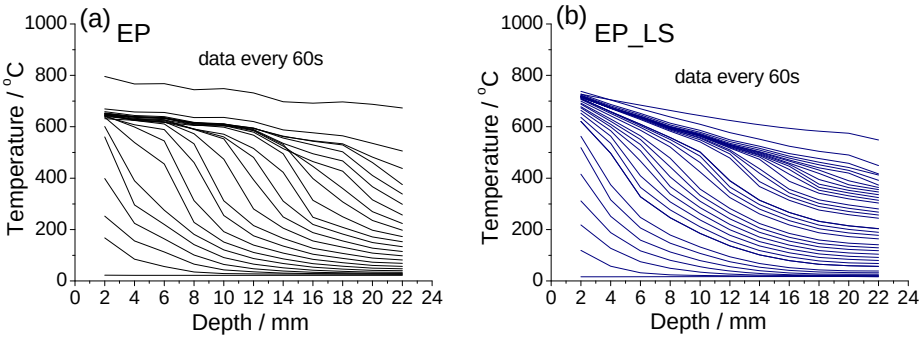

Fig 3.1.3. *Temperature profiles inside burning EP and EP _LS as a function of specimen depth in the cone calorimeter with an external heat flux of 50 kW m^{-2}*

Fig 3.1.3 shows the temperature profiles inside of the burning specimen over the specimen depth for every 60 s. As suggested before [86], the temperature development was attributed to energy transfer processes, mainly to conductive heat transfer through the material, endothermic decomposition and convective mass transfer of volatiles. For a long period, a characteristic temperature gradient showing an exponential decrease was observed between pyrolysis at a temperature above 400^{o} C and the back of the specimen, with temperatures below 200^{o} C for both materials. This typical exponential decrease in temperature depended on the distance between pyrolysis and the back of the sample. For both EP and EP_LS the temperature decrease occurred mainly within the thickness of 6 - 10 mm, defined as the thermal diffusion layer in the solid. Initially, the temperature at the back increased slowly due to thermally thick behaviour when the sample thickness was greater the thermal diffusion layer. When the sample thickness approached or was smaller

than the thermal diffusion layer due to the consumption of material, the temperature at the back increased significantly.

Fig 3.1.4 shows the heating rates inside the burning material over the sample depths between 8 - 16 mm during steady-state burning as a function of temperature. For both EP and EP_LS, at the respective sample depths the heating rate in the condensed phase increased smoothly as temperature increased up to the range of 280 - 380 ^{o}C before reaching pyrolysis. Afterwards it showed a rapid increase in the heating rate, resulting in a maximum at about 420°C. According to previous studies on the combustion behaviour of poly(methyl methacrylate) PMMA based on the same set-up [86], the maximum heating rate indicated the pyrolysis front moving through each thermocouple when pyrolysis began, followed by the material undergoing chemical reactions, thermochemical expansion and/or contraction and changes in various material compositions [129]. A minimum heating rate was observed in both materials due to the endothermic decomposition and vaporization of decomposition products. For EP there was a larger error and uncertainty of heating rate over the sample depth than in EP_LS. This result was attributed to the fact that during pyrolysis and the shift across phase boundaries, the thermocouples in EP were severely disturbed by the movement of decomposition products until they were set free into the gas phase, whereas the thermocouples in EP_LS were fixed in position in the condensed phase. Nevertheless a distinct temperature in the pyrolysis zone ranged from 450 - 600 ^{o}C over the sample depth for both EP and EP_LS. The rather similar pyrolysis temperature was in good agreement with TG results, in which, with a heating rate of 10 ^{o}C min^{-1} in either N_2 or in air atmosphere, the main decomposition of EP occurs between 300 - 500 ^{o}C with a peak mass loss at ~ 420 ^{o}C [115]. Further, the pyrolysis temperatures of both EP and EP_LS during flaming combustion were changed insignificantly with respect to the various irradiations applied, because the LS functioned as inert filler. However, when EP and EP_LS are compared at the same sample depth, the heating rates during pyrolysis and flame-out were significantly reduced in EP_LS, reduction associated with fire residue formation (discussed below).

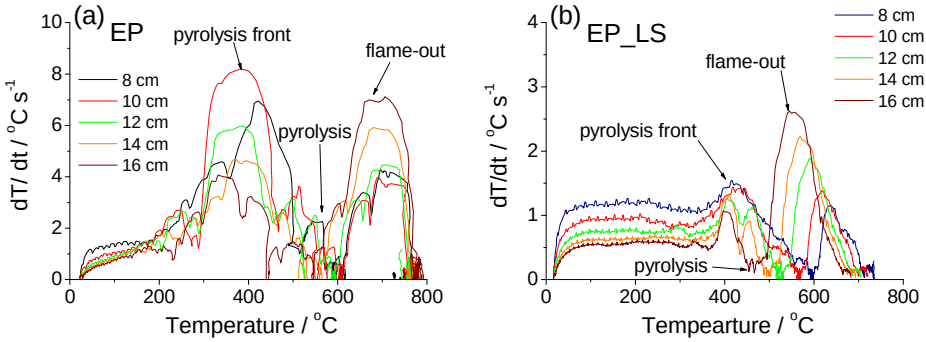

Fig 3.1.4. *Heating rates inside burning material as a function of temperature, monitored by thermocouples at 8, 10, 12, 14, 16 m in the cone calorimeter with an external heat flux of 50 kW m^{-2}; (a) EP and (b) EP _LS*

The different combustion characteristics associated with the fire residue formation between EP and EP_LS are illustrated in Figs 3.1.5 and 3.1.6. In the non-charring material EP (Fig 3.1.5), the thermocouples were set free when the pyrolysis zone passed through since no residue was formed. In fact, the free-standing thermocouples measured the gas-phase temperature above the material surface during burning. It has been proposed that for non-charring materials the material surface during combustion is the actual pyrolysis zone [100, 129]. The surface temperature was thus approximately equal to the pyrolysis temperature ($T_{surface} \approx T_{pyrolysis}$) when the pyrolysis zone moved through the specimen. During flame-out at the end of burning, a sharp temperature peak was attributed to a descending flame, which contacted the free-standing thermocouples directly (indicated in Fig 3.1.2 (a)).

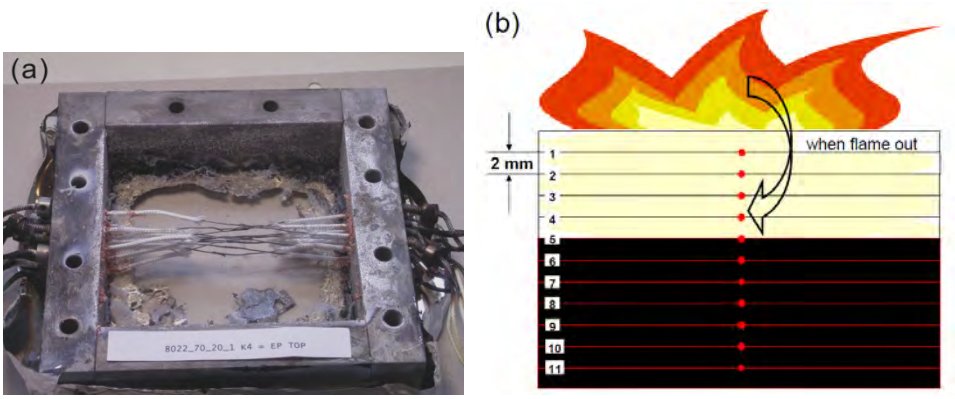

Fig 3.1.5. *(a) Fire residues of EP with free-standing thermocouples obtained in the cone calorimeter with an external heat flux of 70 kW m^{-2} and (b) combustion characteristic of EP*

In contrast, as shown in Fig 3.1.6, due to the inorganic-carbonaceous residue formation in the case of EP_LS, the thermocouples were embedded in the residue when the pyrolysis zone moved down (into the subsequent zone) towards the end of burning. The 11 embedded thermocouples actually measured the temperature distribution over the residue depth. The surface temperature was roughly measured by the thermocouple closest to the residue surface. Thus $T_{surface} \neq T_{pyrolysis}$ during the combustion of EP_LS. At flame-out the high-temperature flame was not able to contact the embedded thermocouples directly since the residue worked as an insulating coating. Thus the increase in temperature measured by the thermocouples in EP_LS was not as significant during flame-out as in EP (indicated in Fig 3.1.2 (b)). Further, the temperature measured by the thermocouples varied over the different residue depths.

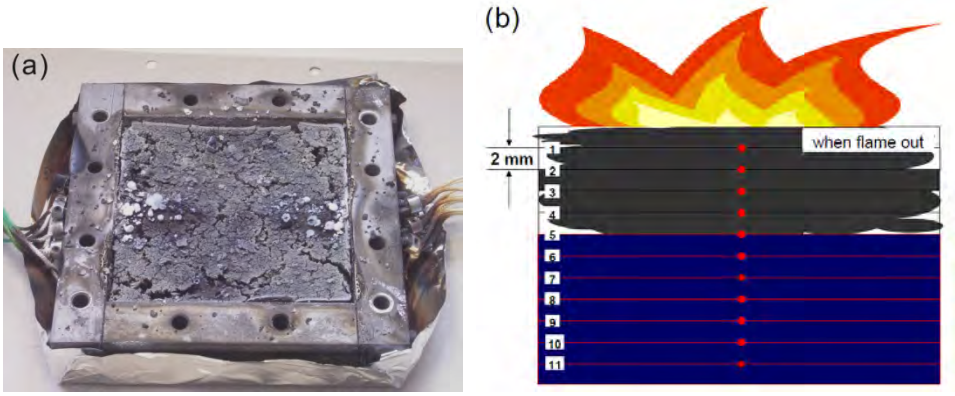

Fig 3.1.6. *(a) Fire residues of EP_LS with embedded thermocouples obtained in the cone calorimeter with an external heat flux of 70 kW m^{-2} and (b) combustion characteristic of EP_LS*

$\dot{q}''_{rerad}$, as one of the main factors to determine the net heat flux, is quantified by the hot surface temperature and defined in a good approximation as

$$\dot{q}''_{rerad} = \sigma \varepsilon T_S^4 \qquad (3),$$

where σ = the Stefan-Boltzmann constant, ε = emissivity (ε is typically 0.9 ± 0.1 for a grey body with a solid surface in fire radiation applications) and T_S = surface temperature [101, 129]. As discussed above, during the combustion of non-charring EP, the gas-phase temperatures measured by the free-standing thermocouples at the top were around 650 - 700°C under various external heat fluxes (shown in Fig 3.1.7 (a)). As the $T_{surface} \approx T_{pyrolysis} \approx 420$°C was approximately constant and independent of the external heat

flux, the calculated $\dot{q}''_{rerad}$ (according to Eq. 3) was around 10 kW m^{-2} and invariable over time and irradiation during the steady-burning stage. In the residue-forming EP_LS, the $T_{pyrolysis}$ was similar to EP and independent of irradiation. With various external heat fluxes applied, the $T_{surface}$ increased with increasing external heat flux (shown in Fig 3.1.7 (b)). $T_{surface}$ was measured approximately by the thermocouple closest to the surface: 680°C (for 35 kW m^{-2}), 720°C (for 50 kW m^{-2}) and 800°C (for 70 kW m^{-2}), respectively. Thus the calculated $\dot{q}''_{rerad}$ values were 42 kW m^{-2} (for 35 kW m^{-2}), 50 kW m^{-2} (for 50 kW m^{-2}) and 68 kW m^{-2} (for 70 kW m^{-2}). The reradiation for EP_LS was considerably larger than that for EP, by a factor of 4.2 to 6.8. The factor increased significantly with increasing irradiation.

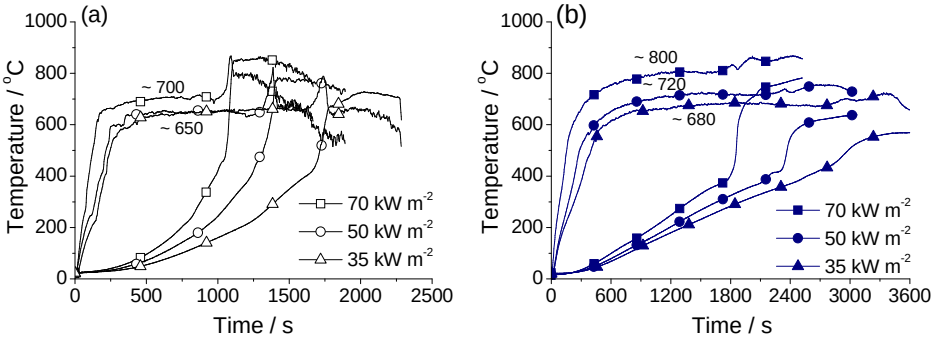

Fig 3.1.7. *Temperature profiles measured by the thermocouples on the top and bottom inside burning EP and EP_LS in the cone calorimeter with an external heat flux of 35, 50 and 70 kW m^{-2}; (a) EP and (b) EP_LS*

In principle, the thermal inertia, representing the product of $\kappa\rho c$, is the primary material property influencing the time to ignition (t_{ig}), while the imposed heat flux contributing to a critical temperature for ignition is the primary environmental impact [101, 102]:

$$t_{ig} \propto \kappa\rho c \cdot \left[\frac{T_{ig} - T_0}{\dot{q}''_{ext} - \dot{q}''_{crit}} \right]^2 \qquad (4),$$

with T_0 = starting specimen temperature and $\dot{q}''_{crit}$ = the critical heat flux necessary for ignition.

In accordance with previous studies [115,116], because the TPPMMT functioned as inert filler, the t_{ig} was hardly changed by the use of organically modified LS in

comparison to EP. The t_{ig} was shortened by applying higher external heat fluxes. Fig 3.1.8 illustrates the linear relationship between the irradiation and $t_{ig}^{-0.5}$ for both EP and EP_LS [102]. A minimum external heat flux of ~8 kW m^{-2} was concluded to ignite both materials. Considering the same pyrolysis temperature, the identical critical heat flux for ignition implied an identical thermal inertia of EP and EP_LS. The heat loss by conductivity through the back of the sample and into the surroundings ($\dot{q}''_{loss}$) was then confirmed to be the same for both materials and below the critical heat flux for ignition (<< 8 kW m^{-2}). In this case, an approximation of $\dot{q}''_{loss}$ = 0 kW m^{-2} was assumed for the equation of $\dot{q}''_{net}$, which can be neglected as contributing to any fire hazard.

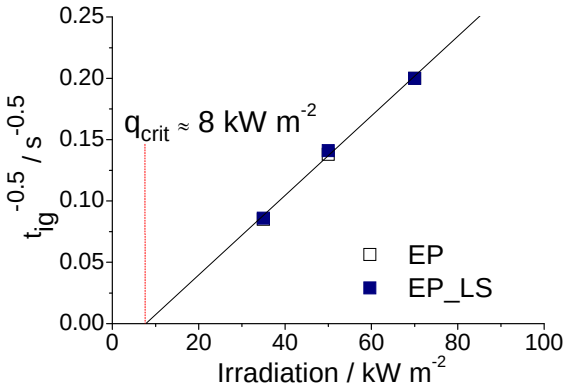

Fig 3.1.8. *Inverse of the square root of time to ignition versus the external heat flux in EP and EP/TPPMMT*

3.1.2 Determination of $\dot{q}''_{net}$

The net heat flux $\dot{q}''_{net}$ was calculated for EP and EP_LS (Eq. (2)) according to the applied different external heat fluxes (data given in Table 3.1.1). For EP, the reradiation emitted by the hot surface was restricted and invariable over the external heat flux; the $\dot{q}''_{net}$ thus clearly depended on the external heat flux. With the defined external heat flux of 35 - 70 kW m^{-2}, the $\dot{q}''_{net}$ of EP was increased to 45 - 80 kW m^{-2}. For EP_LS, since $\dot{q}''_{rerad}$ increased with increasing external heat flux, which counterbalanced the energy impact from the external heat flux, $\dot{q}''_{net}$ was reduced and became less dependent on the external heat

flux than was EP. The $\dot{q}''_{net}$ of EP_LS were decreased to 13 - 22 kW m^{-2}, accordingly. The reduction in $\dot{q}''_{net}$ determining the mass loss rate was decreased by 2 to 3 times. However, the calculated net heat fluxes were still sufficient to ignite the material since they were higher than the critical heat flux for ignition (8 kW m^{-2}).

Table 3.1.1. *Calculated values of various heat fluxes in the steady-burning state*

Unit / kW m^{-2}	EP			EP_LS		
$\dot{q}''_{ext}$	35	50	70	35	50	70
$\dot{q}''_{flame}$	~ 20	~ 20	~ 20	~ 20	~ 20	~ 20
$\dot{q}''_{rerad}$	~ 10	~ 10	~ 10	~ 42	~ 50	~ 68
$\dot{q}''_{net}$	~ 45	~ 60	~ 80	~ 13	~ 20	~ 22

3.1.3 Fire parameters: heating rate, burning velocity, HRR and PHRR

Fig 3.1.9 compares the heating rate profiles close to the pyrolysis front as a function of the sample depth in the two different materials. The high heating rate profile of EP was significant over a depth of ~6 mm for EP and 8 - 10 mm for EP_LS. The highest heating rate near the specimen surface was related to direct high irradiation from the cone heater, with a relatively lower surface temperature from the very beginning of the fire test. The initial decrease in the heating rate in both materials was attributed mainly to the increase in reradiation through preheating the initial surface from room temperature to pyrolysis temperature.

For EP (in Fig 3.1.9 (a)), a plateau-like heating rate was observed between depths of 6 and 16 mm, suggesting that this plateau correlated with the quasi-steady-state burning of the specimen independent of sample thickness [100]. When the material approached the end of combustion, a decrease in the heating rate was observed from 16mm until the end. Overall, for EP, the heating rate profile close to the pyrolysis front was visualized to be an approximately 3rd or 4th polynomial function over the sample depth. Surprisingly this result differs from other proposals [128, 130] indicating that a straightforward decay according to an exponential or a 2nd-order polynomial function is usually expected to satisfy the heat transfer boundary conditions of a non-charring material. Instead, for EP_LS, the heating rate profile close to the pyrolysis front exhibited an exponential decay as a function of depth

(in Fig 3.1.9 (b)). This decay was attributed not only to the thermal diffusivity into the specimen, but also to the increasing thickness of the residue covering the sample. For both materials the application of higher irradiation yielded a higher heating rate close to the pyrolysis front. By applying the same irradiation, the heating rate in EP_LS was reduced in comparison with EP. This decrease was attributed to the increased reradiation in EP_LS, and thus the reduced net heat flux. The differences in the heating rate profiles between the two materials at different irradiations were in good agreement with the corresponding net heat flux imposed on the surface.

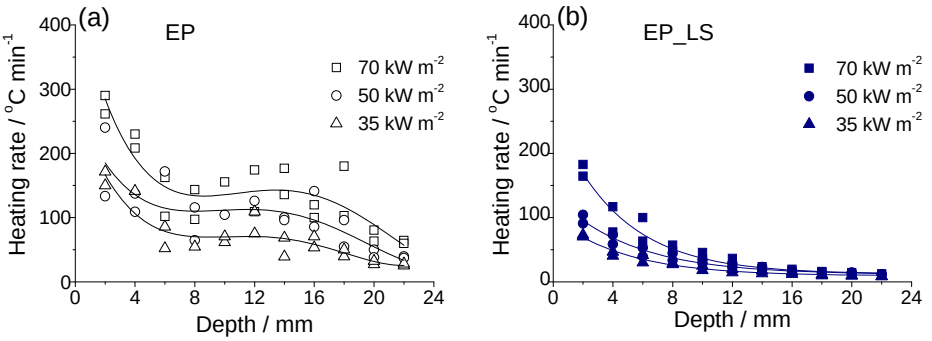

Fig 3.1.9. *Heating rates close to the pyrolysis front as a function of depth under various external heat fluxes; (a) EP and (b) EP_LS*

To explain the different phenomenon of heating rate in EP and EP_LS, it is worth noting that the mechanism of heat transfer to the pyrolysis zone differs between the non-residue and residue forming materials (a proposed model is illustrated in Fig 3.1.10). Generally, heat can flow due to the temperature difference in three distinct mechanisms: radiation, convection and conduction [131-132]. Accurate predictions of the heat and mass transfer for charring and non-charring solids are difficult to determine experimentally and theoretically. As discussed above, the heat conducted through the specimen back is similar for $\dot{q}''_{loss}$ in both EP and EP_LS. For non-charring EP (in Fig 3.1.10 (a)), the heat transferred into the pyrolysis zone is governed directly by radiation and convection at the material surface through the liquid-gas boundary. For EP_LS (in Fig 3.1.10 (b)), as a consequence of residue formation, the radiation and convection heat occur only at the material surface in the solid-gas phase. The major heat transfer through the residue formation into the pyrolysis zone is governed mainly by three mechanisms: bulk conduction through the fire residue, convection by the gas flowing through the residue, and radiation across the pores of the residue [133]. Also, the effective mass flux rate, and thus the burning rate, are influenced by many factors of the residue formation such as thickness,

pore size and shape. In the pyrolysis zone, the main heat mechanisms are conduction and convection for EP and EP_LS, since both are exhibited in the soild/mesophase-liquid phase.

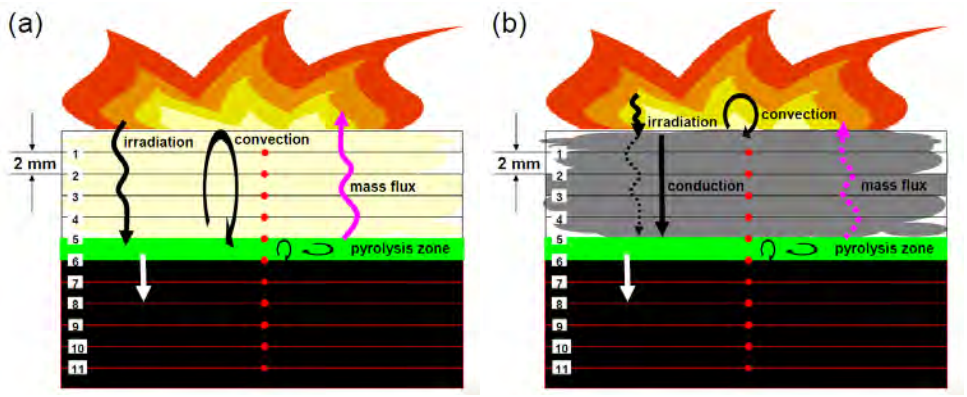

Fig 3.1.10. *Proposed model of different mechanism of heat transfer to the pyrolysis zone for (a) EP and (b) EP_LS*

Other pyrolysis characteristics, including the time to reach the necessary pyrolysis temperature (390°C) and the burning velocity close to the pyrolysis front v_p, are strongly correlated with the heating rate. Higher heat fluxes lead to higher pyrolysis front velocities and quicker temperature rises. In Fig 3.1.11 (a), the time to reach 390°C was prolonged by increasing the sample depth, and also by decreasing the applied irradiation for both materials. The time to reach 390°C was systematically longer in EP_LS than EP, corresponding to the respective net heat fluxes for the two different materials.

Further, the application of higher irradiation resulted in a higher v_p in both materials. In Fig 3.1.11 (b), the v_ps close to the pyrolysis front were almost constant, irrespective of specimen depth. With the applied irradiations of 35 - 70 kW m^{-2}, the v_p was 0.7 - 1.4 mm min^{-1} for EP and 0.5 - 0.7 mm min^{-1} for EP_LS. The systematically reduced v_ps were also in good agreement with the reduced net heat flux imposed on the surfaces of the two different materials.

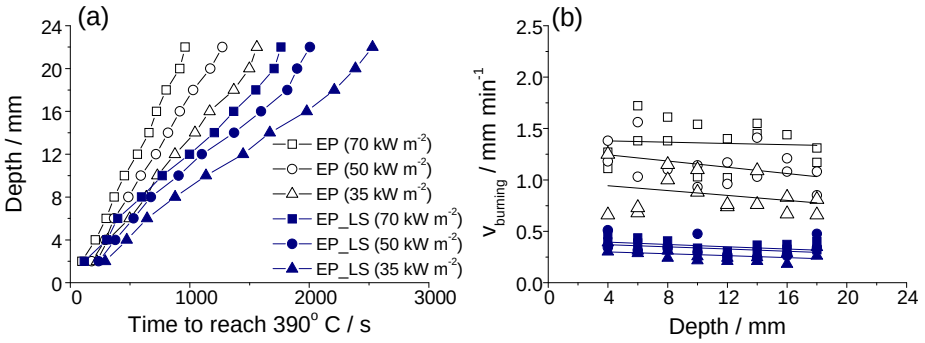

Fig 3.1.11. *Evaluated data for EP and EP/TPPMMT at external heat fluxes of 35, 50 and 70 kW m^{-2} plotted against the depth; (a) time to reach 390 ^{o}C and (b) burning velocity at the pyrolysis front (same legend in (a) and (b))*

Fig 3.1.12 (a) shows the representative HRR of EP and EP_LS during combustion in the cone calorimeter under an irradiation of 50 kW m^{-2}. The fire properties of the investigated materials determined in the cone calorimeter, including HRR, PHRR, THE, and t_{ig}, are given in Table 3.1.2. As explained above, EP showed a typical non-charring burning behaviour, whereas EP_LS showed a typical residue-forming burning behaviour [102]. After ignition, the HRR curves of EP and EP_LS both exhibited a similar initial increase to a reference point at ~410 kW m^{-2} (1st-PHRR). Afterwards the HRR performed differently during the burning process. In EP, a quasi-steady-state HRR (steady-HRR = ~400 kW m^{-2}) was observed between ~100 s and 750 s, then increased to a sharp peak at around 1240 s (2nd-PHRR = ~720 kW m^{-2}) when the remaining material changed from a thermally thick to thermally thin material. The 2nd PHRR at the end of burning was caused by the reduction of heat transfer into the specimen when the pyrolysis zone approached the insulated back of the material [102]. For EP_LS, the HRR from the reference point at 419 kW m^{-2} decreased to 178 kW m^{-2}, then remained steady between ~350 s and 1400 s. This phenomenon was due to the thickening of the residue layer, resulting in a decrease in HRR until an efficient residue layer was formed. Afterwards the HRR increased gradually to a smooth peak (~ 323 kW m^{-2}) at about 2100 s. The prolonged burning time resulted in the delayed flame-out at 2281 s.

In Fig 3.1.12 (b)-(c), the value of steady HRR and the 2nd PHRR increased with increasing irradiation. Compared with EP, both the steady HRR and the 2nd PHRR were reduced in EP_LS. The reductions in steady HRR (about 57 - 61%) and the 2nd PHRR (about 39 - 60 %) increased with increasing irradiation. This phenomenon is typical behaviour for a polymer nanocomposite using LS [49, 51].

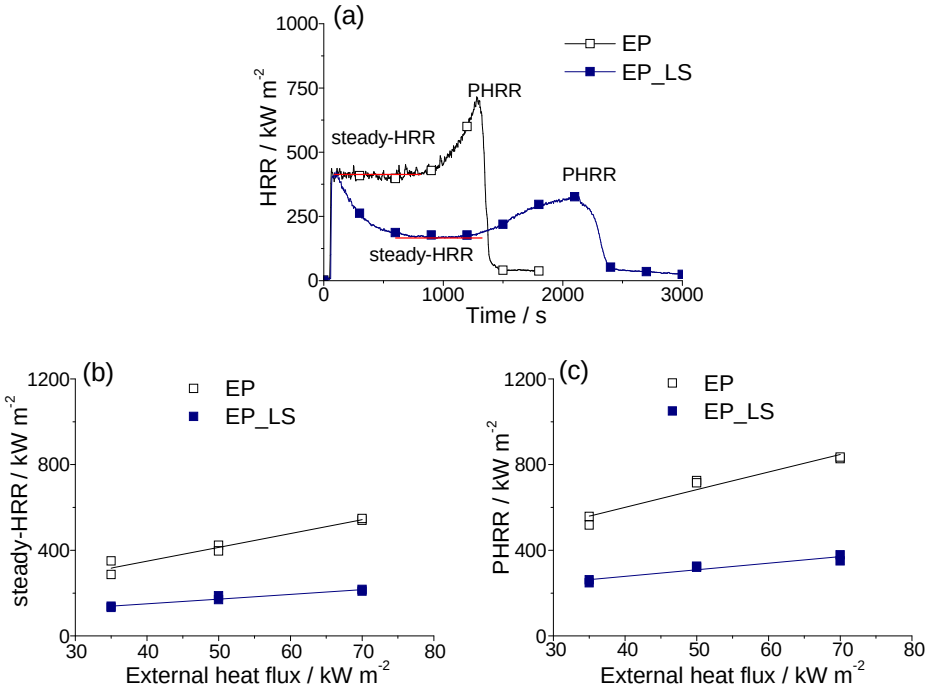

Fig 3.1.12. *(a) A comparison of HRR between EP and EP_LS with an external heat flux of 50 kW m^{-2}; (b) steady HRR as a function of irradiation; (c) 2nd PHRR at the end of burning as a function of irradiation*

Table 3.1.2. *Average data of duplicated cone calorimeter measurements with various external heat fluxes applied for EP and EP_LS*

	EP			EP_LS		
external heat flux / kW m^{-2}	35	50	70	35	50	70
t_{ig} / s	137	52	25	135	60	24
t_{fo} / s	1747	1494	1049	3332	2281	1848
first PHRR / kW m^{-2}	360	410	540	340	419	529
steady HRR / kW m^{-2}	320	400	540	138	178	212
second PHRR / kW m^{-2}	538	720	832	255	323	358

3.1.4 Quantitative assessment of the shielding effect

In Fig 3.1.13, the pyrolysis front velocity, the steady HRR and the 2nd PHRR are plotted against the corresponding $\dot{q}''_{net}$ at the surface of burning material. The results for both EP and EP_LS were elucidated by the same linear relationship of the $\dot{q}''_{net}$. A quantitative assessment of the flame retardancy by the shielding effect in EP_LS was demonstrated by the proportional reduction in the fire parameters against the reduction of $\dot{q}''_{net}$. In the non-charring EP, the higher $\dot{q}''_{net}$ corresponded with higher irradiation, resulting in higher values for v_p, steady HRR and the 2nd PHRR. In EP_LS, due to the increased $\dot{q}''_{rerad}$ defined as the shielding effect, the $\dot{q}''_{net}$ was reduced. Further, the increase in $\dot{q}''_{net}$ with increasing irradiation was largely counterbalanced by an increasing shielding effect. The shielding effect was sufficient to describe the flame retardancy effect with respect to the discussed fire parameters, v_p, steady HRR and PHRR, and was demonstrated to be the only major flame retardancy effect in the use of inert fillers.

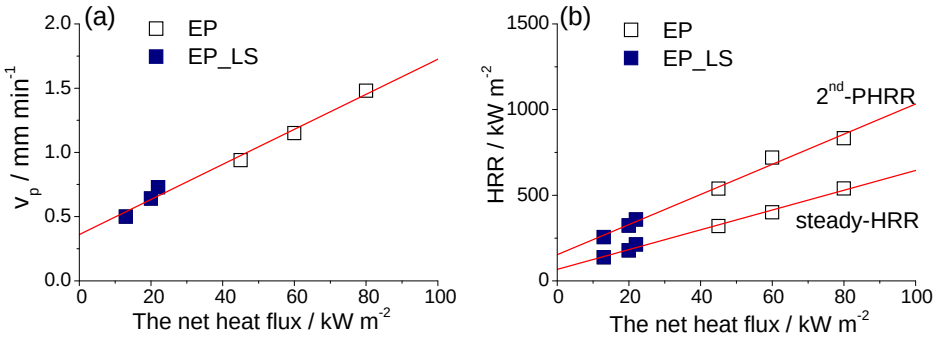

Fig 3.1.13. *(a) The burning velocities at the pyrolysis front and (b) the HRRs during steady state and the 2nd PHRRs at the end of burning are plotted against the calculated net heat flux for EP and EP_LS*

3.1.5 Conclusion

Quantitative experimental insight on the flame retardancy of EP_LS by the shielding effect based on non-charring polymers was explored under various external heat fluxes. The net heat flux was quantified based on several main heat fluxes imposed on the burning material surface, including the defined external heat flux, the estimated heat loss

through the specimen into the surroundings, the incident flame heat flux and the reradiation emitted by hot surface temperatures measured online during combustion.

For both EP and EP_LS, the incident flame heat flux imposed on the burning surface was approximately 20 kW m^{-2}, independent of the defined external heat flux. Concurrently, no major difference was observed between the two different materials.

For the non-charring material EP, the $T_{surface} \approx T_{pyrolysis}$ irrespective of the external heat flux, resulting in an invariable $\dot{q}''_{rerad} \approx$ 10 kW m^{-2} . Hence the net heat flux on the burning surface was strongly dependent on the external heat flux and increased to 45 - 80 kW m^{-2} from applied irradiations of 35 - 70 kW m^{-2}. For the residue-forming material EP_LS, the $T_{surface} \neq T_{pyrolysis}$. The $\dot{q}''_{rerad}$ increased with increasing external heat fluxes, resulting in a reduced dependence of the external heat flux on the net heat flux. The net heat fluxes imposed on the burning surface of EP_LS were thus reduced to 13 - 22 kW m^{-2} accordingly.

Compared to EP, fire parameters including the pyrolysis front velocity, the HRRs in steady-state and the 2nd PHRRs at the end of burning were reduced in EP_LS. A quantitative assessment of the shielding effect for flame retardancy was demonstrated by a linear reduction in the fire parameters against the corresponding net heat flux on the burning surface. Consequently the dependence relation between the $\dot{q}''_{rerad}$ and the external heat flux elucidated the reduction of flame retardancy as function of radiation in nanocomposite when compared to EP. The shielding effect by the inorganic-carbonaceous fire residue surface protection layer is the only major flame retardancy effect in the polymer nanocomposites based on non-charring or low-charring polymers with inert additives.

3.2 Investigations of EP with different organic-modified MMTs

3.2.1 Materials and morphology of the additive dispersion

As discussed in section 2.1.2, layered silicate (montmorillnite) was modified by different organic salts in order to increase the thermal stability of organo-LS. In this section, EP composites with three kinds of MMT, including unmodified NaMMT, organic-modified TPPMMT and 2PIMMT, were investigated in comparison with EP. Samples preparation is described in Appendix: Experimental (materials). The compositions and abbreviations of the investigated materials are summarized in Table 3.2.1.

Table 3.2.1. *Abbreviations and composition of the investigated materials*

Abbreviations	Composition of materials
EP	Bisphenol-A-diglycidylether (GY250 / MHHPA / 1-Methylimidazole)
EP_NaMMT5	EP with 5 wt% sodium montmorillnite
EP_TPPMMT5	EP with 5 wt% tetraphenylphosphonium modified montmorillnite
EP_2PIMMT5	EP with 5 wt% 2-phenylimidazolium modified montmorillnite

The morphologies of layered silicate dispersion in the different EP composites are shown in Fig 3.2.1, which were examined by TEM. The images show that the NaMMT and 2PIMMT were not homogeneously distributed in the EP matrix. Both EP_NaMMT5 and EP_2PIMMT5 appeared mostly in agglomerates or large particles with a size of some micrometers. Further, neither material showed separation of silicate layers under nano-scale magnification, and are thus by definition micro-composites. As reported before [28], the d-spacing of LS was increased to 1.9 nm by the modification of TPP salt. When the TPPMMT was incorporated into the EP matrix, it showed neither dispersion nor exfoliation in a perfect manner. Particles some micrometers in size were randomly distributed at lower magnifications; a mixture of intercalated and exfoliated silicate layers was observed at higher magnifications (shown in Fig 3.3.1). Although the exfoliation into single layers and homogeneous distribution of the layers was rather limited, EP_TPPMMT5 showed some intercalation phases and is thus defined as a nano-composite.

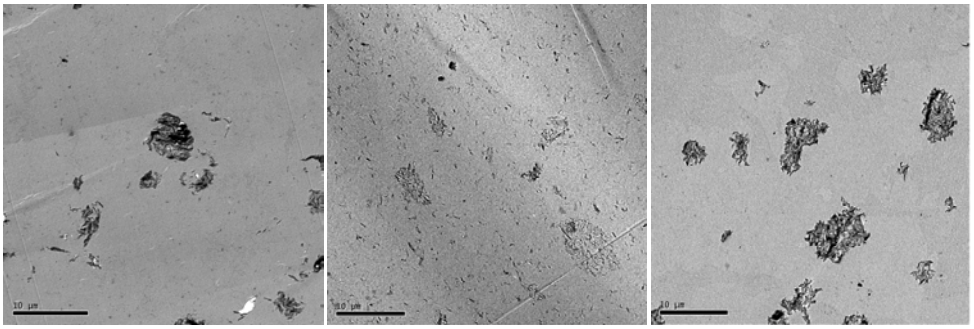

EP_NaMMT5 EP_TPPMMT5 EP_2PIMMT5

Fig 3.2.1. *TEM images of morphology of layered silicate dispersion in epoxy composites with the different fillers* [28]

3.2.2 Pyrolysis behaviour

Decomposition behaviour of the different MMTs (without incorporation into EP resin) was identified individually; their TG-DTG curves are shown in Fig 3.2.2. Corresponding to previous reports [55-57, 110], for all the MMTs the initial mass loss began at a temperature of ~500 K, caused by the release of some free absorbed water and gaseous substances. Two main decomposition regions occurred in the temperature range of 600 - 1000 K. At relatively low temperatures between 600 - 800 K, the unmodified NaMMT exhibited a broad, smooth mass loss step. This phenomenon was caused mainly by the release of some weakly bonded substances residing between the aluminosilicate layers [110]. The first remarkable mass loss step with a peak occurred at ~650 K for TPPMMT, and at ~720 K for 2PIMMT, respectively. These mass losses were attributed to the decomposition of organic moieties from the surfactant [56]. At high temperatures between 800 - 1000 K, the mass loss was caused mainly by dehydroxylation of the alumininosilicate lattice, associated with residual organic carbonaceous charring [110]. Up to 1100 K, when a stable residue stage was reached, the total mass loss was 6 wt% for NaMMT, 18 wt% for TPPMMT and 10 wt% for 2PIMMT, respectively. The additional mass loss in organically modified MMTs was attributed to the organic modification. Comparing the two different organic modified MMTs, 2PIMMT showed slightly higher thermal stability than TPPMMT in correspondence with a relatively higher decomposition temperature and less mass loss.

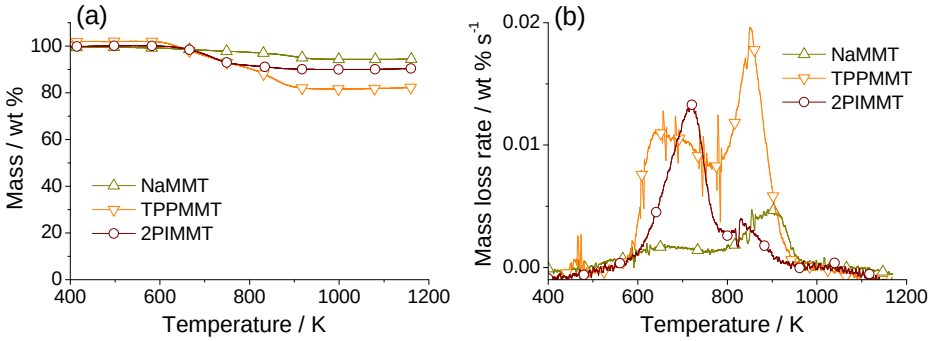

Fig 3.2.2. *Thermo decomposition of different layered silicates in N_2 with a heating rate of 10 K min^{-1}; (a) TG and (b) DTG*

The influence of different MMTs on the thermal stability of EP composites was examined in comparison with EP. The resulting TG-DTG curves are shown in Fig 3.2.3 and the data are summarized in Table 3.2.2. All of the materials showed similar decomposition behaviour with an onset temperature at ~500 K, a result of the evolution of physically absorbed substances (mainly H_2O and CO_2) [110]. One main decomposition step occurred in the temperature range of 600 - 800 K, with a maximum mass loss rate at ~690 K. Up to 1000 K, the residue was increased by using the different fillers. The additional residue in the different composites (Δ = 5 - 6 wt%) was in good agreement with the presence of inert fillers. These results indicated that the thermal stability of EP composites was hardly affected by using the different MMTs.

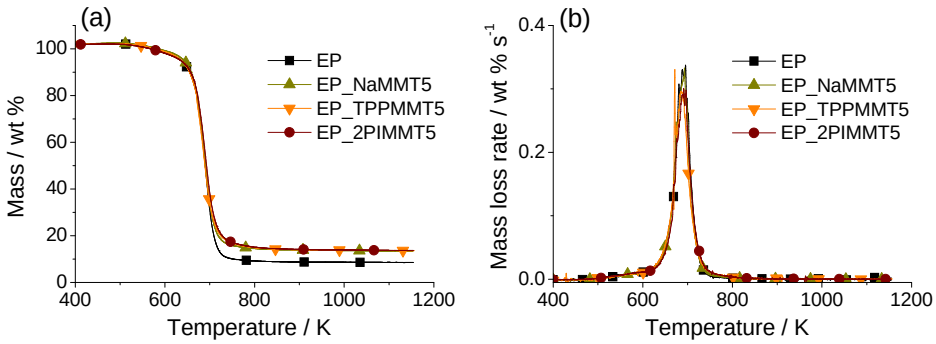

Fig 3.2.3. *Thermo decomposition of EP and EP composites with different fillers in N_2 with a heating rate of 10 K min^{-1}; (a) TG and (b) DTG*

Table 3.2.2. *TG data of the investigated materials in N_2 with a heating rate of 10 K min^{-1}*

Materials in N_2	$T_{5\ wt\%}$ / K	T_{max} / K	Mass loss up to 800 K / wt%	Residue at 1000 K / wt%
EP	636	692	91	8.9
EP_NaMMT5	641	692	86	13.5
EP_TPPMMT5	636	686	85	13.6
EP_2PIMMT5	637	689	84	14.7

Fig 3.2.4 illustrates the thermal oxidative stability of the different EP composites in comparison with EP, which were examined in TG in air atmosphere; the data are summarized in Table 3.2.3. As a typical oxidative decomposition behaviour of EP resin [111], all of the EPs showed similar onset decomposition behaviour, followed by two main mass loss steps in the temperature range of 500 - 1000 K. The first main mass loss step occurred between 600 - 800 K with a peak at a temperature of ~690 K. This result was in good agreement with a similar decomposition temperatures in inert atmosphere as discussed above. At high temperatures between 800 - 1000 K, additional material was consumed during the second mass loss step due to oxidation of the transitory charring network [111]. Compared to EP and EP_NaMMT5, the thermal oxidative stability of the charring network was slightly enhanced by using the organic-modified MMT, since the second peak mass loss rate was shifted to a higher temperature (ΔT = 20 - 30 K) by the use of either TPPMMT or 2PIMMT, while it occurred at ~900 K for EP and EP_NaMMT5. The residue obtained at 1000 K was increased over EP when the various fillers were used. The additional residue in the different composites corresponded well with the presence of inert fillers.

In summary, in either aerobic or anaerobic atmosphere, the overall pyrolysis behaviour of EP composites with the different fillers was changed insignificantly from that of EP.

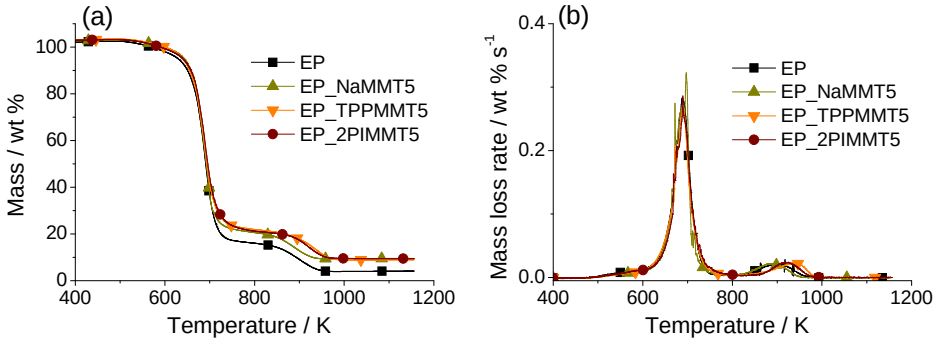

Fig 3.2.4. *Thermo oxidative decomposition of EP and EP composites with different fillers in air with a heating rate of 10 K min^{-1}; (a) TG and (b) DTG*

Table 3.2.3. *TG data of EP and EP composites with different fillers in air with a heating rate of 10 K min^{-1}*

Materials in air	$T_{5\ wt\%}$ / K	$T_{max\ 1}$ / K	Mass loss up to 800 K / wt%	$T_{max\ 2}$ / K	Residue at 1000 K / wt%
EP	629	688	84	900	3.9
EP_NaMMT5	643	689	79	885	9.4
EP_TPPMMT5	640	690	78	930	8.9
EP_2PIMMT5	640	689	79	920	9.5

3.2.3 Flammability and ignitability

The values for flammability in terms of reaction to small flame, characterized by LOI and UL 94 test, are listed in Table 3.2.4. The LOI value was improved slightly over EP by using the different fillers. Among all the materials, EP_TPPMMT5 showed the highest LOI value at 25 %. Only 23 % and 21 % were achieved for EP_NaMMT5 and EP_2PIMMT5, respectively. As has been suggested before [51], this improvement by using inert fillers was caused mainly by a residue protection layer, but also influenced by the organic modification of LS. However, this protection effect was not sufficient to achieve self-extinguishing behaviour in UL 94 test. Although the burning rate of EP_NaMMT5 was reduced slightly in comparison with the other materials, like EP, all of the different composites achieved only a HB classification. As mentioned before, there is no clear correlation between LOI and UL 94 results, since the two tests are applied in different fire scenarios [12,102].

The ignitability of all of the materials was determined by t_{ig} obtained from cone calorimeter tests with a spark ignition and a constant irradiation (data given in Table 3.2.4). In general, t_{ig} shortens with increasing irradiation. Further, higher irradiation levels give better reproducibility [12]. Comparing all of the materials with the same irradiation applied, the t_{ig} was increased marginally by the use of additives, but hardly any difference was found between the various additives.

Table 3.2.4. *Flammability (result of LOI value and UL 94 test) and ignitability (time to ignition obtained in cone calorimeter test) of all the investigated materials*

Samples	LOI / % ±1	UL94 / mm min^{-1} ±1	time to ignition in cone calorimeter		
			35 kW m^{-2}	50 kW m^{-2}	70 kW m^{-2}
EP	20	HB / 21	100 ±6	47 ±1	22 ±3
EP_NaMMT5	23	HB / 5	113 ±2	53 ±2	27 ±4
EP_TPPMMT5	25	HB / 18	110 ±8	53 ±3	25 ±1
EP_2PIMMT5	21	HB / 20	129 ±9	52 ±4	20 ±8

3.2.4 Fire behaviour

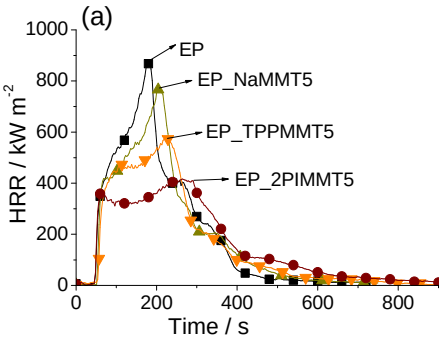

(b)

EP EP_NaMMT5 EP_TPPMMT5 EP_2PIMMT5

Fig 3.2.5. *(a) HRRs and (b) the corresponding fire residue morphologies of EP and EP composites with different MMTs obtained in cone calorimeter under an external heat flux of 50 kW m^{-2}*

The characteristic HRRs of EP and the different EP composites during combustion are shown in Fig 3.2.5 (a). All of the materials showed a similar initial increase in HRR after ignition. As a typical non-charring burning behaviour material of EP, the HRR rapidly increased to a peak before flame-out. For the residue-forming materials of EPs with the different fillers, the HRRs showed a more or less sluggish increase until the PHRR at the end of burning, more pronounced in the EPs with organically modified LS. The reduction in PHRR correlated to the fire residue integrity. As shown in Fig 3.2.5 (b), EP_NaMMT5 produced fragile fragments in a non-integral residue structure, corresponding to a slight reduction in PHRR. EP_2PIMMT5 produced the most compacted and integral residue structure, corresponding to the highest reduction in PHRR among all of the materials.

Fig 3.2.6 (a) shows the PHRR values of each material evaluated under various external heat fluxes. In general, the PHRR increased with increasing external heat flux, more pronounced for the materials forming little or no residue such as EP and EP_NaMMT5. Corresponding well with previous reports [28-29], the PHRRs were reduced by using the different fillers, accompanied by a prolonged burning time. The reduction of PHRR was about 8 - 16 % through the use of unmodified LS (EP_NaMMT5), while a more remarkable reduction was achieved by the use of organically modified LS (34 - 42 % for EP_TPPMMT5 and 52 – 57 % for EP_2PIMMT5). The reduction in PHRR in terms of flame retardancy tended to increase with increasing the external heat flux applied.

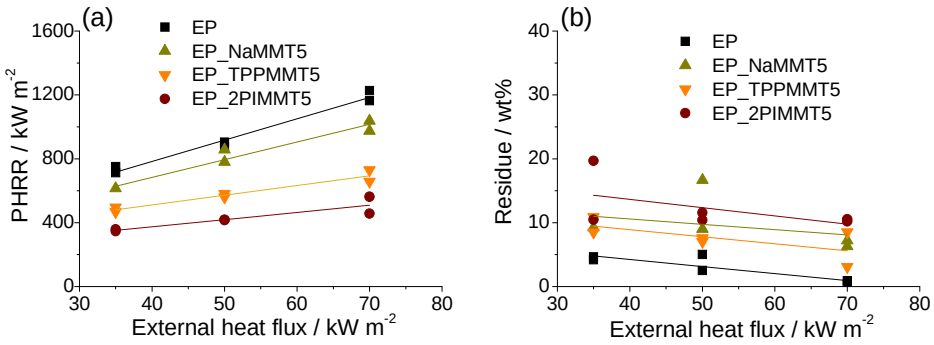

Fig 3.2.6. *(a) PHRR and (b) the amount of residue of EP and EP with different fillers evaluated under various external heat fluxes in cone calorimeter*

Other fire parameters, including the amount of residue after the end of combustion, THE , THE/ML in terms of the effective heat of combustion efficiency, CO and smoke production evaluated from cone calorimeter measurements with various external heat fluxes, are summarized in Table 3.2.5.

For each material the residue was decreased marginally as higher external heat fluxes were applied. Compared to EP, the amount of fire residue was increased through the use of different fillers (illustrated in Fig 3.2.6 (b)). The additional residue (Δ = 4 - 10 wt%) was related mainly to the amount of inorganic filler, with limited carbonaceous charring. Compared with the EPs with different fillers, EP_2PIMMT5 generated a slightly higher amount of carbonaceous char than would be expected. In general, THE strongly depends on the total mass loss, char yield, and effective heat of combustion efficiency in the flame zone, and is also influenced slightly by irradiation [12]. Due to the presence of LS working mainly as an inert filler, as compared to non-filled EP, the fire load (THE) and effective heat of combustion (THE/ML) were insignificantly lower in all of the EPs with the different additives, as were the CO and smoke yield. These results further showed that flame inhibition hardly occurred in the gas phase, demonstrating the various additive's contribution to flame retardancy. The flame retardancy was attributed mainly to a shielding effect through residue formation in the condensed phase.

3.2.5 Conclusions

For the dispersion of LS in EP matrix, only EP_TPPMMT5 exhibited the intercalation morphology defining it as a nano-composite, whereas both EP_NaMMT5 and EP_2PIMMT5 showed no delamination of silicate layers, defining them as micro-composites. Insignificant influence was observed on the degree of curing and glass transition of EP matrices with the different MMTs. Although the thermal oxidation process at high temperatures was enhanced marginally through the use of organically modified TPPMMT and 2PIMMT, the overall pyrolysis behaviour of all the composites, in either aerobic or in anaerobic atmospheres, was hardly changed in comparison with EP.

The LOI values of EP composites were improved slightly over EP by using the different additives. EP_TPPMMT5 showed the highest LOI value among all of the materials. However, no significant change was found in UL 94 test, since all of the materials achieved only a HB classification. The time to ignition was increased slightly by using the additive under the same irradiation, but barely any difference was detected when various fillers were used.

The PHRR was reduced compared to EP by using the different additives. The reduction in PHRR corresponded very well with the structural integrity of the fire residue. Among all of the materials, EP_2PIMMT5, which had the most integral residue structure, exhibited the greatest reduction in PHRR. The additional residue in the different composites

was mainly related to the original amount of additive with limited carbonaceous charring. No flame inhibition occurred in the gas phase due to the different MMTs acting as inert fillers.

In conclusion, although the microcomposite EP_2PIMMT5 showed better fire performance than the nanocomposite TPPMMT, the intercalated or exfoliated morphology of LS dispersion is a mandatory prerequisite for the efficiency of flame retardancy since the exfoliation of LS can be further induced during heating process. The flame retardancy was attributed mainly to a shielding effect through residue formation in the condensed phase. It is demonstrated that higher fire residue integrity provided for more efficient of flame retardancy.

Table 3.2.5. *Cone calorimeter results for all the investigated materials at various external heat fluxes of 35, 50 and 70 kW m^{-2} applied. (*one measurement was done)*

	PHRR	t-PHRR	Residue	THE	THE / ML	COY	TSR /ML
	kW m^{-2}	s	%	MJ m^{-2}	MJ $m^{-2}g^{-1}$	g g^{-1}	g^{-1}
irradiation of 35 kW m^{-2}							
EP	733 ±19	248 ±17	4.4 ±1	141 ±1	2.48	0.046	82
EP_NaMMT5*	615	279	9.2	148	2.47	0.044	82
EP_TPPMMT5	482 ±14	306 ±21	9.7±2	140 ±5	2.43	0.051	85
EP_2PIMMT5	353 ±6	141 ±6	15.2 ±5	138 ±6	2.44	0.041	76
irradiation of 50 kW m^{-2}							
EP	891 ±14	182 ±2	3.8 ±1	151 ±3	2.46	0.044	82
EP_NaMMT5	819 ±39	204 ±3	12.8 ±4	146 ±1	2.55	0.046	89
EP_TPPMMT5	571 ±11	228 ±3	7.3 ±1	138 ±3	2.36	0.051	89
EP_2PIMMT5	418 ±2	285 ±21	11 ±1	136 ±4	2.42	0.040	84
irradiation of 70 kW m^{-2}							
EP	1196 ±32	134 ±2	0.7 ±1	147 ±5	2.40	0.047	85
EP_NaMMT5	1006 ±32	150 ±6	4.2 ±1	138 ±1	2.41	0.044	90
EP_TPPMMT5	694 ±36	195 ±3	3.8 ±2	140 ±1	2.34	0.051	94
EP_2PIMMT5	510 ±53	257 ±2	10.4 ±1	137 ±2	2.36	0.040	94

Chapter 3.3 Investigations of EP_LS with triphenylphosphate

3.3.1 Materials and morphology of LS dispersion

As discussed in section 2.1.3, in order to improve the dispersion of LS, triphenylphosphate (TriPP) salt was introduced as spacer for expansion of the d-spacing of silicate layers. Three kinds of EP/TPPMMT were investigated, with and without the spacer TriPP, respectively, in comparison with EP and EP with 1 wt% TriPP. Sample abbreviations and compositions of the investigated materials are summarized in Table 3.3.1. The 'normal' designation means the organic-modified TPPMMT without further treatment. The 'loaded' clay means TPPMMT preloaded with the spacer TriPP before being blended into the EP matrix. The 'mixed directly' designates the material that resulted when the TPPMMT and the spacer were mixed into the EP resin at the same time. The details of preparing the materials are described in Appendix: Experimental (materials).

Table 3.3.1. *Abbreviations and Composition of the investigated materials*

Abbreviations	Composition of materials
EP	GY250 / MHHPA / 1-Methylimidazole
Tripp_1	with 1 wt% spacer of triphenylphosphate (TriPP)
TPPMMT_5	with 5 wt% "normal" clay
TPPMMT_6	with 6 wt% "loaded" clay
TPPMMT_5+1	with "simple mixed" 5 wt% Clay + 1 wt% spacer

The dispersion morphology of TPPMMT_5 (refer to EP_TPPPMMT5) without TriPP was discussed in section 3.2. Comparing TPPMMT_5 to the other two composites containing TriPP, TEM images exhibit a similar morphology of LS dispersion (shown in Fig 3.3.1). The overall distribution of LS in micrometer-sized particles was dispersed homogenously in the EP matrix at lower magnifications. On the nanometer scale, a limited mixture of intercalated and exfoliated structure was exhibited in all of the EPs with various fillers. In fact, no improvement in the dispersion of LS was observed through either the methods of preloading or simple mixing with the spacer TriPP, since the presence of TriPP did not affect the morphology of LS with a d-spacing of ~1.9 nm in the EP matrix.

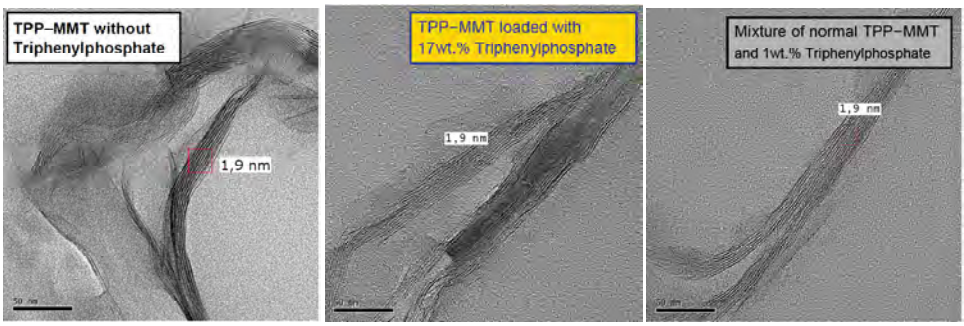

TPPMMT_5 TPPMMT_6 TPPMMT_5+1

Fig 3.3.1. *Morphology of the different layered silicate dispersion in the different EP/TPPMMT* [28]

3.3.2 Pyrolysis behaviour

The different EPs showed a similar thermal stability in inert atmosphere (illustrated in Fig 3.3.2). All of the materials started to decompose at a temperature of ~500 K. A slight mass loss at the early stage was mainly related to the release of some physically absorbed substances like moisture and CO_2 [110]. One main decomposition step occurred in the temperature range of 600 - 750 K, with a peak mass loss rate at ~680 K. The residue obtained at 1000 K was increased through the use of different additives (in Table 3.3.2). TriPP_1, in particular, generated more residue than expected (additional 3 wt%). The additional carbonaceous char was due to the beneficial effect of a compound containing phosphorus enhancing charring in the condensed phase [90]. For all of the EPs with varying TPPMMT content, the derivations of mass loss during the main decomposition step (4 - 7 wt%) and the additional residues (4 - 5 wt%) were related to the amount of inorganic additive applied.

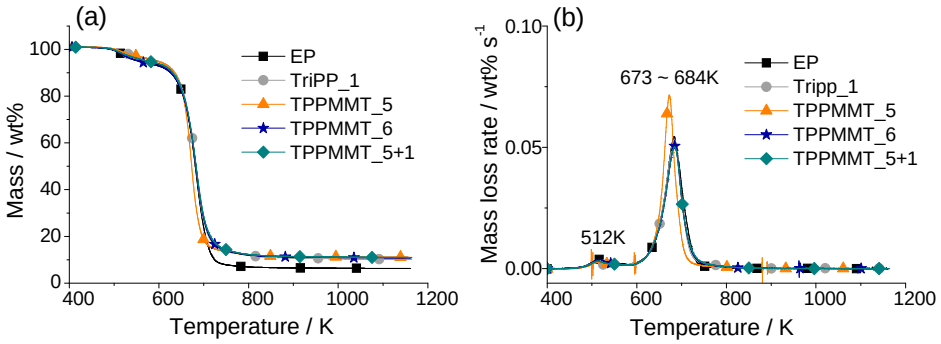

Fig 3.3.2. *Thermal stability of EP and EP/TPPMMTs in different modification in N_2 with a heating rate of 10 K min^{-1}; (a) TG and (b) DTG*

Table 3.3.2. *TG data of the EP and the different nanocomposites in N_2 with a heating rate of 10 K min^{-1}*

Materials in N_2	$T_{5\ wt\%}$ / K	T_{max} / K	Mass loss up to 720 K / wt%	Residue at 1000 K / wt% ±1
EP	571	684	89	6
TriPP_1	597	684	83	10
TPPMMT_5	595	673	85	11
TPPMMT_6	556	684	83	11
TPPMMT_5+1	575	684	82	11

The thermal-oxidative stability of the different EPs in air is shown in Fig 3.3.3. and Table 3.3.3. The onset decomposition temperature of all the materials occurred at ~500 K with a slight mass loss at the beginning. Two main oxidative decomposition steps were exhibited in the temperature range of 600 - 950 K. The first peak mass loss occurred at ~650 K, resulting in a mass loss of about 63 - 67 wt%. The second peak mass loss occurred at ~830 K, with additional materials consumed (30 - 33 wt%) during the oxidation of char. At a temperature of 1000 K the residue was increased slightly by the presence of inorganic additive.

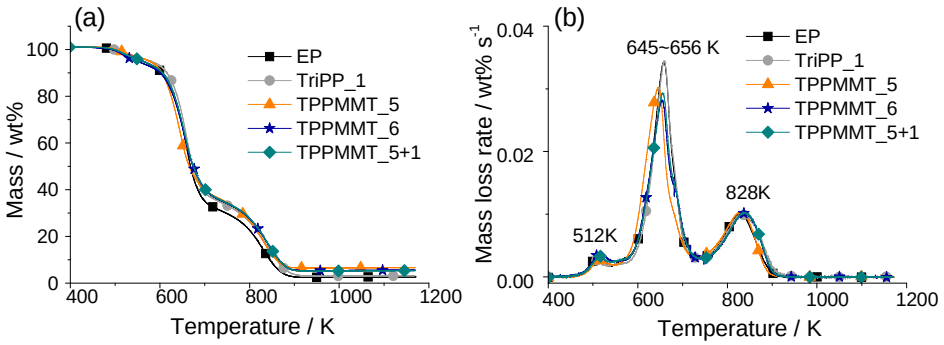

Fig 3.3.3. *Thermo oxidative stability of EP and different EP nanocomposites in air with a heating rate of 10 K min^{-1}; (a) TG and (b) DTG.*

Table 3.3.3. *TG data of the investigated materials with modified TPPMMT with a spacer of TriPP in air with a heating rate of 10 K min^{-1}*

Materials in air	$T_{5\ wt\%}$ / K ± 2	$T_{max\ 1}$ / K ±2	Mass loss up to 720 K / wt% ± 1	$T_{max\ 2}$ / K ± 5	Residue at 1000 K / wt% ± 2
EP	560	658	67	828	3
TriPP_1	579	659	64	830	3
TPPMMT_5	577	645	63	828	6
TPPMMT_6	549	654	63	838	5
TPPMMT_5+1	560	655	63	839	5

3.3.3 Flammability and ignitability

Table 3.3.4 shows the flammability and ignitability results for all of the different materials. The LOI value was increased slightly through the use of various additives. In comparison with EP at 21 %, it was increased by 2 % for TriPP_1, and by 4 % for TPPMMT_5. For the composites containing both additives, however, it clearly showed a superposition effect on flammability, since the LOI value was increased by 5 - 7 %. The TPPMMT_5+1 showed a slightly better performance than TPPMMT_6. However, this improvement was not shown in UL 94 test since the burning behaviour hardly changed in any of the materials. All of the materials were classified as only HB.

Table 3.3.4. *Flammability (result of LOI value and UL 94 test) and ignitability (time to ignition obtained in cone calorimeter test) of all the investigated materials*

Samples	LOI / % ±1	UL94 / mm min^{-1} ±1	time to ignition in cone calorimeter		
			35 kW m^{-2}	50 kW m^{-2}	70 kW m^{-2}
EP	21	HB / 21	92 ±5	50 ±2	26±3
Tripp_1	23	HB / 23	103 ±10	51 ±1	24 ±1
TPPMMT_5	25	HB / 18	110 ±5	50 ±1	27 ±2
TPPMMT_6	26	HB / 19	107 ±2	48 ±3	25 ±2
TPPMMT_5+1	28	HB / 19	107 ±5	45 ±5	25 ±2

With various irradiations applied, the time to ignition was about 92 - 110 s at an irradiation of 35 kW m^{-2}, 45 - 51s at an irradiation of 50 kW m^{-2} and 24 - 27s at an irradiation of 70 kW m^{-2}, indicating a strong dependence on irradiation. The time to ignition was slightly improved when additives were used at relatively low irradiation, but not with high irradiation applied. Nevertheless this minor influence of additives on ignitability was negligible in the application of fire behaviour.

3.3.4 Fire behaviour

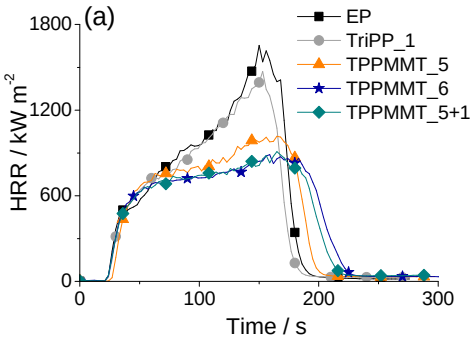

(b)

TPPMMT_5 TPPMMT_6 TPPMMT_5+1

Fig 3.3.4. *(a) HRR curves and (b) the corresponding fire residue morphologies of epoxy resin and different composites obtained in cone calorimeter under an external heat flux of 70 kW* m^{-2}

The characteristic HRRs of the different materials during combustion are shown in Fig 3.3.4 (a). EP and TriPP_1 displayed the similarity that after ignition the HRR increased to sharp peak before flame-out, with no or little residue obtained after complete combustion. A minor influence on the PHRR and the time to flame-out was observed when 1 % TriPP was added. For the other EPs containing various amounts of LS, they showed an plateau-

like HRR up to a smooth PHRR before the end of combustion, also accompanied by prolonged burning time. The HRRs during combustion were reduced in the EPs containing LS, which was attributed mainly to the formation of residue as a protective layer (shown in Fig 3.3.4 (b)). However, a minor difference was observed between the three different TPPMMTs applied. A similar effect on reducing the HRR corresponded to the similar fire residue morphology and structural integrity.

With various irradiations in cone calorimeter, the PHRR was reduced slightly (Δ = 6 %) through the use of TriPP when compared to EP (shown in Fig 3.3.5 (a)). TriPP performed as a promising, effective flame retardant for EP, but a content of only 1 wt% TriPP was not sufficient to improve flame retardancy. The EPs containing TPPMMT showed greater reductions in PHRR (Δ = 20 - 33 % for TPPMMT_5, Δ = 29 - 40 % for both TPPMMT_6 and TPPMMT_5+1). As shown in the literature [49], the flame retardancy effect of EPs containing LS increases with increasing irradiations. A clear superposition effect on the reduction of PHRR occurred for the materials when both additives TPPMMT and TriPP were used. However, the two materials prepared using different methods (TPPMMT_6 vs. TPPMMT_5+1) exhibited hardly any difference in their flame retardancy effects.

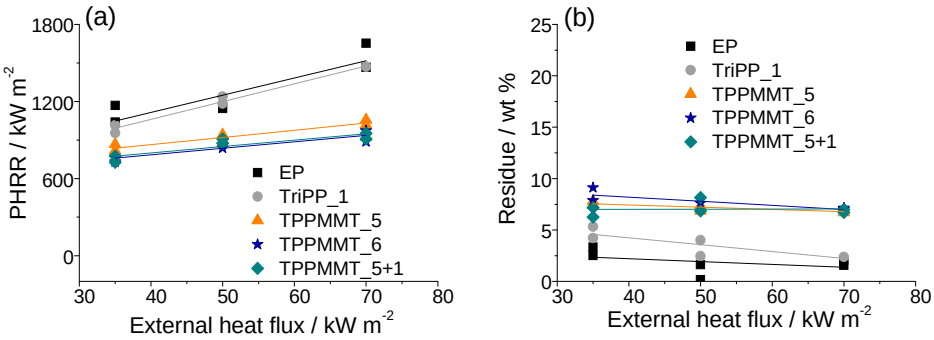

Fig 3.3.5. *(a) PHRRs and (b) amount of fire residues of epoxy resin and different epoxy composites obtained in cone calorimeter with various external heat fluxes of 35, 50 and 70 kW m^{-2}*

Fire properties evaluated from cone calorimeter measurements are given in Table 3.3.5. An almost complete combustion of EP generated a little residue under various irradiations. All of the residues were increased through the use of different additives (shown in Fig 3.3.5 (b)). The TriPP_1 produced slightly more residue than expected under relatively low irradiation. This result was in good agreement with the pyrolysis residue in TG in inert atmosphere. The additional residue (Δ = 5 - 6 wt%) of the EPs containing TPPMMT was

related to the presence of inorganic additive. Further, a minor influence on the fire properties including THE, the effective heat of combustion, CO and smoke yields, was observed due to the presence of different additives. These results indicate that no significant flame inhibition occurred in the gas phase.

Table 3.3.5. *Cone calorimeter results for all the investigated materials with various external heat fluxes of 35, 50 and 70 kW m^{-2}. (* one measurement was done)*

	PHRR kW m^{-2}	t-PHRR s	Residue % ±1	THE MJ m^{-2}	THE / ML MJ m^{-2}g^{-1}	COY g g^{-1}	TSR / ML g^{-1}
irradiation of 35 kW m^{-2}							
EP	1053 ±13	268 ±7	2	148 ±3	2.42	0.055	75
TriPP_1	985 ±30	266 ±5	5	134 ±4	2.21	0.069	75
TPPMMT_5	842 ±25	281 ±11	8	131 ±1	2.17	0.073	81
TPPMMT_6	750 ±19	305 ±2	8	126 ±5	2.10	0.072	79
TPPMMT_5+1	751 ±24	299 ±5	7	128 ±3	2.11	0.075	79
irradiation of 50 kW m^{-2}							
EP	1150 ±5	197 ±5	2	136 ±1	2.19	0.056	72
TriPP_1	1211 ±28	195 ±1	3	134 ±3	2.17	0.068	73
TPPMMT_5	909 ±33	200 ±20	7	129 ±2	2.14	0.063	76
TPPMMT_6	852 ±14	228 ±3	8	124 ±3	2.06	0.063	78
TPPMMT_5+1	892 ±18	201 ±9	8	125 ±2	2.10	0.068	78
irradiation of 70 kW m^{-2}							
EP	1559 ±94	153 ±3	2	144 ±8	2.31	0.062	72
TriPP_1*	1471	153	2	136	2.21	0.069	72
TPPMMT_5	1037 ±20	158 ±8	7	131 ±2	2.18	0.063	80
TPPMMT_6	930 ±42	167 ±8	7	131 ±3	2.16	0.067	79
TPPMMT_5+1	931 ±22	170 ±5	7	131 ±3	2.16	0.068	82

3.3.5 Conclusions

TPPMMT was preloaded or mixed directly with TriPP in the EP composites, and compared to EP with or without TriPP. A mixture of intercalated and exfoliated morphology was exhibited in all of the EPs containing TPPMMT. However, the dispersion of LS was not affected by the use of TriPP. The thermal and thermal oxidative stability of EPs were insignificantly changed by the use of different additives according to EP. The pyrolysis residue obtained in the inert condition was enhanced slightly by a small amount of single-used TriPP. For the EPs with the different layered silicates, the additional residue was attributed mainly to the presence of inorganic additives.

The LOI value was increased through the use of different additives. A clear superposition effect on flammability was exhibited when both TPPMMT and TriPP were added. The composite produced by the simple mixture of the two additives (TPPMMT_5+1) showed slightly better performance than the one with the preloaded organic clay (TPPMMT_6). However no improvement was found in UL 94 since all the materials were classified only as HB. A minor improvement in ignitability through the use of different additives was exhibited when low irradiations were applied.

The use of TriPP showed a promising effect on the reduction in PHRR. However the flame retardancy was not sufficient when only 1 wt% was used. Significant reduction in PHRR was observed in the different EPs with TPPMMT, attributed to the formation of residue as protective layers. A clear superposition effect on the reduction in HRR occurred when both additives were used (TPPMMT + TriPP), but no difference was observed for the different material preparations (preloaded vs. directly mixed). A similar reduction in HRR corresponded to the similar fire residue morphology and structural integrity. Further, due to limited carbonaceous charring, fire properties including the fire load, the effective heat of combustion, the production of CO and smoke was changed insignificantly through the use of different additives, suggesting that no significant flame inhibition occurred in the gas phase.

In conclusion, although no improvement in the dispersion of LS was found to be caused when TriPP was used as a spacer, the combination of TPPMMT and a small amount of TriPP shows a promising effect on flammability and flame retardancy. The flame retardancy effect corresponds well to the fire residue morphology and structural integrity.

Chapter 3.4 Investigations of EP_LS with low-melting glasses

3.4.1 Combined with inorganic Ceepree and sulphate glasses

3.4.1.1 Materials and morphology of the additive dispersion

As discussed in section 2.1.4, combining LS with low-melting glasses was used to enhance the fire residue integrity thus for flame retardancy. In this section two kinds of inorganic low-melting glasses, silicate glass available under the Ceepree trademark (CP) and sulphate glass (SG), were applied to EP and EP/TPPMMT, respectively. Partial results of this chapter have been prepared for publication [112]. The compositions of the two systematic materials are listed in Table 3.4.1.1. The preparation methods for all of the investigated materials are described in Appendix: Experimental (materials).

The morphology of EP_LS5 (EP_TPPMMT5) was discussed in Chapter 3.2. It showed neither dispersion nor exfoliation in a perfect manner. The overall distribution of LS was characterized by a blend demixed on the micrometer scale, with one phase being a nanocomposite characterized by intercalated and exfoliated structures. With micrometer-sized glass particles, the EPs containing glass were defined as common micro-composites.

Table 3.4.1.1. *Abbreviations and compositions of the investigated materials*

Abbreviations	Composition of materials
EP	GY250 / MHHPA / 1-Methylimidazole
EP_LS5	EP with 5 wt% tetraphenylphosphonium modified montmorillite
EP_CP10	EP with 10 wt% Ceepree glass
EP_CP15	EP with 15 wt% Ceepree glass
EP_LS5+CP10	EP with combination of 5 wt% TPPMMT and 10 wt% Ceepree
EP_SG10	EP with 10 wt% sulphate glass
EP_SG15	EP with 15 wt% sulphate glass
EP_LS5+SG10	EP with a combination of 5 wt% TPPMMT and 10 wt% sulphate

3.4.1.2 Pyrolysis behaviour

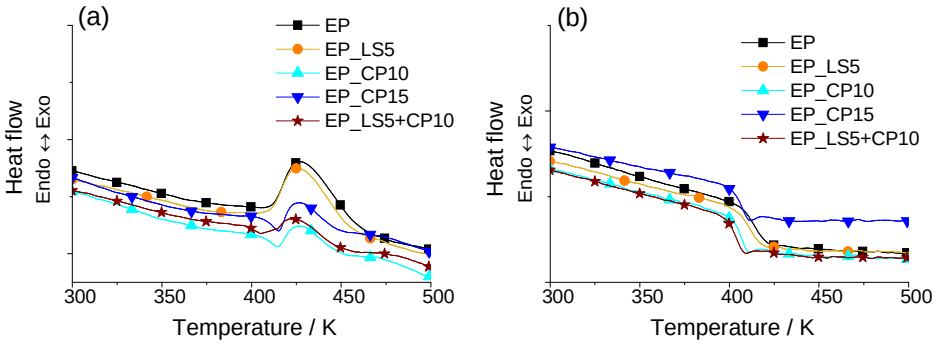

Fig 3.4.1.1 *DSC curves of EP and the different EP composites with layered silicate and Ceepree glass in N_2 with a heating rate of 10 K min^{-1}; (a) first heating and (b) second heating*

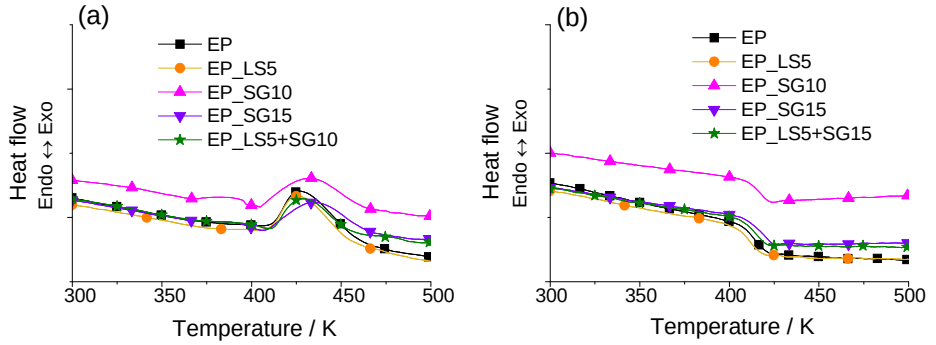

Fig 3.4.1.2 *DSC curves of EP and the different EP composites with layered silicate and sulphate glass in N_2 with a heating rate of 10 K min^{-1}; (a) first heating and (b) second heating*

In general, the formation of polymeric networks can be affected by the use of additives or by the thermal history of the material [52]. DSC curves of all the investigated materials are shown in Fig 3.4.1.1 (for the CP system) and Fig 3.4.1.2 (for the SG system). The first heating showed a post-cure reaction for all the materials in the temperature range of 400 - 470 K with a peak at 426 K, which is typical behaviour of EP cured at 393 K, indicating a slight increase in the degree of curing. The exothermic reaction enthalpy of EP was about 21 J/g and the glass transition temperature (T_g) was about 415 K (Table 3.4.1.2). The reaction peak and T_g were hardly influenced by using TPPMMT alone.

EPs containing CP exhibited endothermic and exothermic reactions during post-curing, resulting in reduced peak exothermic reaction enthalpies to 4 – 11 J/g. The T_g was decreased slightly, by about 10 K. This result may also be influenced by other phenomena

such as an increased free volume. The exothermic reaction peak and T_g were hardly influenced by the use of SG. Overall, only minor effects on the degree of curing and the glass transition temperature of EP occurred through the use of various inorganic additives, which is marginal with respect to decomposition and fire behaviour.

Pyrolysis behaviour of single additives and their binary mixtures was characterized in order to identify any potential chemical interaction between the components (Fig 3.4.1.3 for CP and Fig 3.4.1.4 for SG). As explained in chapter 3.2, due to the release of physically absorbed substances and organic moieties from the surfactant, the decomposition of TPPMMT occurred in sequential steps with two peak mass loss rate at 650 and 850 K, respectively. In Fig 3.4.1.3, CP glass showed a relatively high thermal stability, with very little mass loss up to the temperature of 1000 K (Δ = 8 wt% considered as moisture and weakly bonded substances). For the binary mixture of CP and TPPMMT, no dramatic change was observed during the main decomposition of TPPMMT, except that the peak mass loss rate of dehydroxylation of aluminosilicate was somewhat reduced at higher temperatures. These results implied that chemical reaction between the components of CP and TPPMMT played a minor role.

Corresponding to the literature [113-114], SG glass (consists mainly of Na_2SO_4, K_2SO_4 and $CaSO_4$) decomposed significantly at temperature above 1000 K, resulted from thermal decomposition reactions such as:

$$Na_2SO_4 \rightarrow Na_2O + SO_3 \qquad (1)$$

$$2SO_3 \rightarrow 2SO_2 + O_2 \qquad (2)$$

In Fig 3.4.1.4 *(b)*, during the decomposition of the mixture of SG and TPPMMT, a significant mass loss with several peaks occurred at 650, 870 and 970 K, respectively. The mixture of SG and carbon (in a ratio of 1:4) showed a slight mass loss between 900 -1100 K and dramatically decomposed at temperatures above 1100 K. These phenomena were related mainly to the respective decomposition of TPPMMT and SG, as well as some possible chemical interactions between the various substances, such as Na_2SO_4 from SG, SiO_2 from LS and carbon from the organic moieties under certain conditions (temperature, the atmosphere and the sulphate to carbon molar ration) suggested as [114]:

$$Na_2SO_4 + 2C \rightarrow Na_2S + 2CO_2 \quad (3)$$

$$Na_2SO_4 + 4C \rightarrow Na_2S + 4CO \quad (4)$$

$$Na_2SO_4 + Na_2S + 2SiO_2 \rightarrow 2Na_2SiO_3 + SO_2 + S \quad (5)$$

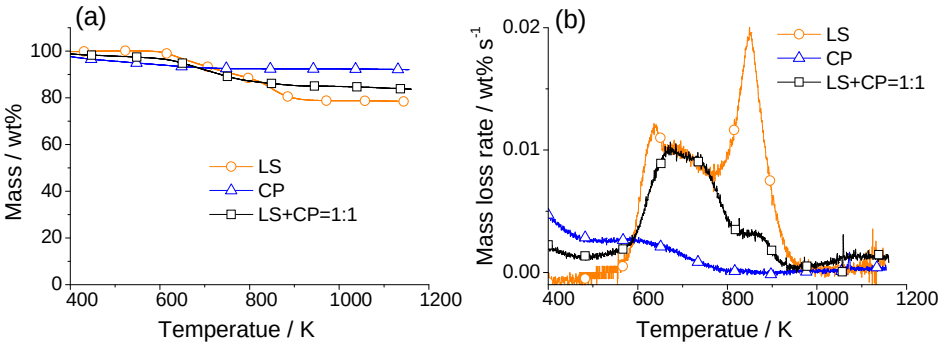

Fig 3.4.1.3. *Pyrolysis of the additives TPPMMT, Ceepree glass and their binary mixture in a ratio of 1:1 in N_2 at a heating rate of 10 K min^{-1}; (a) TG and (b) DTG*

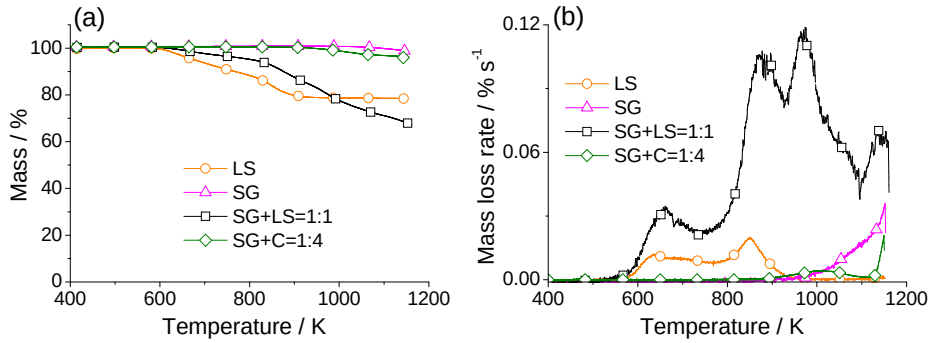

Fig 3.4.1.4. *Pyrolysis of the additives TPPMMT, sulphate glass and their binary mixture in N_2 at a heating rate of 10 K min^{-1}; (a) TG and (b) DTG*

For the EPs containing CP, no significant influence on thermal stability was observed to result from the use of the different additives in comparison with EP, shown in Fig 3.4.1.5 and Table 3.4.1.2. All of the materials showed one main decomposition step in the temperature range of 500 - 800 K with a peak mass loss rate at 685 K, resulting in a main mass loss of 70 - 82 wt% for the composites and 88 wt% for EP. The residues obtained at 1000 K were increased over EP when various inorganic additives were used. The deviation of mass loss during the decomposition step (Δ = 8 - 16 wt%) and the additional residues (Δ = 6 - 12 wt% at 1150 K) corresponded to the amount of inorganic additives.

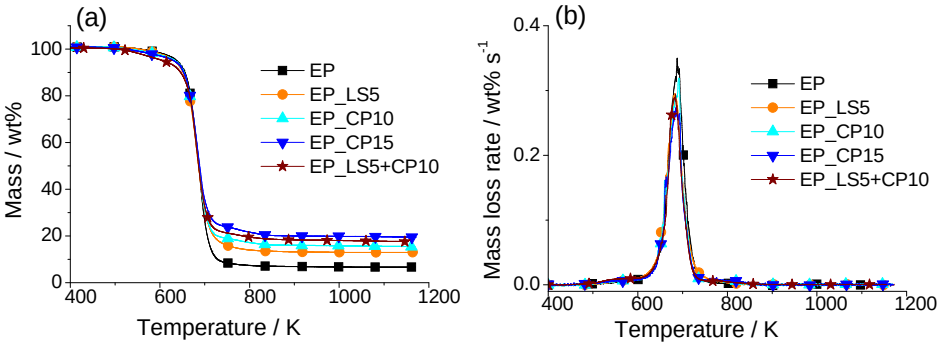

Fig 3.4.1.5. *Pyrolysis of EP and EP with the different additives in N_2 at a heating rate of 10 K min^{-1}; (a) TG and (b) DTG*

For the EPs containing SG, compared to EP and EP_LS5, the thermal stability of the composite was predominately affected by the use of SG (Fig 3.4.1.6). Not only was the peak mass loss temperature shifted to a temperature 20 K lower, a second minor decomposition step took place at a high temperature approaching 1050 K, while the residues of EP and EP_LS5 remained stable. The residue of the composite was increased slightly when the different additives were used. The additional residue (Δ = 4 - 11 wt%) was attributed mainly to the remaining inorganic substances. However more materials were consumed in the EPs containing SG than would be expected according to the SG content. These results were attributed to the chemical interactions proposed, as in reactions (1) - (5).

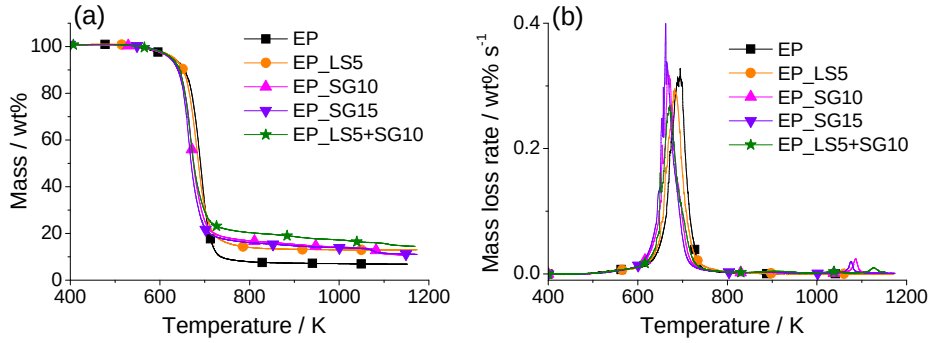

Fig 3.4.1.6. *Pyrolysis of EP and EP with the different additives in N_2 at a heating rate of 10 K min^{-1}; (a) TG and (b) DTG*

Table 3.4.1.2. *DSC and TG data of the materials in N_2 with a heating rate of 10 K min^{-1}*

Materials in N_2	DSC			TG	
	T_g / K ±2	$T_{5\ wt\%}$ / K ±2	T_{max} / K ±2	Mass loss up to 720 K / wt% ±1	Residue at 1150 K / wt% ±2
EP	415	637	685	88	7
EP_LS5	415	637	685	80	13
EP_CP10	405	637	689	79	15
EP_CP15	405	639	689	72	19
EP_LS5+CP10	405	639	685	76	18
EP_SG10	415	622	667	80	11
EP_SG15	415	623	664	80	11
EP_LS5+SG10	415	626	670	75	15

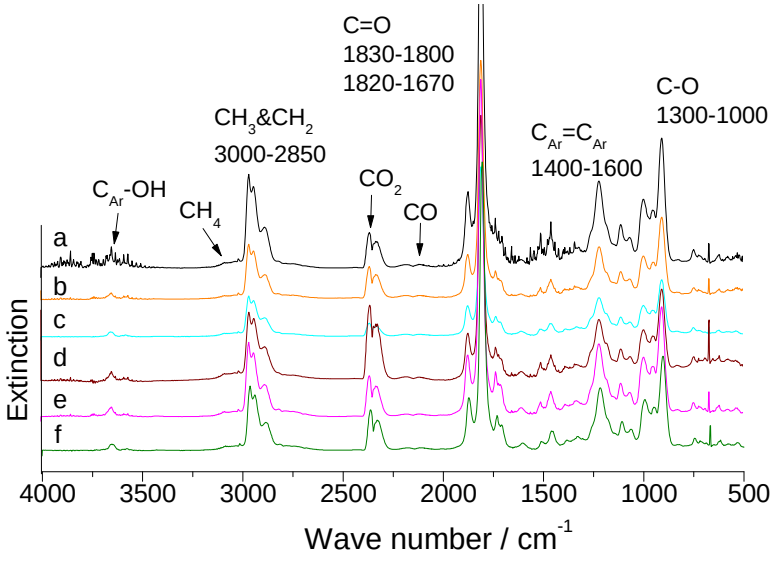

Fig 3.4.1.7. *FTIR spectra of the investigated materials at the maximum mass loss rate (at 38 min / 680 K) with the characteristic bands used for products identification. (a) EP, (b) EP_LS5, (c) EP_CP10, (d) EP_LS5+CP10, (e) EP_SG10, (f) EP_LS5+SG10*

Decomposition products in the gas phase during different decomposition steps were identified for all of the investigated materials. Fig 3.4.1.7 shows the representative spectra with several products identified during the peak mass loss step. The main gaseous products were indentified as CO_2 (2354 cm^{-1}), CO (2176 cm^{-1}), H_2O (3853 cm^{-1}), methane (3015 cm^{-1}) and some other organic substances containing carboxylic acid (1729 cm^{-1}), anhydride (1806 cm^{-1}), phenolic derivatives (3647 cm^{-1}) and ester compounds (1216 cm^{-1}) as previously reported [115-116]. However, when the spectra corresponding to the same decomposition steps were compared with EP, no additional decomposition products were detected in the gas phase in sufficient quantity for any of the composites, neither in the CP system nor in the SG system. Therefore the chemical interactions between the components played a minor role, since there was no significant change in the gaseous decomposition products of EP.

According to EP, the product release rate of several gaseous products as a function of decomposition time was influenced slightly when any of the different additives was used. For EPs containing CP-containing EPs (Fig 3.4.1.8), because LS and CP function as inert fillers, a minor change in the release rates of gaseous products was attributed mainly to the amount of additive used. For EPs containing SG (Fig 3.4.1.9), due to some chemical interactions occurring in the EPs containing SG, the peak time / temperature for the release of the main decomposition products in the gas phase were shifted slightly along with the release rates of these products. Additionally, remarkable CO_2 and CO production was observed at high temperatures due to the decomposition of SG. The pyrolysis residue appeared to be the same light-yellowish colour as the fire residue and soluble in water. These results further implied the chemical interactions between the existence of Na_2SO_4, SiO_2 and carbon as discussed above.

The thermal oxidative stability of the investigated materials in air is shown in Fig 3.4.1.10 (for the CP system) and Fig 3.4.1.11 (for the SG system). The data are given in Table 3.4.1.3. All of the materials exhibited two main mass loss steps under aerobic conditions, which is typical thermo-oxidative decomposition behaviour by EP [111]. For all of the investigated materials under either aerobic or anaerobic conditions, the first main mass loss step exhibited a similar decomposition temperature as a consequence of heating, with the first peak mass loss rate occurring at the same temperature of 688 K for the CP system, and at 670 K when SG was used. Nevertheless the mass loss was 67 - 74 wt% for the composites and 78 wt% for EP under aerobic conditions, which was slightly less than the mass loss reported under anaerobic conditions due to the influence of the oxidizing process.

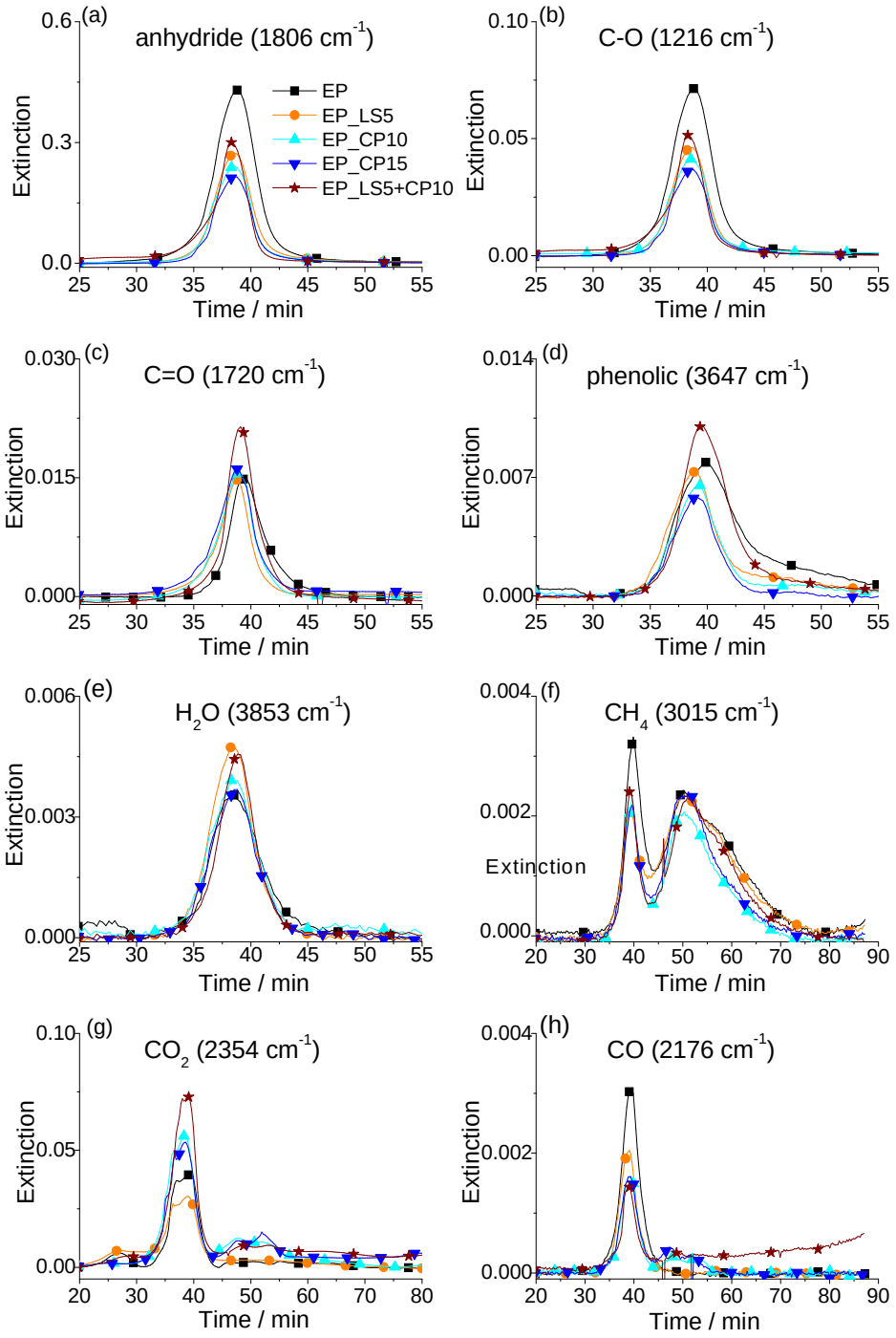

Fig 3.4.1.8. *Gaseous product release rates for EP and EP composites with LS and CP*

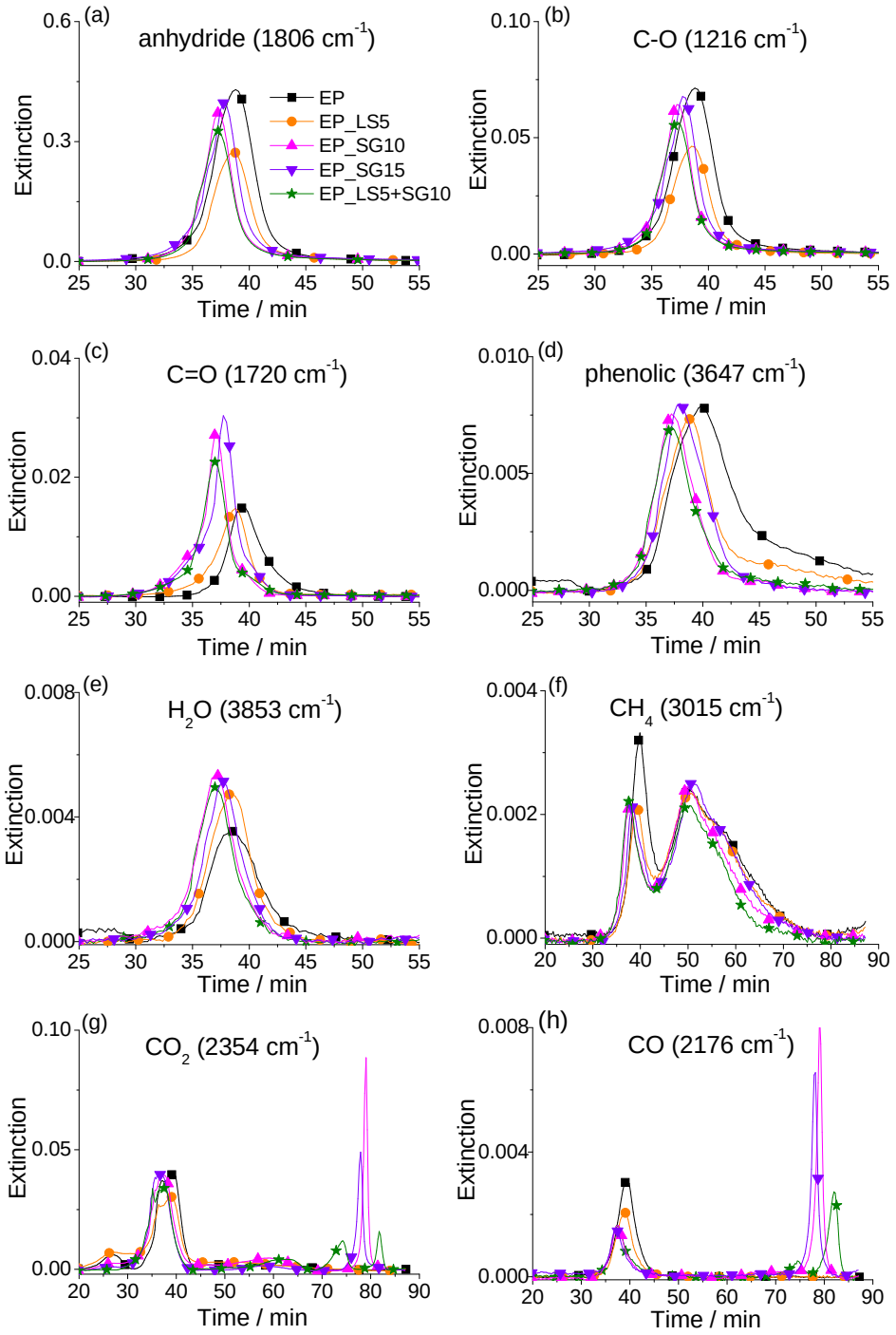

Fig 3.4.1.9. *Gaseous product release rates for EP and EP composites with LS and SG*

Surprisingly, at high temperatures in the range of 750 - 950 K, the oxidation of the transitory charring network was facilitated by using either CP or SG. The second mass loss step occurred earlier than for EP and EP_LS5 (at about 90 K when CP was used and 70 K when SG was used). In particular, the stability of the charring network deteriorated in the presence of the inorganic glasses. The oxidative decomposition led to greater material consumption than under anaerobic conditions. The additional residue of the composites after complete oxidation (Δ = 10 - 11 wt% for the use of CP and Δ = 4 - 8 wt% for the use of SG) was attributed to the existence of inert substances.

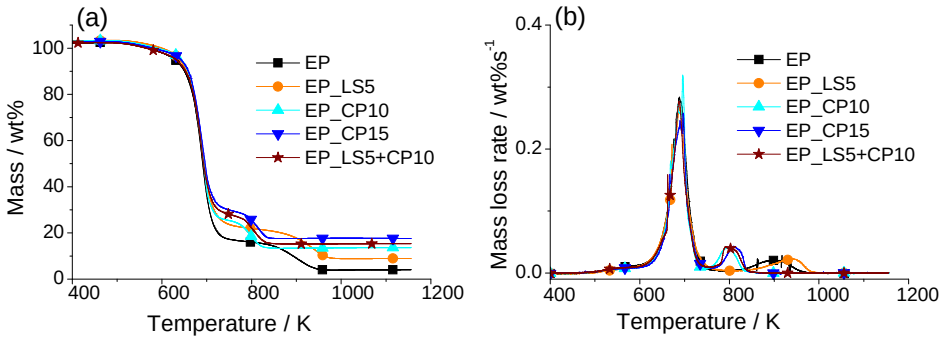

Fig 3.4.1.10. *Pyrolysis of EP and EP composites with LS and Ceepree in air with a heating rate of 10 K min^{-1}; (a) TG and (b) DTG*

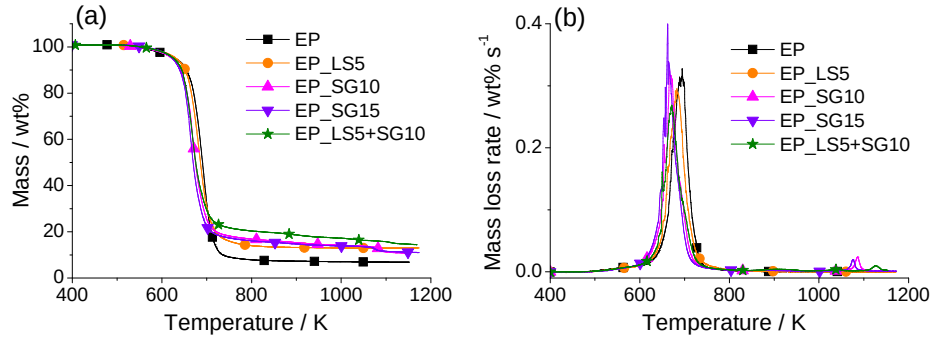

Fig 3.4.1.11. *Pyrolysis of EP and EP composites with LS and sulphate glass in air with a heating rate of 10 K min^{-1}; (a) TG and (b) DTG*

Table 3.4.1.3. *TG data of the investigated materials in air at a heating rate of 10 K min^{-1}*

Materials in air	$T_{5\ wt\%}$ / K ± 2	$T_{max\ 1}$ / K ±2	Mass loss up to 720 K / wt% ± 1	$T_{max\ 2}$ / K ± 5	Residue at 1150 K / wt% ± 2
EP	635	688	78	892	4
EP_LS5	631	688	74	883	9
EP_CP10	630	688	71	800	14
EP_CP15	635	690	67	809	18
EP_LS5+CP10	632	688	71	800	15
EP_SG10	626	670	73	825	8
EP_SG15	622	668	73	829	8
EP_LS5+SG10	625	675	69	832	12

3.4.1.3 Flammability and ignitability

The LOI and UL 94 values are listed in Table 3.4.1.4. Compared to EP (LOI: 20 %), the LOI value was increased by the different additives. This improvement through the use of inorganic additives was caused mainly by formation of residue as a protective layer [51]. There was no distinctive change in the composites through the use of either LS or CP, since the LOI was increased similarly by 4 - 5 %. A better performance was achieved in the composite with SG alone, as the LOI increased to 27 - 29 % depending on the SG content. However, a pronounced antagonistic effect occurred in both of the combined systems, since the LOI was limited to 25 % for EP_LS5+CP10 and 24 % for EP_LS5+SG10.

In UL 94, after a while burning, melt flow and slight dripping behaviour occurred in EP, resulting in liquid decomposition products of the thermoset accumulating to a melt. The behaviour of melt flow and dripping was prevented when the various inorganic additives were incorporated. Particularly, the burning rate of the material in the horizontal orientation was reduced slightly when the inorganic glass was used alone. However, the residue protection effect was not sufficient to achieve self-extinguishing behaviour, since all of the different composites were classified as HB, as EP was.

The time to ignition (t_{ig}) obtained in the cone calorimeter shortened with higher irradiations. The difference between the materials' ignitability was more distinct at lower

irradiations. The t_{ig} of the different materials was around 89 - 110 s for an irradiation of 35 kW m^{-2}, 42 - 53 s for an irradiation of 50 kW m^{-2} and 19 - 25 s for an irradiation of 70 kW m^{-2}. In general, comparing EP to the different composites, a marginal improvement in ignitability occurred when LS was used alone, hardly any change through the use of CP, and a slight deterioration when SG was used at low irradiation. Such a minor effect on ignitability with the different additives is negligible in the application of fire behaviour.

Table 3.4.1.4. *Flammability data of LOI and UL 94 test and ignitability of materials in cone calorimeter*

Samples	LOI / %	UL94 / mm min^{-1}	time to ignition in cone calorimeter		
	±1	±1	35 kW m^{-2}	50 kW m^{-2}	70 kW m^{-2}
EP	20	HB / 21	100 ±6	47 ±1	22 ±3
EP_LS5	25	HB / 18	110 ±8	53 ±3	25 ±1
EP_CP10	25	HB / not burning	101 ±3	44 ±2	20 ±1
EP_CP15	24	HB / 1.8	89 ±3	46 ±4	19 ±1
EP_LS5+CP10	25	HB / 20	101±3	48 ±1	22 ±1
EP_SG10	27	HB / not burning	95 ±4	42 ±1	21 ±1
EP_SG15	29	HB / not burning	92 ±2	43 ±2	21 ±1
EP_LS5+CP10	24	HB / 20	96 ±4	46 ±1	19 ±2

3.4.1.4 Fire behavior

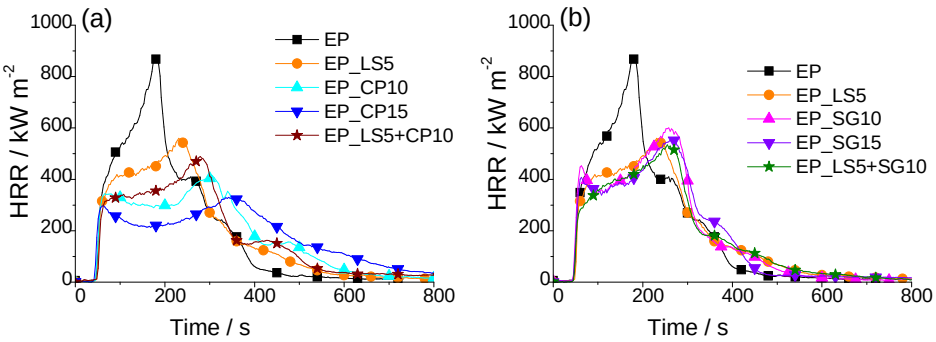

Fig 3.4.1.12. *Heat release rate curves obtained under irradiation of 50 kW m^{-2} in cone calorimeter from the epoxy resin and the different composites; (a) the use of LS and Ceepree glass and (b) the use of LS and sulphate glass*

After ignition all of the EPs with additives showed a smoothly burning flame rather than EP burning with a vigorous sputtering flame and some dripping. Fig 3.4.1.12 illustrates characteristic HRR curves for all of the investigated materials, separated into (a) for the CP system and (b) for the SG system for a clear comparison. After a close initial increase in HRR for all of the materials, EP reached a rather sharp peak, which is typical behaviour for a non-charring material — also indicated by the almost complete consumption of EP. All of the EPs with the different additives displayed more plateau-like curves when approaching the PHRR at the end of burning. Because some material was covered below the sample holder frame edges, and most of it was consumed after the PHRR, this resulted in a subsequent extension in HRR with prolonged burning time and afterglow.

For EPs containing CP, the average HRRs were clearly reduced by the use of CP depending on the fraction of glass loading. The dominant PHRR at the end of burning was significantly decreased by using the different inorganic additives. Under various irradiations the reduction of PHRR was around 32 - 42% for EP_LS5, around 57 - 53% for EP_CP10, and about 63 - 51% for the higher loading of EP_CP15 (Fig 3.4.1.13 (a)). Similar to other EP nanocomposites studied before [49], the efficiency of flame retardancy tended to increase with increasing irradiation when the LS was used. In contrast, a better performance occurred at lower external heat flux when CP was used. In the case of EPs containing SG, the reduction in PHRR was not changed significantly by varying the amounts of the different additives. Under various irradiations the reduction of PHRR was around 32 – 39 % for EP_SG10, around 39 – 42 % for EP_SG15 (Fig 3.4.1.13 (b)).

For the EPs to which a combination of additives was applied, the reduction in the PHRR was 47 - 52 % for EP_LS5+CP10 and 41 - 45 % for EP_LS5+SG10, obtained for all of the irradiations applied. Compared to the EPs with a single additive, flame retardancy was only better than that achieved with EP_LS5. Further, it is clearly less than expected assuming a superposition of the flame retardancy effects through the combination of two additives. A clear antagonism in flame retardancy was thus defined for both combinations of additives used.

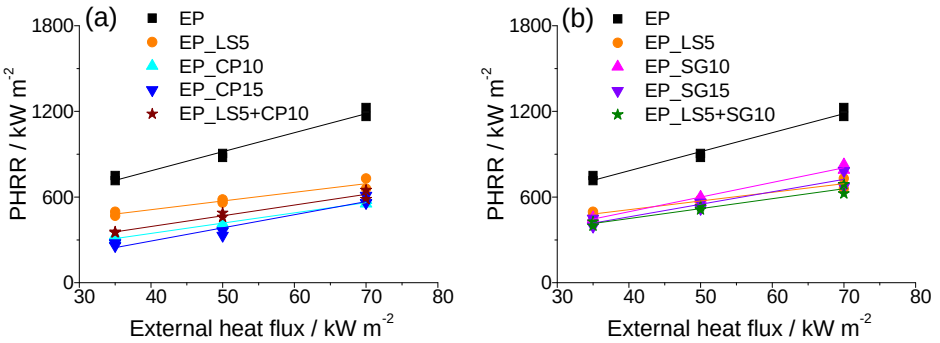

Fig 3.4.1.13. *PHRR values of epoxy resin and different epoxy composites obtained in cone calorimeter with various external heat fluxes of 35, 50 and 70 kW m^{-2}; (a) the use of LS and Ceepree glass, (b) the use of LS and sulphate glass*

Since the different additives made no significant contribution to flame retardancy in the gas phase, these remarkable reductions of PHRRs were mainly attributed to the shielding effects by the residual protection layer. The representative fire residue morphologies of the EPs with the different additives are shown in Fig 3.4.1.14. The observed morphology of fire residue structure explained well the difference between all of the composites and the non-residue forming EP in terms of the relationship between structural integrity and fire properties. In a general view, greater integrity in the residue structure provided a greater reduction in PHRR. As shown in Fig 3.4.1.14 (a)-(d), the residue of EP_CP10, which exhibited the most integral structure and a fully closed surface, provided the highest flame retardancy efficiency. The antagonistic effect on flame retardancy in EP_LS5+CP10 corresponded to some extent with a visually worsened, fragmented structure. In contrast, when EP_LS5+CP10 was compared to EP_LS5, macro-length scale viewing revealed the contradiction that the fire residue of the combination systems on macro-length scale viewing showed larger cracks on the surface than did EP_LS5, but a greater reduction in PHRR. This contradiction raised the demand for addressing fire residue morphology more intensively to clarify the structure integrity-fire property relationship governing flame retardancy.

(a) EP

(b) EP_LS5

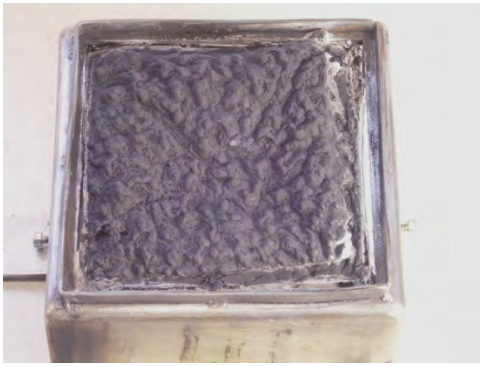

(c) EP_CP10

(d) EP_LS5+CP10

(e) EP_SG10

(f) EP_LS5+SG10

Fig 3.4.1.14. *The corresponding fire residues obtained under irradiation of 50 kW* m^{-2} *in cone calorimeter from the epoxy resin and the different composites*

Micro-scale inspections of the fire residue in cross-section (Fig 3.4.1.15) and top view (Fig 3.4.1.16) were examined by SEM. In principle, several factors such as purity, homogeneity, temperature and heating rate, are critical conditions for suitable glass micro-

structuring [113]. Under severe fire conditions, both the residue of composites with glass alone (EP_CP10 and EP_SG10) showed some imperfect films with pores resulting from glass forming during combustion. EP_CP10, with higher flame retardancy efficiency, was supported by a more solid and interconnected multilayer structure. The pores on the layers were considered to be pathways for the emission of volatile decomposition products. Rather than layered films, the fire residues of all the composites containing LS exhibited a similarity in columnar structure. The columns were attributed to the agglomeration of layered silicate during burning, enhanced by ablation and probably the release of pyrolysis products. With a lack of integral structure, the large gap between the columns formed some defined channels for the release of decomposition products. As to the antagonism in flame retardancy produced in combinations of the additives, the dominant columnar feature in the fire residue structure turned out to be a key factor contributing to this antagonism.

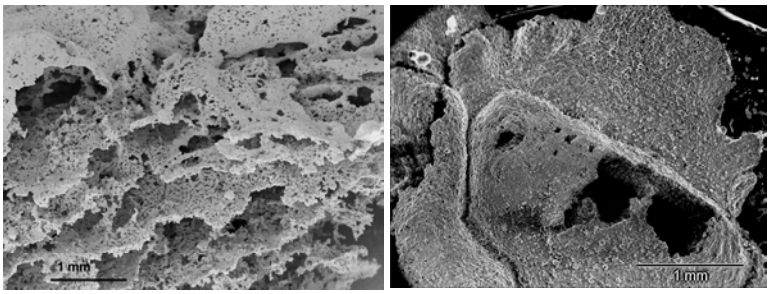

(a) EP_CP10 (b) EP_SG10

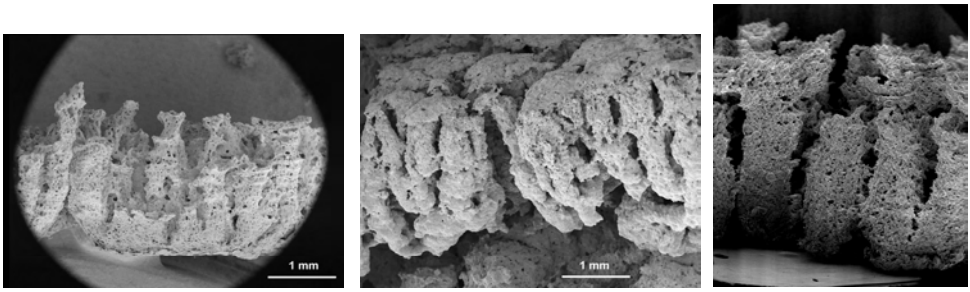

(c) EP_LS5 (d) EP_LS5+CP10 (e) EP_LS5+SG10

Fig 3.4.1.15. *Cross-section view of SEM imagines of fire residues obtained from Cone Calorimeter under an external heat flux of 50 kW m^{-2}*

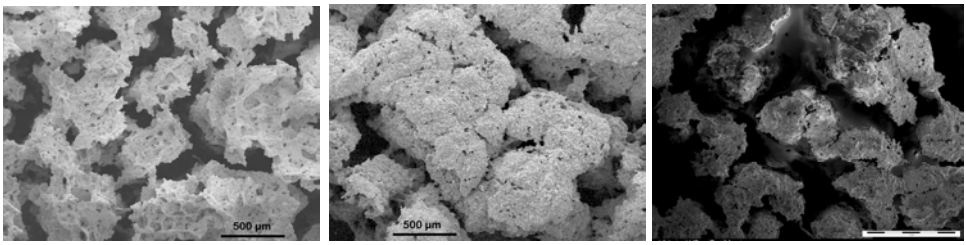

(a) EP_LS5 (b) EP_LS5+CP10 (c) EP_LS5+SG10

Fig 3.4.1.16. *Top-view of SEM imagines of fire residues obtained from cone calorimeter under an external heat flux of 50 kW m^{-2}*

A further comparison of the fire residue from the top views between EP_LS5 and EP_LS5+CP/SG10 showed that both EP_LS5 and EP_LS5+SG10 exhibited a similar feature, which consisted of some detached craggy islands in a loose texture, corresponding to a similar reduction in PHRR. In contrast, EP_LS5+CP10 displayed a cauliflower-like morphology at the top of the residue surface. Despite the columns in the cross-section, the top surface of the columns seemed to be coated and glued together into larger units. A more integral residue structure on the micrometer scale, albeit not upon macroscopic visual observation, explained well why the EP_LS5+CP10 showed a better performance despite the cracks and openings on the residue surface.

Fire properties with various irradiations applied were evaluated in Table 3.4.1.5. As discussed above, both TPPMMT and CP worked as inert fillers; despite a minor influence by chemical interactions in the use of SG, the flame retardancy of all of the EPs with the different additives occurred mainly in the condensed phase. There was barely any relevant additional carbonaceous charring corresponding to the presence of inorganic additives. Since THE (fire load) and THE/ML (the effective heat of combustion) hardly changed with limited replacement by inert fillers, no flame inhibition or fuel dilution occurred in the gas phase.

Generally the smoke and CO release rate showed a strong correlation with the heat or mass release rate as the counterparts of combustion. In this case, the smoke and CO release rate were suppressed at the main stage of burning, followed by a prolonged afterglow. Disregarding the afterglow, the CO and smoke yields during the flaming combustion were not significantly influenced by the use of different additives.

Table 3.4.1.5. *Cone calorimeter results for all the investigated materials with various external heat fluxes of 35, 50 and 70 kW m^{-2} applied*

	PHRR	t-PHRR	Residue	THE	THE / ML	COY	TSR / ML
	kW m^{-2}	s	% ±2	MJ m^{-2}	MJ m^{-2}g^{-1}	g g^{-1}	g^{-1}
			irradiation of 35 kW m^{-2}				
EP	733 ±19	248 ±17	4	141 ±1	2.48	0.046	82
EP_LS5	482 ±14	306 ±21	10	140 ±5	2.43	0.051	85
EP_CP10	315 ±13	120 ±6	15	139 ±1	2.50	0.040	76
EP_CP15	268 ±10	371 ±14	20	132 ±8	2.47	0.039	76
EP_LS5+CP10	353 ±3	350 ±20	19	131 ±2	2.37	0.049	83
EP_SG10	450 ±6	315 ±18	14	140 ±7	2.43	0.042	76
EP_SG15	422 ±28	326 ±8	15	137 ±2	2.41	0.043	77
EP_LS5+SG10	412 ±14	315 ±12	17	132 ±1	2.36	0.050	81
			irradiation of 50 kW m^{-2}				
EP	891 ±14	182 ±2	4	151 ±3	2.46	0.044	82
EP_LS5	571 ±11	228 ±3	7	138 ±3	2.36	0.051	89
EP_CP10	408 ±6	308 ±2	14	136 ±2	2.38	0.042	89
EP_CP15	346 ±16	344 ±2	16	134 ±1	2.30	0.041	83
EP_LS5+CP10	474 ±14	272 ±8	16	130 ±3	2.33	0.049	88
EP_SG10	593 ±8	255 ±3	11	141 ±3	2.39	0.040	79
EP_SG15	541 ±22	279 ±12	13	140 ±1	2.33	0.042	79
EP_LS5+SG10	523 ±11	257 ±2	14	134 ±3	2.30	0.049	85
			irradiation of 70 kW m^{-2}				
EP	1196±32	134 ±2	1	147 ±5	2.40	0.047	85
EP_LS5	694 ±36	195 ±3	6	140 ±1	2.34	0.051	94
EP_CP10	565 ±12	252 ±3	12	137 ±2	2.34	0.044	93
EP_CP15	585 ±26	269 ±8	17	129 ±4	2.33	0.046	92
EP_LS5+CP10	617 ±33	224 ±11	16	130 ±7	2.31	0.049	89
EP_SG10	808 ±19	194 ±11	9	148 ±3	2.43	0.045	87
EP_SG15	728 ±55	216 ±9	11	141 ±1	2.42	0.044	86
EP_LS5+SG10	656 ±32	200 ±8	14	133 ±2	2.31	0.049	90

3.4.1.5 Conclusions

The degree of curing of EP matrices and glass transition temperatures were influenced slightly by the use of CP, but hardly changed when LS or SG was used. The decomposition temperature of the main mass loss was hardly changed by the use of LS or CP under either aerobic or anaerobic atmosphere. Due to SG is lack of thermal stability at high temperatures, the thermal and thermal-oxidative stability of EPs containing SG were decreased slightly compared to EP and EP_LS5. The thermal oxidative stability of char at high temperatures was decreased slightly when both inorganic low-melting glasses were used. The different additives played a minor role on the decomposition of EP since no additional gaseous decomposition products were found.

The LOI value was increased through the use of different additives, more remarkably by the use of SG. The improvement in UL 94 was not sufficient as all the materials were classified as HB. A marginal improvement on ignitability was achieved through the use of TPPMMT alone, but not observed for materials with CP or SG. A clear antagonistic effect on flammability and ignitability occurred when additives were used in combination.

The PHRR was reduced by the use of different additives, attributed to the shielding effect by the residual protective layer in the condensed phase. The reduction in PHRR correlated to the fire residue integrity, as a more integral structure on the different length scales provided higher flame retardancy efficiency. Upon the different observations from the macro to the micro-scale, a dominant columnar feature was discovered, caused by the accumulation of layered silicates, and resulting in antagonistic effects on the flame retardancy of EPs using a combination of additives. Further, no significant flame inhibition occurred in the gas phase, as THE, the effective heat of combustion, CO and smoke productions were hardly changed by the use of various additives.

In conclusion, overall the use of the combination LS+CP/SG does not improve the flame retardancy of EP since the fire residue integrity is not enhanced on macro-scale length. However the improved residue surface integrity on micro-scale length by the combination additives resulted in more efficient flame retardancy than the use of LS alone. It has been demonstrated that a more integral residue structure with a more closed surface on different length scales contributes to higher flame retardancy efficiency.

3.4.2 Combined with phenylsiloxane $(PhSiO_{1.5})_n$ glass

3.4.2.1 Materials and morphology of the additive dispersion

All of the composites in this chapter were based on epoxy resin of bisphenol-A, which was cured with 4-methyl hexahydrophthalic anhydride and catalyzed by 2,4,6-tris (dimethylaminomethyl) phenoal. The synthesis of two kinds of additives: (a) low-melting phenylsiloxane glass and (b) organically tetraphenylphosphonium modified layered silicate is introduced in section Appendix: Experimental (Materials). The abbreviation for and composition of all of the investigated materials are listed in Table 3.4.2.1. The results of this part have been prepared for publication [117-118].

Table 3.4.2.1. *Abbreviations and compositions of the investigated materials*

Abbreviations	Composition of materials
EP	GY250 / MHHPA / 5 wt% ancamine K54
EP_G5	EP with 5 wt% phenylsiloxane glass
EP_G10	EP with 10 wt% phenylsiloxane glass
EP_G15	EP with 15 wt% phenylsiloxane glass
EP_LS5	EP with 5 wt% tetraphenylphosphonium modified montmorillite (TPPMMT)
EP_LS5+G5	EP with a combination of 5 wt% phenylsiloxane glass and 5 wt% TPPMMT
EP_LS5+G10	EP with a combination of 10 wt% phenylsiloxane glass and 5 wt% TPPMMT

The morphology of additive dispersion was examined by TEM [118]. Fig 3.4.2.1 shows the representative TEM images of EP_G10 and EP_LS5+G5 with the same magnification. The image of EP_G10 (Fig 3.4.2.1 (a)) shows that the glass droplets with smooth edges were randomly dispersed in the epoxy matrix. The particle size distribution was rather broad, from approximately 10 nm up to 10 μm. Further, smaller particles with a round shape were observed at higher magnifications, indicating that glass particles became soft at 423 K during the post-curing process. The image of EP_LS5+G5 (Fig 3.4.2.1 (b)) shows a random mixture dispersion of large and small glass particles and intercalated and exfoliated LS. As a similar dispersion of layered silicate with a d-spacing of about 1.9 nm in intercalation phase has been reported before (refer to EP_TPPMMT5 in section 3.2), the dispersion of LS was not improved by the additional filler G. Overall the size of glass particles in EP_LS5+G5 was generally smaller than in the EP_G10, suggesting that the LS may hinder the glass particles growth during the curing process.

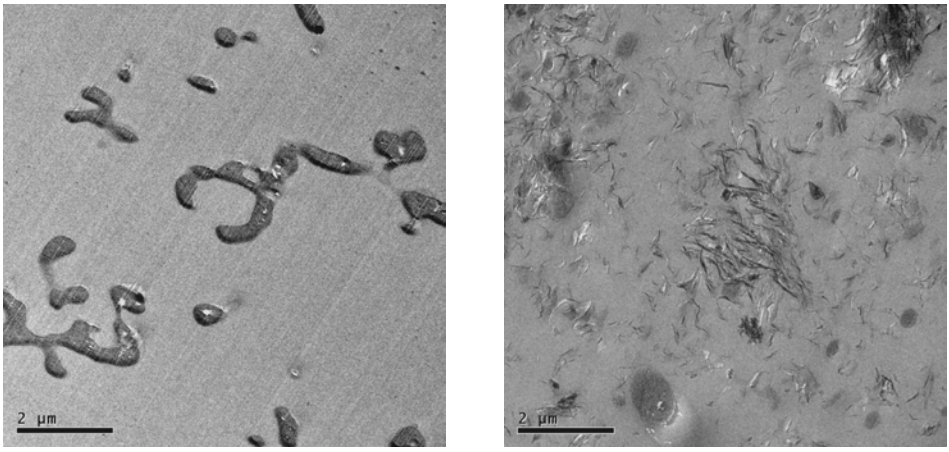

(a) EP_G10 (b) EP_LS5+G5

Fig 3.4.2.1. *Morphology of the additive dispersion in epoxy matrix characterized by TEM [118]*

3.4.2.2 Pyrolysis behaviour

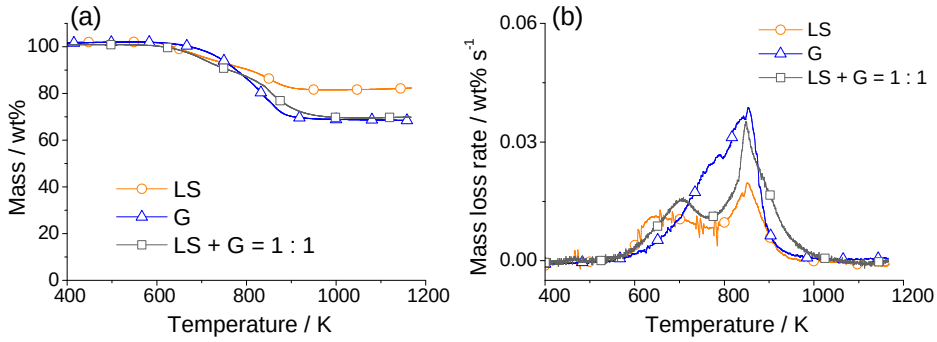

Fig 3.4.2.2. *(a) TG and (b) DTG curves of the different additives of layered silicate, glass and their binary mixture in N_2 at a heating rate 10 K min^{-1}*

Pyrolysis of the single components LS, G and their binary mixture LS+G (in a ratio of 1:1) were examined in TG under N_2. The main mass loss step occurred in the temperature range from 600 - 1000 K for the respective components, caused by the release of organic moieties presented in both LS and G (shown in Fig 3.4.2.2 (a)). The organically modified LS showed two main distinctive decomposition steps with the peak mass loss rate at 650 K and 850 K, respectively. The decomposition of organic-inorganic glass showed one broad step with a peak mass loss rate at about 850 K (shown in Fig 3.4.2.2 (b)). Up to 1100 K the total mass loss was 18 wt% for LS and 32 wt% for G. For the binary mixture LS+G, the DTG curve corresponded to the decomposition of each component. The total

mass loss up to high temperature of 1100 K (Δ = 30 wt%) was slightly more than expected (Δ = 25 wt%) if both additives are regarded as inert filler.

The influence of additives on the curing degree of EP matrix and the glass transition temperature was determined in DSC measurements. During the first heating in the temperature range of 350 - 430 K all of the materials showed a post-cure peak with the maximum at about 393 K. The residual exothermic enthalpy was about 10 - 16 J g^{-1}. This phenomenon corresponded to about 5% of enthalpy for the completed cross-linking of the EP network. The glass transition temperature T_g was hardly changed by the use of different additives, and observed at about 405 K similar to EP (Table 3.4.2.2).

Fig 3.4.2.3 shows the thermal stability of the different materials in N_2, and the data are summarized in Table 3.4.2.2. According to EP, no significant change in decomposition temperature was observed through the use of different additives. The onset decomposition temperature ($T_{5wt\%}$) occurred at 550 K, except that it was slightly lower for the EP_LS5+G5 than for all the other materials (at about 519 K). The main mass loss step occurred between 600 K and 750 K, with a similar peak at temperatures around 675 K. Compared to EP, the maximum mass loss rate was not changed significantly for EP_LS5, but decreased slightly for all of the G-containing composites. Up to 1000 K the residue was increased by the use of different additives in comparison with EP. Except for the fact that the residue of EP_G5 (17 wt%) showed slightly more carbonaceous char than expected (13 wt%), the additional residue in the other composites was related mainly to the presence of inert filler.

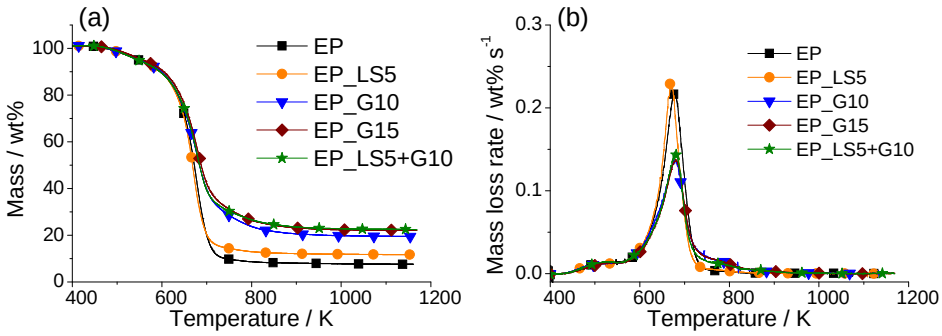

Fig 3.4.2.3. *(a) TG and (b) DTG curves of EP and EP composites with TPPMMT, glass and the combination, respectively, in N_2 at a heating rate of 10 K min^{-1}*

Table 3.4.2.2. *Data of differential scanning calorimeter (DSC) and thermogravimetry (TG) in N_2 of all the investigated materials at a heating rate of 10 K min^{-1}*

	DSC	TG			
	T_g / K ± 1	$T_{5\ wt\%}$ / ± 5	T_{max} / K ± 5	Mass loss rate / wt% s^{-1}	Residue at 1000K / % ± 3
EP	407	546	677	0.22	8
EP_G5	406	554	675	0.15	17
EP_G10	404	550	679	0.14	20
EP_G15	405	550	679	0.14	22
EP_LS5	406	549	670	0.22	12
EP_LS5+G5	402	519	675	0.15	19
EP_LS5+G10	403	546	679	0.14	23

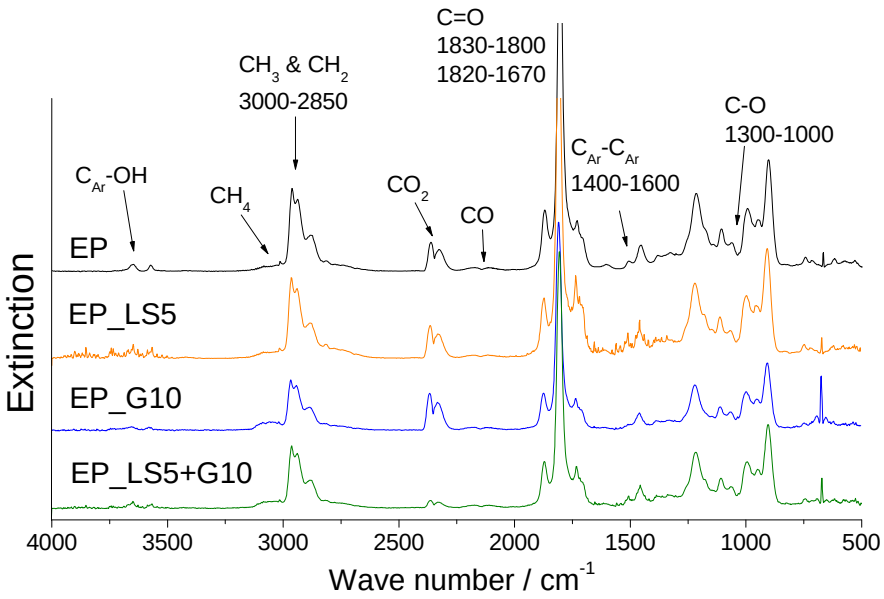

Fig 3.4.2.4. *FTIR spectra of the investigated materials EP and the different EP composites for evolved gaseous products at the peak mass loss rate (at 38 min / 680 K)*

The spectra of the main gaseous products were observed during decomposition of the materials in FTIR. Fig 3.4.2.4 shows the gas-phase spectra, with some products identified at the peak mass loss stage (at 38 min / 680 K) for the composites with the various additives. Corresponding well with the literature [114, 119-120], the major

decomposition products in detectable quantities in the gas phase were identified as H_2O (3852 cm^{-1}), CO_2 (2358 cm^{-1}), CH_4 (3015 cm^{-1}), and also other organic derivatives containing anhydride (1806 cm^{-1}), phenol (3647 cm^{-1}), carbonyl (1729 cm^{-1}), and ester groups (1216 cm^{-1}). Similar to the results reported in the previous section, no additional gaseous decomposition products during the same decomposition step were observed when LS and G were used compared to EP, implying that no critical chemical interaction occurred to interrupt decomposition of the EP matrix.

Further, the product release rate (PRR) of several gaseous products was plotted as a function of decomposition during heating for the materials containing the different additives (in Fig 3.4.2.5). In general, these decomposition products were released in three main stages during pyrolysis between 20 - 88 min. During 20 - 32 min (in the temperature range of 500 - 620 K), CO_2 was released first in all the materials, which was associated with the release of freely absorbed substances at an early stage [115]. In the period 32 - 42 min (between 620 and 720 K), most gaseous products were detected, including CO_2, CO, H_2O, CH_4 and other derivatives containing anhydride, allylic ester, carbonyl and phenolic groups. The anhydride derivatives were released in larger quantities than other products as a consequence of the hardener used, 4-methyl hexahydrophthalic anhydride. For most of the gaseous products observed, the respective peak of PRR was affected slightly by using the different additives at marginal intervals. In the period 42 - 88 min (between 720 and 1150 K), CH_4 and CO_2 were the two main products generated due to a charring process after the main mass loss step. The G-containing composites, in particular, produced more significant CH_4 than EP and LS_5 during charring.

Based on the TG and TG-FTIR results and according to the literature [115, 119-120], the decomposition of EP is sketched in Fig 3.4.2.6. The initial polymer non-chain scission occurs via a dehydration reaction of the secondary alcohol in the cured resin structure, leading to the formation of H_2O and vinylene ethers (a). As the resulting allylic ester C-O bond is the weakest bond, chain scission occurs mainly at the allylic position. At this stage, in anhydride-cured resin, MHHPA is regenerated in large quantities (b). Upon further decomposition, the anhydride structure undergoes decomposition, producing CO, CO_2 and aliphatic substituted rings (c). In addition to the main process of chain scission, other secondary reactions may take place, for example, a radical decomposition of bisphenol A structure yields more products like CH_4 and hydrocarbons (d). At higher pyrolysis temperatures, a further breakdown or rearrangement of the aromatic segments from the bisphenol A structure leads to the formation of phenol and some aromatic derivatives.

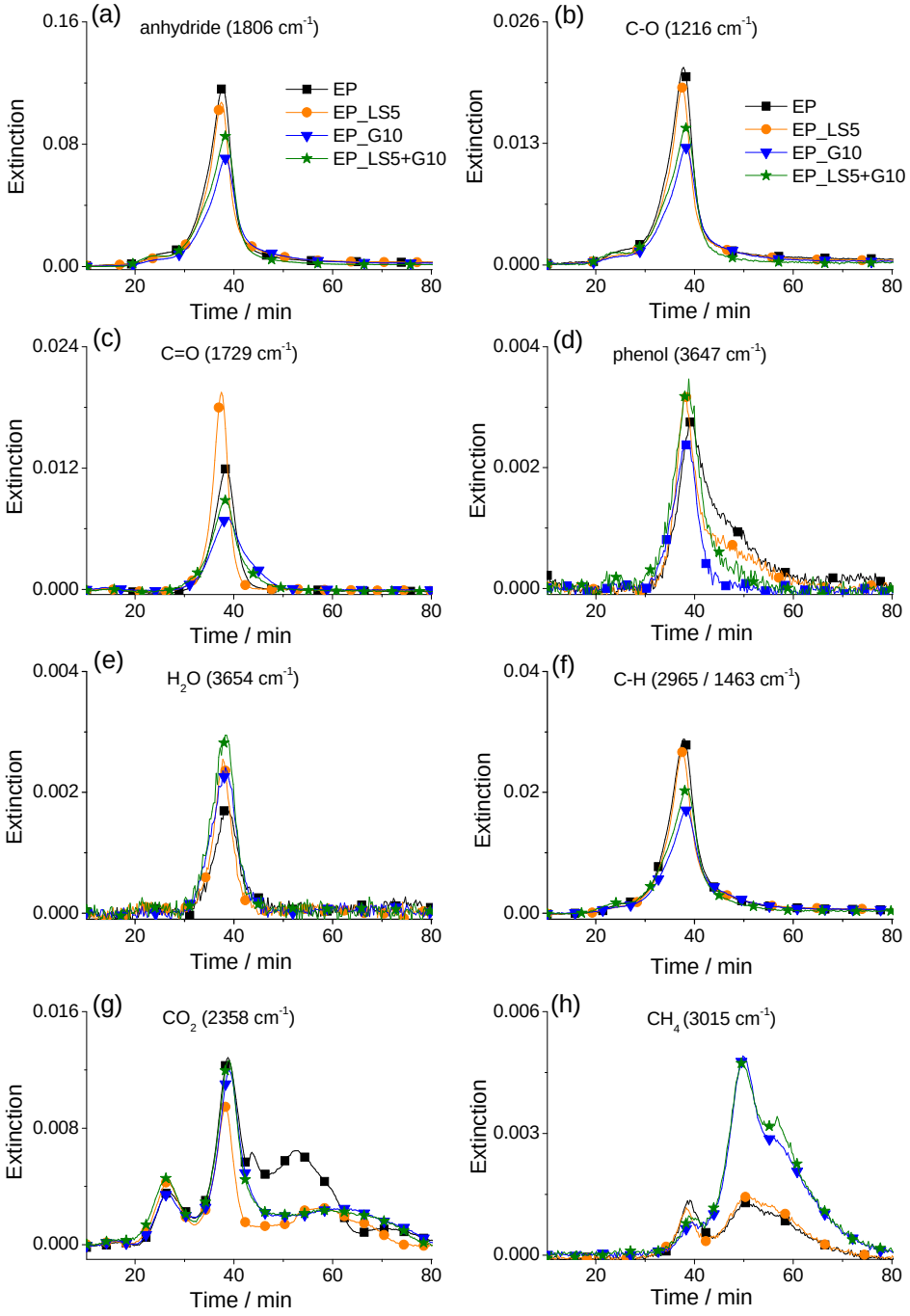

Fig 3.4.2.5. *Gaseous product release rates for EP and the different EP composites with LS, G and LS+G, respectively*

Structure of epoxy resin

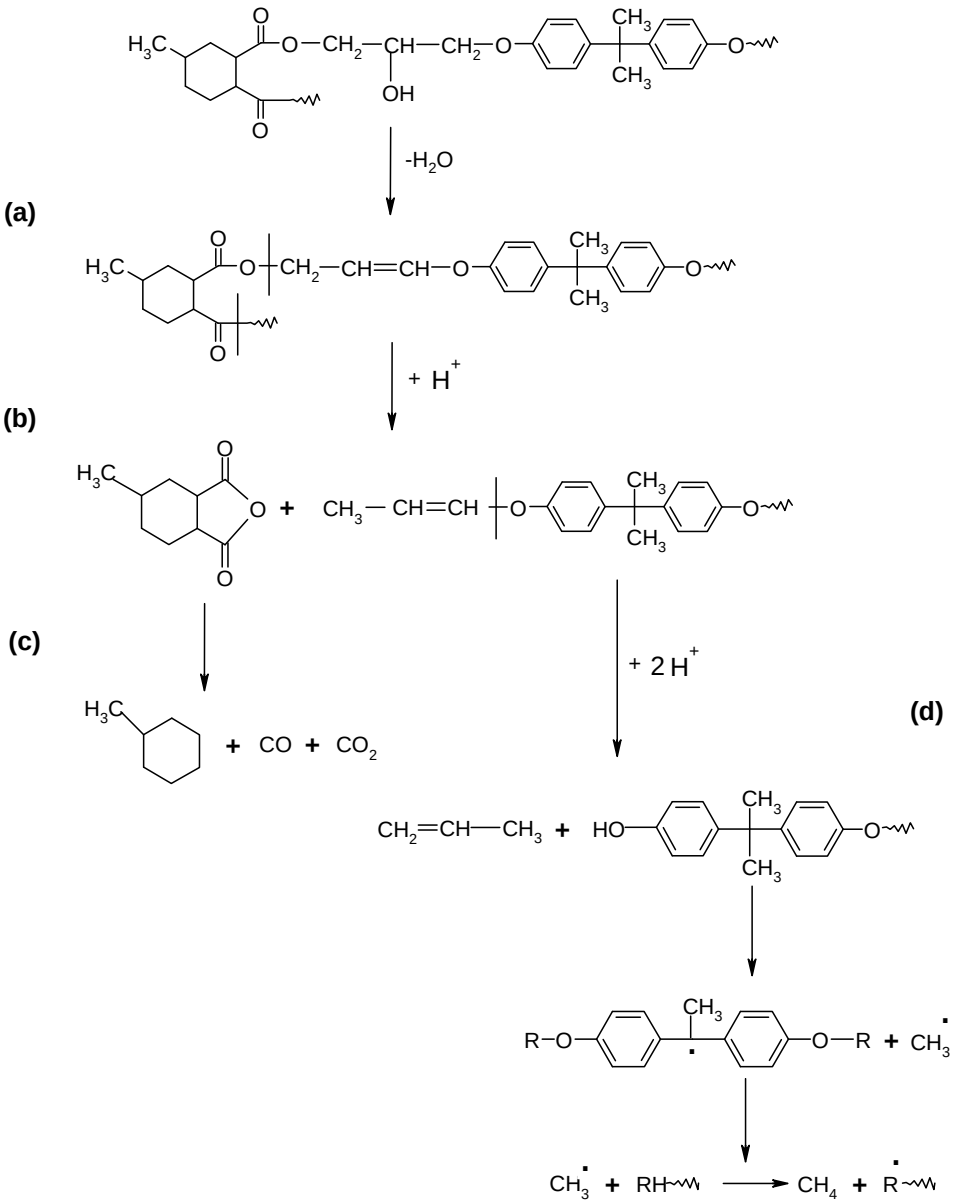

Fig 3.4.2.6. *Proposed main decomposition scheme of EP*

The thermo oxidative stability of the EPs with the different additives were compared to EP (shown in Fig 3.4.2.7 and data given in Table 3.4.2.3). Based on the typical oxidative decomposition of EP with two main mass loss steps, all of the materials showed a similar onset decomposition temperature with 5 wt% mass loss occurring at about 540 K, except that for the EP_LS5+G5 it occurred at a slightly lower temperature (511 K) than the other materials. The first peak mass loss rate occurred at about 635 - 653 K and the second main mass loss occurred at about 830 K. The residue after complete oxidation process at 1000 K increased slightly (Δ = 2 - 6 wt%) due to the presence of inorganic additives.

Overall, according to the insignificant change on the pyrolysis behaviour of EPs in either aerobic or anaerobic atmosphere, the different additives functioned mainly as inert fillers during the decomposition of the EP matrix.

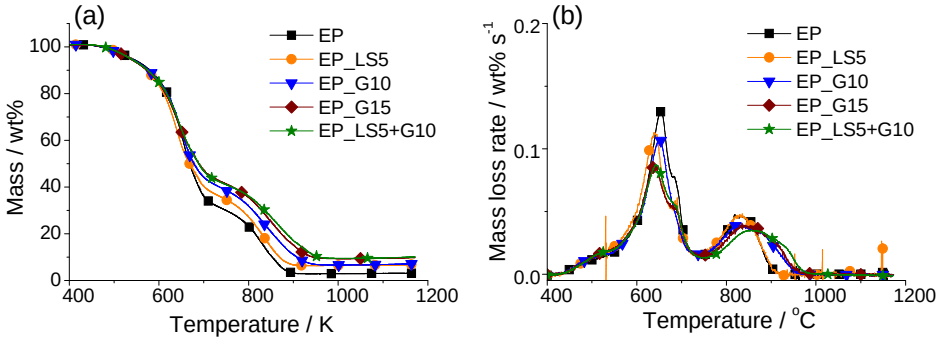

Fig 3.4.2.7. *(a) TG and (b) DTG curves of EP and EP composites with TPPMMT, glass and the combination, respectively, in N_2 at a heating rate of 10 K min^{-1}*

Table 3.4.2.3. *TG data of all the materials in air at a heating rate of 10 K min^{-1}*

	$T_{5\ wt\%}$ / K ± 5	T_{max1} / K ± 5	T_{max2} / K ± 5	Residue at 1000K / % ± 2
EP	540	653	831	3
EP_G5	545	653	825	5
EP_G10	537	650	823	6
EP_G15	543	640	833	8
EP_LS5	537	640	823	7
EP_LS5+G5	511	635	823	9
EP_LS5+G10	543	643	823	9

3.4.2.3 Flammability and ignitability

Flammability results from LOI and UL 94 tests are given in Table 3.4.2.4. Compared to EP, only EP_LS5 showed a slight improvement in flammability, which not only increased the LOI value by 4 %, but also reduced the burning rate from 21.5 mm min^{-1} of EP to 4.7 mm min^{-1} in UL 94 test. No improvement was found by the use of G, since the LOI values of all the G-containing composites were similar to EP, remaining at 21%, and were classified as HB in UL 94 test. Concurrently an antagonism effect on flammability was observed in the use of combination additives (EP_LS+G), attributed to the predominate influence by G.

In cone calorimeter, the higher the irradiation applied, the shorter time to ignition for all of the materials [12]. The t_{ig} was obtained between 86 - 96 s at the applied irradiation of 35 kW m^{-2}, 37 - 50 s at the applied irradiation of 50 kW m^{-2} and 17 - 23 s at the applied irradiation of 70 kW m^{-2}. Compared to the EP, ignitability hardly changed in EP_LS5, but shortened slightly in the G-containing composites with relatively low irradiation applied. This minor effect on ignitability through the use of different additives was negligible with regard to fire applications.

Table 3.4.2.4. *Flammability results of LOI and UL 94 test and ignitability in cone calorimeter (t_{ig} = time to ignition) for all of the materials*

	LOI	UL 94	t_{ig} in cone calorimeter / s		
	/ % ±1	/ mm min^{-1} ±1	35 kW m^{-2}	50 kW m^{-2}	70 kW m^{-2}
EP	22	HB / 21.5	94±4	50±2	17±2
EP_G5	26	HB / 4.7	96±3	45±4	23±1
EP_G10	21	HB / 24.4	87±1	38±2	21±1
EP_G15	21	HB / 22.2	89±3	39±7	19±1
EP_LS5	21	HB / 22.9	87±8	37±5	17±1
EP_LS5+G5	21	HB / 24.2	93±5	43±1	19±1
EP_LS5+G10	21	HB / 22.2	86±4	40±1	20±1

3.4.2.4 Fire behaviour

Fig 3.4.2.8 shows the representative HRR curves for all of the investigated materials in cone calorimeter with an irradiation of 35 kW m^{-2}, separated into (a) and (b) for a clear comparison with regard to the amount of additive applied. After ignition, the initial increase in HRR exhibited a minor difference between the different materials, except that EP_G5 showed the first PHRR at an early stage. Afterwards EP showed a sharp increase in the PHRR before flame-out. In contrast, the increase in HRR until the peak at the end of burning was decelerated in all of the composites with the different additives, caused by residue forming and exerting a shielding effect during combustion. A plateau-like HRR was related to a steady-burning state when a sufficient residue layer was formed. Compared to EP the av-HRR and the PHRR were reduced significantly when various additives were used, accompanied by a prolonged burning time. This effect was more pronounced in the G-containing composites with higher amounts of additive.

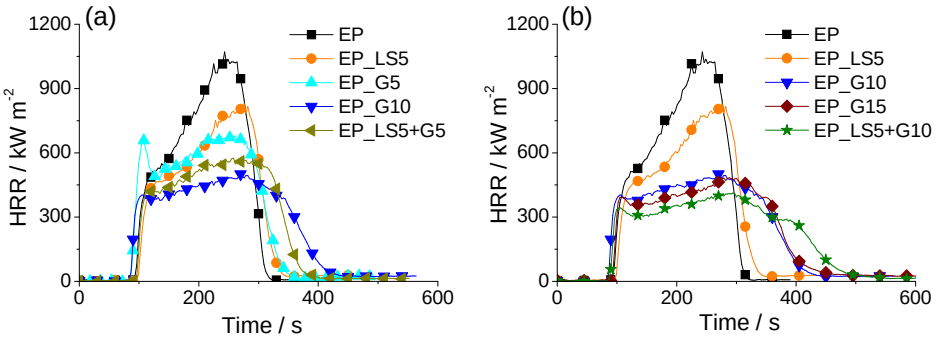

Fig 3.4.2.8. *HRR of the EP and all the EP composites with different filler content in cone calorimeter at irradiation of 35 kW* m^{-2}

The HRR's characteristic corresponded well with the respective fire residue morphology of the various composites (EP_LS, EP_G and EP_LS+G). With the use of only G (Fig 3.4.2.9 (a) - (c)), the fire residue of EP_G displayed some foam-like segments with a porous surface. Higher G loading displayed larger openings and cracks on the residue surface, which may have been caused by the flow of molten glass during combustion. However, irrespective of the visual size of cracks and openings on the surface, PHRR was reduced in the order: G_15 > G_10 > G_5, due to the fact that higher amount of additive produced more densely compacted fire residue. Similar to a previous study [115], the fire residue of EP_LS (Fig 3.4.2.9 (d)) displayed fragmental islands in a loose structure,

contributing to a slight reduction in PHRR. The fire residue of EP_LS+G (Fig 3.4.2.9 (d) - (e)) showed not only relatively high structural integrity, but also an intact surface with a few cracks, contributing to the high reduction in PHRR.

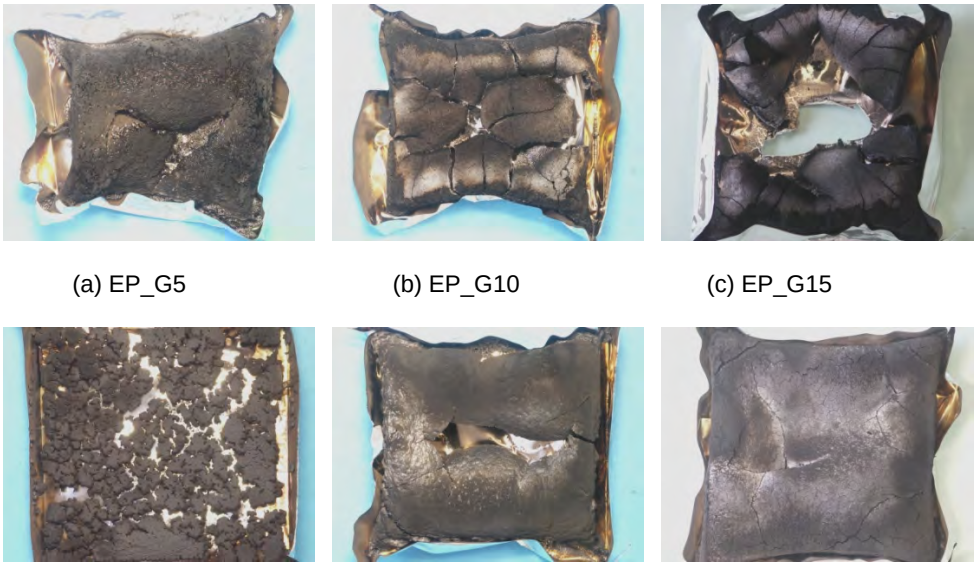

(a) EP_G5 (b) EP_G10 (c) EP_G15

(d) EP_LS5 (e) EP_LS5+G5 (f) EP_LS5+G10

Fig 3.4.2.9. *Morphology of fire residues of the EPs with different additives obtained with an irradiation of 35 kW m^{-2} in cone calorimeter*

Further, under a micro-scale length of view by SEM, the fire residue of EP_G (Fig 3.4.2.10 (a)), displayed a rough and porous surface. While the fire residue of EP_LS+G (Fig 3.4.2.10 (b)) displayed an intact and smooth surface with a few holes, it was further enhanced by a solid and interconnected structure with multilayers underneath (Fig 3.4.2.10 (c)). The integrity of residue from the surface to the inner structure was successfully enhanced through the combination of additives. Overall, more compact and higher-integrity residue structure corresponded to higher efficiency of flame retardancy.

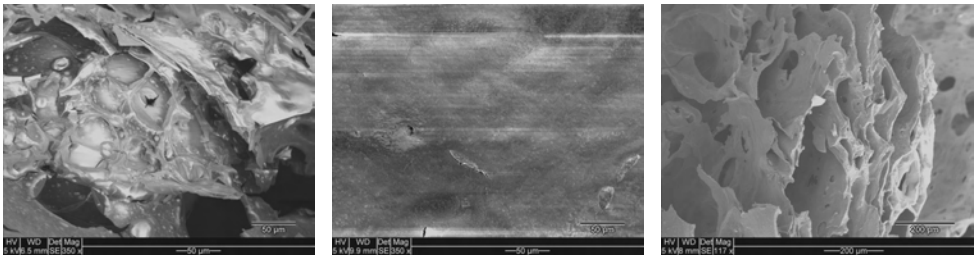

(a) EP_G10 (b) EP_LS5+G5 (c) EP_LS5+G5

Fig 3.4.2.10. *SEM images of fire residues of EPs under micro-scale length view; (a) Top view of EP_G10; (b) top view of EP_LS5+G5 and (c) cross-section of EP_LS5+G*

The PHRRs obtained under various irradiations are illustrated in Fig 3.4.2.11 (a). In general, the application of higher irradiation yielded a higher PHRR for all of the materials. The PHRR was systematically reduced by the use of different additives, with a minor difference influenced by the irradiation. The term ΔPHRR% is defined as the percentage of PHRR reduction yield caused by the total amount of additive. With various irradiations the ΔPHRR% was 10 -17 % for EP_LS, 34 - 52 % for EP_G and 43 - 60 % for EP_LS+G. In many cases, flame-retardant effects as a function of concentration are often represented by a nonlinear functional relationship [121-122].

Fig 3.4.2.11 (b) plots the ΔPHRR% at an irradiation of 35 kW m^{-2} as a function of the percentage of additive for the different composites. For the material EP_G, the ΔPHRR% increased with increasing G content, but leveled off at a percentage of around 10 - 15 %. Comparing the ΔPHRR% for the same percentage of additive but varying irradiations, the performance was compared as EP_G5 > EP_LS5, EP_G10 > EP_LS5+G5 and EP_LS5+G10 ≥ EP_G15.

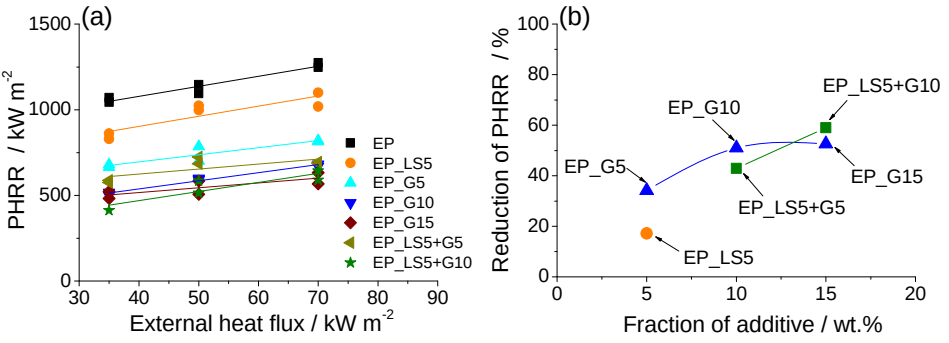

Fig 3.4.2.11. *Reduction of PHRR in the different composites obtained in cone calorimeter with an irradiation of 35 kW m^{-2} plotted against the percentage of additive applied*

Table 3.4.2.4. *Flame retardancy related to the reduction of PHRR in cone calorimeter evaluated at various irradiations of 35, 50 and 70 kW m^{-2}. ($\Delta PHRR_{sp}$% means specific reduction of PHRR per unit additive, SE means synergistic effect index calculated by equations (1),(3)-(5))*

Samples	PHRR / kW m^{-2}	ΔPHRR / %	$\Delta PHRR_{sp}$ / % wt%$^{-1}$	$SE_{abs}^{(1)}$	$SE_{abs}^{(3)}$	$SE_{rel}^{(4)}$	$SE_{rel}^{(5)}$
irradiation of 35 kW m^{-2}							
EP	1021	-	-				
EP_G5	672	34	6.8				
EP_G10	509	50	5				
EP_G15	503	51	3.4				
EP_LS5	845	17	3.4				
EP_LS5+G5	582	43	4.3	0.84	1.02	0.94	1.13
EP_LS5+G10	412	60	4	0.89	1.17	1.02	1.32
irradiation of 50 kW m^{-2}							
EP	1121	-	-				
EP_G5	744	34	6.8				
EP_G10	595	47	4.7				
EP_G15	546	51	3.4				
EP_LS5	1011	10	2				
EP_LS5+G5	705	37	3.7	0.85	1.12	0.92	1.20
EP_LS5+G10	550	51	3.4	0.90	1.16	0.98	1.25
irradiation of 70 kW m^{-2}							
EP	1261	-	-				
EP_G5	817	35	7				
EP_G10	676	46	4.6				
EP_G15	601	52	3.5				
EP_LS5	1059	16	3.2				
EP_LS5+G5	690	45	4.5	0.88	1.15	0.99	1.28
EP_LS5+G10	618	51	3.4	0.82	1.00	0.93	1.13

The reduction of PHRR is also related to the additive content and the amount of polymer matrix. Another term, $\Delta PHRR_{sp}$%, is defined as the specific reduction of PHRR per unit of additive used, to measure the effectiveness of a flame retardant (eff-FR) with regard to its concentration effect [123]. The calculated values are given in Table 3.4.2.4. EP_G5

showed the highest eff-FR among all of the composites. However, for the EP_G materials the eff-FR decreased with increasing G content, as in EP_G5 > EP_G10 > EP_G15. Comparing the materials with a single additive, the eff-FR of EP_LS5 exhibited the same efficiency as EP_G15. With regard to the same additive content used, the eff-FR of EP_LS5+G5 was slightly less than EP_G10 corresponding to about 7 % less reduction in the PHRR. In contrast, the eff-FR of EP_LS5+G10 was slightly more than EP_G15, corresponding to about 9 % more reduction in the PHRR.

Throughout the literature, the terminology of synergistic effects through the use of combined additives is arguable and not used consistently. Strictly speaking, superposition is defined as the sum of effects of each additive taken independently. A synergism is an actual effect greater than the superposition, while antagonism is an effect less than the superposition [121-123]. Weil and Lewin have proposed mathematical quantitative descriptions defining a synergistic effect index (SE) for LOI or PHRR, respectively [122-123]. However, such quantitative descriptions are rarely used in the literature. Many reports of synergism are often misapplied to cases where two or more additives merely work better together than either does alone, disregarding the question of whether the effect is greater than superposition, not to mention the question of the concentration-effect relationship prevailing in the polymer matrix.

Disregarding the presence of any additives, the SE for EP_LS+G relates to the absolute reduction of PHRR (SE_{abs}) as the ratio of the actual effect between the combination additive and the sum of the single additives taken independently, defined by the equation (1):

$$SE_{abs}^{(1)} = \frac{PHRR(EP) - PHRR(EP\_xLSyG)}{PHRR(EP) - PHRR(EP\_xLS) + PHRR(EP) - PHRR(EP\_yG)} \qquad (1)$$

$$= \frac{\Delta PHRR(EP\_xLSyG)}{\Delta PHRR(EP\_xLS) + \Delta PHRR(EP\_yG)}$$

where x denotes the amount of LS and y the amount of G in EP_LS+G. A SE of 1 indicates superposition, while above means 1 synergism and below 1 antagonism [123]. Using equation 1, synergism occurs only if there is an additional advantageous interaction between the two flame retardants.

For the same additive content and thus the same amount of EP matrix, equation 2 may be used:

$$SE_{abs}^{(2)} = \frac{\Delta PHRR(EP\_xLSyG)}{\frac{x}{x+y}\Delta PHRR(EP\_(x+y)LS) + \frac{y}{x+y}\Delta PHRR(EP\_(x+y)G)} \quad (2)$$

Using Equation 2 assumes a linear concentration-response relationship between the flame retardant and flame retardancy effect. In practise, however, this relationship is usually not linear, particularly when larger ranges of concentration are discussed. Thus in Equation (2) synergisms also become apparent, resulting from the addition of nonlinear effects versus concentration of the flame retardants. Such pseudosynergisms [122], or synergisms created by non-linearity [121], are not artefacts, but in practice often successful routes to superior products.

Unfortunately, since in EP_LS with concentrations above 5 wt% the viscosity became too high for proper processing, it was not possible to prepare the EP composites with 10 or 15 wt% LS. The effect of LS with different percentages of additive is thus not discussed here. Only for the effect of G were materials with the same percentage of filler taken into account, such that equation 2 was replaced by equation 3:

$$SE_{abs}^{(3)} = \frac{\Delta PHRR(EP\_xLSyG)}{\Delta PHRR(EP\_xLS) + \frac{y}{x+y}\Delta PHRR(EP\_(x+y)G)} \quad (3)$$

Since the reduction in PHRR is only relative to the additive content and the amount of polymer matrix in a non-linear relationship, it is not always appropriate to consider only the absolute reductions of PHRR as used in the equations (1) - (3). For instance, starting from the reduction observed for EP_G5, an addition of the absolute reduction (EP_G10 = EP_G5+5 and EP_G15 = EP_G5+5+5) should result in a much more pronounced reduction for EP_G10 and EP_G15. For the latter a value of PHRR ≤ 0 would be expected, namely three times the absolute reduction observed for EP_G5. Therefore, using the addition of absolute reduction of PHRR is hardly the best model. Assuming that the reduction in PHRR due to a protection layer is described better by a reduction factor, equations (1) and (3) can be replaced by equations (4) and (5), respectively, defined as a relative SE factor (SE_{rel}):

$$SE_{rel}^{(4)} = \frac{1 - \frac{PHRR(EP\_xLSyG)}{PHRR(EP)}}{1 - \frac{PHRR(EP\_xLS)}{PHRR(EP)} \cdot \frac{PHRR(EP\_yG)}{PHRR(EP)}} \quad (4)$$

$$SE_{rel}^{(5)} = \frac{1 - \frac{PHRR(EP\_xLSyG)}{PHRR(EP)}}{1 - \frac{PHRR(EP\_xLS)}{PHRR(EP)} \cdot (1 - (1 - \frac{PHRR(EP\_(x+y)G)}{PHRR(EP)}) \cdot \frac{y}{(x+y)})} \quad (5)$$

Both the values of SE_{abs} (equations 1 and 3) and SE_{rel} (equations 4 and 5) are summarized in Table 3.4.2.4. According to the absolute reduction in PHRR, EP_LS5+G5 and EP_LS5+G10 showed a slight antagonism when $SE_{abs}^{(1)}$ (0.82 - 0.9) was used, whereas they showed a slight synergism based on $SE_{abs}^{(3)}$ (1.02 - 1.17). According to the relative reduction of PHRR, the results for $SE_{rel}^{(4)}$ (0.92 - 0.99) indicated superposition, whereas $SE_{rel}^{(5)}$ (1.1 - 1.3) clearly proved synergism. The SE based on equations (1) and (4) showed the slight antagonism / superposition due to the non-linearity of the concentration-effect relationship for the use of inert fillers. The SE based on equations (3) and (5) showed a clear synergistic tendency in good agreement with the enhanced fire residue integrity through the use of LS+G.

Other fire parameters evaluated in cone calorimeter with various irradiations, including the amount of residue, THE, smoke and CO productions, are given in Table 3.4.2.5. Comparing the different composites with different additives to EP, the amount of fire residue each composite yielded increased as a consequence of the presence of inert fillers. Due to limited carbonaceous charring, THE was hardly changed by varying irradiations. A slight deviation in the THE for the different materials was related to the amount of additive used in the EP matrix. Moreover, the effective smoke and CO yield upon incomplete combustion were changed insignificantly by the use of different additives. These results indicated that no flame inhibition occurred in the gas phase during combustion as the additive worked as an inert filler. The flame retardancy effect was contributed mainly by the shielding effect through residue formation in the condensed phase.

Table 3.4.2.5 *Residue amount, total heat evolved and effective smoke and CO yield from all the materials obtained at various irradiations in cone calorimeter*

	Residue	THE	THE/ML	TSR / ML	COY
	% ±1	MJ m^{-2} ±5	MJ / m^2 g	g^{-1}	g g^{-1}
irradiation of 35 kW m^{-2}					
EP	4	147	2.4	73	0.052
EP_G5	9	134	2.3	66	0.065
EP_G10	13	127	2.3	69	0.045
EP_G15	15	120	2.2	69	0.060
EP_LS5	8	129	2.1	75	0.054
EP_LS5+G5	12	125	2.2	73	0.046
EP_LS5+G10	16	118	2.1	76	0.055
irradiation of 50 kW m^{-2}					
EP	3	135	2.2	70	0.054
EP_G5	9	132	2.2	71	0.060
EP_G10	12	127	2.2	70	0.044
EP_G15	15	123	2.2	72	0.057
EP_LS5	8	128	2.1	75	0.048
EP_LS5+G5	12	127	2.2	73	0.046
EP_LS5+G10	15	119	2.1	78	0.055
irradiation of 70 kW m^{-2}					
EP	2	135	2.2	72	0.056
EP_G5	9	135	2.3	76	0.060
EP_G10	11	132	2.3	72	0.048
EP_G15	14	120	2.2	74	0.054
EP_LS5	7	129	2.1	78	0.046
EP_LS5+G5	11	126	2.2	76	0.046
EP_LS5+G10	15	119	2.2	80	0.054

3.4.2.5 Conclusion

In general, the curing degree and the glass transition temperature of EP matrix were hardly influenced by the additives LS and G. Pyrolysis behaviour of the different composites was changed insignificantly in comparison with EP, since the main mass loss occurred at a similar decomposition temperature in N_2 or in air. Further, no additional decomposition product was observed in the gas phase during different decomposition stages, indicating that both additives worked mainly as inert fillers. The additional residue in the different composites was related to the presence of inorganic filler with very limited carbonaceous char.

The flammability and ignitability of the material improved only slightly in EP_LS5, but hardly changed in the G-containing composites. All the materials were classified as HB in UL 94 test. An antagonism in reaction to a small flame was observed in EP_LS+G due to a predominant influence by the additive G.

The average HRR and the PHRR were reduced by the use of different additives in comparison with EP. The reduction in PHRR increased with increasing the additive content, but leveled off at around 10 - 15 %. The effectiveness flame retardant of per unit decreased with increasing amounts of G. Disregarding the presence of an additive, based on either the absolute reduction of PHRR or the relative reduction factor, EP_LS+G showed slight antagonism / superposition due to the non-linearity of the concentration-effect relationship for the use of inert fillers. With regard to the same percentage of additive and thus the same amount of EP matrix, the EP_LS+G displayed a clear synergistic tendency in good agreement with the enhanced fire residue integrity through the combination of additives.

No flame inhibition was observed in the gas phase, since both of the additives functioned as inert fillers during combustion. The flame retardancy effect was contributed mainly by a shielding effect in the condensed phase in association with the fire residue's structure-property relationship. Overall, more compacted and higher-integrity residue from the surface to the inner structure, which was related to the higher amount of additive used, corresponded to higher efficiency of flame retardancy. The fire residue of EP_LS+G was enhanced not only through an intact, smooth surface, but also an interconnected structure on a different length scale, contributing to the defined superposition in flame retardancy.

In conclusion, EP_LS+G composite was successfully developed as a promising halogen-free flame retarded material by enhancing the fire residue integrity, which is not a common effect found when only two inert fillers are used.

Chapter 4. Summary and Conclusions

The motivation of this study was search for effective eco-friendly and economical flame retarded polymer materials. With wide-ranging advantages such as improved fire and physical properties, halogen-free and relatively low cost, layered silicate / polymer nanocomposite (LSPN) was targeted for high efficiency of flame retardancy. The main goals of this study were to increase the understanding of the flame retardancy phenomenon in LSPN by assessing the shielding effect of the protection layer experimentally and quantitatively, and also to optimize the flame retardancy by the shielding effect in epoxy / layered silicate nonocomposites (EP_LS).

Through the approach to quantify the shielding effect of flame retardancy, the net heat flux in the pyrolysis zone was calculated by determining several important factors as in equation $\dot{q}''_{net} = \dot{q}''_{ext} + \dot{q}''_{flame} - \dot{q}''_{rerad} - \dot{q}''_{loss}$. The $\dot{q}''_{flame}$ and the $\dot{q}''_{rerad}$ through the online heat flux and the temperature at the burning surface. In comparison between the non-charring or low-charring material EP and residue forming EP_LS,

- a similar incident flame heat flux imposed on the burning surface was approximately 20 kW m^{-2} for both EP and EP_LS, independent of the defined external heat flux;
- for the non-charring material EP, the $T_{surface} \approx T_{pyrolysis}$ irrespective of the external heat flux, resulting in an invariable $\dot{q}''_{rerad} \approx$ 10 kW m^{-2} . Hence the net heat flux on the burning surface was strongly dependent on the external heat flux and increased to 45 - 80 kW m^{-2} from an applied external heat flux of 35 - 70 kW m^{-2}. For the residue-forming material EP_LS, the $T_{surface} \neq T_{pyrolysis}$. The $\dot{q}''_{rerad}$ increased with increasing external heat flux, resulting in a reduced dependence of the external heat flux on the net heat flux. The net heat fluxes imposed on the burning surface which penetraets into the material EP_LS were thus reduced to 13 – 22 kW m^{-2}, accordingly;
- compared to EP, combustion parameters including the pyrolysis front velocity, the steady-state HRRs and the 2nd PHRRs at the end of burning were reduced in EP_LS. A quantitative assessment of the shielding effect for flame retardancy was demonstrated by a linear reduction in the fire parameters against the corresponding net heat flux on the burning surface;

- Consequently the dependence relation between the $\dot{q}''_{rerad}$ and the external heat flux elucidated the reduction of flame retardancy as a function of radiation in nanocomposite.

Through the approaches to optimize the efficiency of halogen-free and low-cost flame-retarded EP_LS composites by shielding effect, various organically modified LSs were used for improving the thermal stability of LS and increase the dispersion of LS. Combination of LS and various low-melting glass was used for enhancing the fire residue integrity. All the investigated materials were examined for the materials' pyrolysis behaviour, flammability and fire behaviour.

When EP was combined with the various LSs (NaMMT, TPPMMT and 2PIMMT),

- the degree of curing and the glass transition temperature were insignificantly influenced by the use of different LSs according to EP. The overall decomposition behaviour was hardly changed by the addition of different LSs, in either aerobic or in anaerobic atmospheres. The additional pyrolysis residue obtained in the different composites was related to the presence of inorganic additive with limited carbonaceous char;
- the LOI value was slightly increased by the use of different LSs; EP_TPPMMT5, in particular, showed the highest LOI among all of the materials. However no improvement was observed in UL 94 since all of the materials achieved only a HB rating. Further, the ignitability of the material was slightly improved by adding LS, but barely any difference was detected between the various additives;
- the PHRR was reduced by adding different LSs. The reduction in PHRR corresponded very well with the fire residue structural integrity. Although EP_2PIMMT5 displayed the morphology of a microcomposite at room temperature, it exhibited the highest reduction of PHRR among of all the materials, which was attributed to its fire residue having the most integral structure. The material with higher stability of LS showed more efficient flame retardancy. Due to the different LSs acting as inert fillers, fire properties including the THE, the effective heat of combustion in the gas phase, CO and smoke production yield were hardly changed by adding different LSs, indicating that no flame inhibition occurred in the gas phase;

- The flame retardancy effect was concluded to be exerted by a shielding effect through residue formation in the condensed phase.

When EP/TPPMMT was preloaded or simply mixed with the phosphorous compound TriPP,

- the thermal and thermal oxidative stability of EPs were hardly changed by the use of different additives. The pyrolysis residue obtained in an inert condition was slightly enhanced by small amounts of TriPP alone. For the EPs with the different additives, the additional residue was attributed mainly to the presence of inorganic additives;
- in general, the LOI value was increased by the use of different additives. A clear superposition effect on flammability was observed for the combination of TPPMMT and TriPP. All of the materials achieved a UL94 rating of only HB. The ignitability of EPs was marginally improved by the use of different additives when low irradiations were applied in the cone calorimeter;
- PHRR was reduced significantly by adding different TPPMMTs, attributed to the physical barrier and shielding effect from the residue formation. A clear superposition effect on the reduction in HRR was exerted by the combination of TPPMMT and TriPP during combustion. No difference was observed between the two methods of adding either preloaded or simply mixed TPPMMT+TriPP, corresponding to their similar residue structures. Further, due to limited carbonaceous charring, fire properties including the fire load, the effective heat of combustion, the CO and smoke production were barely influenced by the use of different additives, suggesting that no significant flame inhibition occurred in the gas phase;
- Although no improvement in the dispersion of LS was found to be caused when TriPP was used as a spacer, the combination of TPPMMT and a small amount of TriPP shows a promising effect at a start point on flammability and flame retardancy.

When EP/TPPMMT was combined with the low-melting glasses CP, SG and phenylsiloxane glass, all of the glass-containing composites were visualized as microcomposites in a mixture of micro-sized glass particles and nano-sized LS dispersion. In comparison with EP,

- the degree of curing and the glass transition temperature were not significantly affected by the use of LS and the different glasses. The thermal stability of the material was decreased slightly when SG was added due to SG's lack of high thermal stability at high temperatures, but not when LS, CP and phenylsiloxane glass were added. At high temperatures, thermal oxidative charring stability was decreased slightly by the use of CP and SG, but hardly changed by phenylsiloxane glass. The additional pyrolysis residue obtained from the composites was attributed mainly to the presence of different inorganic additives. Although the product release rate of the main gaseous decomposition products was influenced slightly by the use of different additives, no spectra of additional decomposition products were observed in the gas phase during different decomposition steps. Chemical interactions between the components played a minor role during the decomposition of EP matrix, since these different additives functioned as inert fillers;
- the LOI value was increased through the use of LS, CP and SG, particularly when high amounts of SG were added. But it was hardly changed by the use of phenylsiloxane glass, due to a predominant influence by the phenylsiloxane glass. Just like EP, all of the materials achieved a HB classification. When the three different low-melting glasses were used, no improvement in flammability or ignitability was achieved by adding the combination of LS+G;
- no flame inhibition was observed in the gas phase since all of the different additives functioned as inert fillers during combustion, resulting in barely any influence on the fire load, effective heat of combustion, or production of CO and smoke. The average HRR and the PHRR were reduced significantly by the use of different inorganic additives, attributed to the physical barrier and shielding effect through residue formation in the condensed phase;
- addition of the inorganic glasses (Ceepree and Sulphate glass) showed antagonistic effects on the reduction of PHRR. The antagonism was attributed to a dominant columnar structure on the micro-scale resulting when LS was added, which also appeared as a less efficient fire residue structure on the macro-scale. Nevertheless, the characteristics of the fire residue surface demonstrated that the enhanced fire residue integrity on the micro-scale by the combination additives (LS + CP/SG) contributes to the efficiency of flame retardancy;
- when phenylsiloxane glass was used, the combination of organo-LS and phenylsiloxane glass showed a clear superposition / pseudosynergism in reducing

PHRR during combustion, which is not a common effect found when only two inert fillers are used. This promising effect on flame retardancy was attributed to the enhanced integrity of the fire residue structure.

Several conclusions are drawn from this study,

- It was evident that the shielding effect by the inorganic-carbonaceous fire residue surface protection layer is the only main flame retardancy effect in the polymer nanocomposites based on non-charring or low-charring polymers with inert additives;
- It was proved that the intercalated and exfoliated structure of LS dispersion by organic modification is a prerequisite for high efficiency of EP composites. Further fire behaviour of EPs with the different organo-LSs indicated that although no improvement on the dispersion of LS was observed at room temperature, the exfoliation of LS can be affected significantly by several important factors, such as heating, decomposition, evaporation of decomposition products and accumulation during combustion;
- Although the combination of LS and low-melting glass was not universally effective for all the glass selections, a promising effect was possible and available when the fire residue integrity was enhanced. A new route was discovered that the fire residue integrity on the macro and the micro-scales is critical for flame retardancy efficiency.

References

1. Levchik SV. Introduction to flame retardancy and polymer flammability. In: *Flame Retardant Polymer Nanocomposite*, Morgan AB, Wilkie CA, eds. John Wiley & Sons, Inc. **2007**; Chap 1

2. Hall Jr JR, Bukowsli RW. Fire-hazard and fire-risk assessment of fire-retardant polymers. In: *Fire Retardancy of Polymeric Materials*, Grand AF, Wilkie CA, eds. Marcel Dekker, Inc. **2000**; Chap 14

3. Joseph P, Ebdon JR. Recent developments in flame-retarding thermoplastics and thermosets. In: *Fire Retardant Materials*, Horrocks AR, Price D, eds. Woodhead Publishing Ltd. **2001**; Chap 7

4. Martin FJ, Price KR. Flammability of epoxy resin. *J. Appl. Polym. Sci.* **1968**; 12: 143-158

5. Lyon RE. Pyrolysis kinetics of char forming polymers. *Polym. Degrad. Stab.* **1998**; 61: 201-210

6. Van Krevelen DW. Some basic aspects of flame resistance of polymeric materials. *Polymer*. **1975**; 16: 615-620

7. Grand AF, Wilkie CA, eds. *Fire Retardancy of Polymeric Materials*. Marcel Dekker, Inc. **2000**; Chap 5-10

8. Laoutid F, Bonnaud L, Alexandre M, Lopez-Cuesta JM, Dubois Ph. New prospects in flame retardant polymer materials: from fundamentals to nanocomposites. *Mater. Sci. Enginee. R* **2009**; 63: 100-125

9. Wilkie CA, Morgan AB, eds. *Fire Retardancy of Polymeric Materials.* Taylor and Francis Group, LLC **2010**; Chap 4-12

10. Horrocks AR, Price D, eds. *Fire Retardant Materials*. Woodhead Publishing Ltd. **2001**; Chap 7-10

11. Hornsby P. Fire-Retardant Fillers. In: *Fire Retardancy of Polymeric Materials*. Wilkie CA, Morgan AB, eds. 2nd Edition, CRC Press, **2010**; Chap 7

12. Schartel B. Use of fire tests in materials flammability development. In: *Fire Retardancy of Polymeric Materials.* Wilkie CA, Morgan AB, eds. Taylor and Francis Group, LLC **2010**; Chap 15

13. Lopez-Cuesta JM, Laoutid F. Muticomponet FR systems: Polymer nanocomposites combined with additional materials. In: *Fire Retardancy of Polymeric Material,* Wilkie CA, Morgan AB, eds. Taylor and Francis Group, LLC **2010**; Chap 12

14. Lewin M. Synergistic and catalytic effects in flame retardancy of polymeric materials-An overview. *J. Fire. Sci,* **1999**; 17: 3-19

15. Beyer G. Flame Retardant Properties of EVA-nanocomposites and Improvements by Combination of Nanofillers with Aluminium Trihydrate. *Fire Mater.* **2001**; 25: 193–197

16. Morgan AB, Wilkie CA, eds. *Flame Retardant Polymer Nanocomposite.* John Wiley and Sons Inc, Hoboken, **2007**; Chap 2-7

17. Kiliaris P, Papaspyrides CD. Polymer/layered silicate (clay) nanocomposites: An overview of flame retardancy. *Progress in Polymer Sci* **2010**; 35: 902-958

18. Wang D, Wilkie CA. Fire properties of polymer nanocomposites. In: *Fire Properties of Polymer Composite Materials,* Mouritz AP, Gibson AG, eds. Springer, **2006**; Chap 9

19. Bourbigot S, Dequesne S, Jama C. Polymer nanocomposites: How to reach low flammability. *Macromol. Symp.* **2006**; 233: 180-190

20. Schartel B, Pötschke P, Knoll U, Abdel-Goad M. Fire behaviour of polyamide 6/multiwall carbon nanotube nanocomposites. *Eur. Polym. J.* **2005**; **41**: 1061-1070

21. Gilman JW. Flammability and thermal stability studies of polymer layered-silicate _clay/ nanocomposites. *Appl. Clay. Sci*. **1999**; 15: 31-49

22. Paul DR, Robeson LM. Polymer nanotechnology: Nanocomposites. *Polymer* **2008**; 49: 3187-3204

23. Hackman I, Hollaway L. Epoxy-layered silicate nanocomposites in civil engineering. *Composite: Part A.* **2005**; DOI:10.1016

24. Gilman JW. Flame retardant mechanism of polymer-clay nanocomposites. In: *Flame Retardant Polymer Nanocomposites,* Morgan AB, Wilkie CA, eds. John Wiley and Sons Inc, Hoboken **2007**; Chap 3

25. Kandola B. Nanocomposite. In: *Fire Retardant Materials*, Horrocks AR, Price D, eds. Woodhead Publishing Ltd **2001**; Chap 6

26. Yano K, Usuki A, Okada A, Kurauchi T, Kamigaito O. Synthesis and properties of polyimide-clay hybrid. *J. Polym. Sci. A.* **1993**; 31: 2493-2498

27. Schartel B, Braun U, Knoll U, Bartholmai M,Goering H, Neubert D, Pötschke P. Mechanical, thermal, and fire Behavior of bisphenol A polycarbonate/multiwall carbon nanotube nanocomposites*. Polym. Enginee. Sci*. **2008**; DOI 10.1002/pen

28. Schartel B, Knoll U, Hartwig A, Pütz D. Phosphonium-modified layered silicate epoxy resins nanocomposites and their combinations with ATH and organo-phosphorus fire retardants. *Polym. Adv. Technol.* **2006**; 17: 281-293

29. Hartwig A, Pütz D, Schartel B, Bartholmai M, Wendschuh-Josties M. Combustion behaiour of epoxide based nanocomposites with ammonium and phosphonium bentonites. *Macromol. Chem. Phys.* **2003**; 204: 2247-2257

30. Lakshmi MS, Narmadha B, Reddy BSR. Enhanced thermal stability and structural characteristics of different MMT-Clay/epoxy-nanocomposite materials. *Polym. Degrad. Stab*. **2007**; 92: 425-436

31. Jang BN, Wilkie CA. The thermal degradation of polystyrene nanocomposite. *Polymer* **2005**; 46: 2933-2942

32. Bourbigot S, Gilman JW, Wilkie CA. Kinetic analysis of the thermal degradation of polystyrene-montmorillonite nanocomposite. *Polym. Degrad. Sta.* **2004**; 84: 483-492

33. Burnside SD, Giannelis EP. Synthesis and properties of new polydimethylsiloxane nanocomposites. *Chem. Mater.* **1995**; 7: 1597-1600

34. Hartwig A, Sebald M. Preparation and propeties of elastomers based on a cycloaliphatic diepoxide and poly(tetrahydrofuran). *Eur. Polym. J.* **2003**; 39: 1975-1981

35. Gilman JW, Kashiwagi T. Nanocomposites: A revolution new flame retardant approach. *42nd International SAMPE Symposium* **1997**; May 4-8

36. Gilman JW, Jackson CL, Morgan AB, Jr. RH, Manias E, Giannelis EP, Wuthenow M, Hilton D, Phillips SH. Flammability properties of polymer-layered silicate nanocomposites. Polypropylene and polystyrene nanocomposites. *Chem. Mater.* **2000**; 12: 1866-1873

37. Morgan AB. Flame retarded polymer layered silicate nanocomposites: a review of commercial and open literature systems. *Polym. Adv. Technol.* **2006**; 17: 206-217

38. Zanetti M, Kashiwagi T, Falqui L, Camino G. Cone calorimeter combustion and gasification studies of polymer layered silicate nanocomposites. *Chem. Mater.* **2002**; 14: 881-887

39. Gilman JW, Kashiwagi T, Giannelis EP,Manias E, Lomakin S, Lichtenham JD, Jones P. Nanocomposites: Radiative gasfication and vinyl polymer flammability. In: *Fire Reatrdancy of Polymers: The Use of Intumescence*. Le Bras M, Camino G, Bourbigot S, Delobel R eds,. Royal Society of Chemistry. London **1998**; 203-221

40. Kashiwagi T, Danyus R, Liu MF, Zammarano M, Shield JR. Enhancement of char formation of polymer nanocomposites using a catalyst. *Polym. Degrad. Stab.* **2009**; DOI: 10.1016

41. Gilman JW, Kashiwagi T. Polymer-layered silicate nanocomposites with conventional flame retardants. In: *Polymer-Clay Nanocomposites*, Pinnavaia TJ, Beall GW eds., John Wiley & Sons, Chichester **2000**; Chap 10

42. Gilman JW, Harris RH, Shields JR, Kashiwagi T, Morgan AB. A study of the flammability reduction mechanism of polystyrene-layered silicate nanocomposite: layered silicate reinforced carbonaceous char. *Polym. Adv. Technol.* **2006**; 17: 263-271

43. Kashiwagi T, Mu MF, Winey K, Cipriano B, Raghavan SR, Pack SC, Rafailovich M, YangY, Grulke E, Shileds J, Harris R, Douglas J. Relation between the viscoelastic and flammability properties of polymer nanocomposites. *Polymer* **2008**; 49: 4358-4368

44. Beyer G. Filler blend of carbon nanotubes and organoclays with improved char as a new flame retardant system for polymers and cable applications. *Fire Mater*. **2005**; 29:61–69

45. Gilman JW, Ritchie SJ, Kashiwagi T, Lomakin SM. Fire retardant additives for polymeric materials-I. Char formation from silica gel-potassium carbonate. *Fire Mater.* **1997**; 21: 23-32

46. Kashiwagi T, Gilman JW, Butler KM, Harris RH, Shields JR, Asano A. Flame retardant mechanism of silica gel/silica. *Fire Mater.* **2000**; 24: 277-289

47. Morgan AB, Harris RH, Kashiwagi T, Chyall LJ, Gilman JW. Flammability of polystyrene layered silicate(clay) nanocomposites: Carbonaceous char formation. *Fire Mater.* **2002**; 26: 247-253

48. Schartel B. Considerations of regarding specific impacts of the principal fire retardancy mechanisms in nanocomposites. In: *Flame Retardant Polymer Nanocomposite*. Morgan AB, Wilkie CA, eds. John Wiley & Sons, Inc. **2007**; Chap 5

49. Bartholmai M, Schartel B. Layered silicate polymer nanocomposites: New appoach or illusion for fire retardancy? Investigations of the potentials and the tasks using a model system. *Polym. Adv. Technol.* **2004**; 15: 355-364

50. Schartel B, Weiß A, Sturm H, Kleemeier M, Hartwig A, Vogt C, Fisher RX. Layered silicate epoxy nanocomposites: formation of the inorganic-carbonaceous fire protection layer. *Polym. Adv. Technol.* **2010**; DOI: 10.1002/pat. 1644

51. Schartel B, Bartholmai M, Knoll U. Some comments of the main fire retardancy mechanisms in polymer nanocomposites. *Polym. Adv. Technol.* **2006**; 17: 772-777

52. Zammarano M. Thermoset fire retardant nanocomposites. In: *Flame Retardant Polymer Nanocomposites*, Morgan AB, Wilkie AW, eds. John Wiley and Sons, Inc, **2007**; Chap 9

53. Vaccari A. Preparation and catalytic properties of cationic and anionic clays. *Catalysis Today* **1998**; 41: 53-71

54. Meyn M, Beneke K, Lagaly C. Anion-exchange reactions of hydroxy double salts. *Inorg. Chem.* **1993**; *32,* 1209-1215

55. Xie W, Gao ZM, Pan WP, Hunter D, Singh A, Vaia R. Thermal degradation chemistry of alkyl quaternary ammonium montmorillonite. *Chem. Mater.* **2001**; 13: 2979-2990

56. Xie W, Xie RC, Pan WP, Doug Hunter D, Koene B, Tan LS,| Vaia R. Thermal stability of quaternary phosphonium modified montmorillonites. *Chem. Mater.* **2002**; 14: 4837-4845

57. Gilman JW, Awad WH, Davis RD, Shields J, Harris Jr RH, Davis C, Morgan AB, Sutto TE, Callahan J, Trulove PC, Delong HC. Polymer/layered silicate nanocomposites from thermally stable trialkylimidazolium-treated montmorillonite. *Chem. Mater.* **2002**; 14: 3776-3785

58. Park JH, Jana SC. Mechanism of exfoliation of nanoclay particles in epoxy-clay nanocomposites. *Macromolecules* **2003**; 36: 2758-2768

59. Schartel B. Fire retardancy based on polymer layered silicate nanocomposites. In: *Advanced in Polymeric Nanocomposite,* Okamoto M ed. CMC Publishing: Osaka, **2004**; Chap 2-3, 242-257

60. Krishnamoorti R, Vaia RA, Giannelis EP. Structure and dynamics of polymer-layered silicate nanocomposites. *Chem. Mater.* **1996**; 8: 1728-1734

61. Wang Z, Pinnavaia TJ. Hybrid organic-inorganic nanocomposites: exfoliation of magadiite nanolayers in an elastomeric epoxy polymer**.** *Chem. Mater.* **1998**; 10: 1820-1826

62. Carrado KA. Synthetic organo- and polymer–clays: preparation, characterization, and materials applications. *Appl. Clay. Sci*. **2000**; 17: 1–23

63. Yang F, Nelson GL. Polymer/silica nanocomposites prepared via extrusion. *Polym. Adv. Technol*. **2006**; 17: 320–326

64. Triantafillidis CS, LeBaron PC, Pinnavaia TJ. Homostructured mixed inorganic-organic ion clays: A new approach to epoxy polymer-exfoliated clay nanocomposites with a reduced organic modifier content. *Chem. Mater.* **2002**; 14: 4088-4095

65. Pastore HO, Frache A, Boccaleri E, Marchese L, Camino G. Heat induced structure modifications in polymer-layered silicate nanocomposites. *Macromol. Mater. Enginee*. **2004**; 289: 783–786

66. Adhikari R, Henning S, Michler GH. Nanostructured composites with layered morphology: structure and properties*. Macromol. Symp*. **2006**; 233: 26–35

67. Fina A, Bocchini S, Camino G. Thermal behaviour of nanocomposites and fire testing performance. In: *Fire and Polymers V: Materials and Concepts for Fire Retardancy*, Wilkie CA, Morgan AB, Nelson GL eds, ACS Symposium Series 1013. **2009**; Chap 2

68. Jang BN, Wilkie CA. The effect of clay on the thermal degradation of polyamide 6 in polyamide 6 / clay nanocomposites. *Polymer* **2005**; 46: 3264-3274

69. Tang Y, Lewin M. New aspects of migration and flame retardancy in polymer nanocomposites. *Polym. Degrad. Stab.* **2008**; 93: 1985-1995

70. Lewin M. Reflections on migration of clay and structural changes in nanocomposites. *Polym. Adv. Technol*. **2006**; 17: 758-763

71. Lewin M. Some comments on the modes of action of nanocomposites in the flame retardancy of polymers. *Fire Mater.* **2003**; 27: 1-7 (DOL: 10.1002/fam.813)

72. Tang Y, Lewin M, Pearce EM. Effects of annealing on the migration behaviour of PA6/Clay nanocomposites. *Macromol. Rapid. Commun.* **2006**; 27: 1545-1549

73. Lewin M, Pearce EM, Levon K, Mey-Marom A, Zammarano M, Wilkie CA, Jang BK. Nanocomposites at elevated temperatures: migration and structural changes. *Polym. Adv. Technol*. **2006**; 17: 226–234

74. Kashiwagi T, Harris Jr RH, Zhang X, Briber RM, Cipriano BH, Raghavan SR, Awad WH, Shields JR. Flame retardant mechanism of polyamide 6- clay nanocomposites. *Polymer* **2004**; 45: 881-891

75. Samyn F, Bourbigot S, Jama C, Bellayer S. Fire retardancy of polymer clay nanocomposites: Is there an influence of the Nanomorphology. *Polym. Degrad. Stab.* **2008**; 93: 2019–2024

76. Zanetti M, Camino G, Mülhaupt R. Combustion behaviour of EVA/fluorohectorite nanocomposites. *Polym. Degrad. Stab.* **2001**; 74: 413-417

77. Zanetti M, Camino G, Reichert P, Mülhaupt R. Thermal behaviour of poly(propylene) layered silicate nanocomposites. *Macromol. Rapid Commun.* **2001**; 22: 176-180

78. Zanetti M, Camino G, Thomann P, Mülhaupt R. Synthesis and thermal behaviour of layered silicate-EVA nanocomposite. *Polymer* **2001**; 42: 4501-4507

79. Lewin M, Weil E. Mechanisms and modes of action in flame retardancy of polymers. In: *Fire Retardant Materials*, Horrocks AR, Price D, eds. Woodhead Publishing, Cambridge **2001**; Chap 2: 31-57.

80. Bourbigot S, Le Bras M, Duquesne S, Rochery M. Recent advances for intumescent polymers. *Macromol. Mater. Enginee.* **2004**; 289: 499–511

81. Kashiwagi T, Gilman JW, Butler KM, Harris1 RH, Shields JR, Asano A. Flame retardant mechanism of silica gel*/*silicas. *Fire Mater*. **2000**; 24: 277-289

82. Duquesne S, Jama C,Le Bras M, Delobel R, Recourt P, Gloaguen JM. Elaboration of EVA-nanoclay systems-characterization,thermal behaviour and fire performance. *Compo. Sci. Technol.* **2003**; 63: 1141–1148

83. Kandola BK, Horrocks AR. Complex char formation in flame-retarded fibre-intumescent combinations IV. Mass loss and thermal barrier properties. *Fire Mater*. **2000**; 24: 265-275

84. Bourbigot S, Le Bras M, Dabrowski F, Gilman JW, Kashiwagi T. PA-6 clay nanocomposite hybrid as char forming agent in intumescent formulations. *Fire Mater*. **2000**; 24: 201-208

85. Bellucci F, Camino G, Frache A, Sarra A. Catalytic charring evolatilization competition in organoclay nanocomposites. *Polym. Degrad. Stab*. **2007**; 92: 425-436

86. Schartel B, Weiß A. Temperature inside burning polymer specimens: Pyrolysis zone and shielding. *Fire Mater*. **2010**; 34: 217-235

87. Wu GM, Schartel B, Bahr H, Kleemeier M, Yu D, Hartwig A. Experimental and quantitative assessment of flame retardancy by the shielding effect in layered silicate epoxy nanocomposites. *Combust. Flame.* **2010**; submitted

88. Zhang J, Delichatsios M, Bourbigot S. Experimental and numerical study of the effects of nanoparticles on pyrolysis of a polyamide 6 (PA6) nanocomposite in the cone calorimeter *Combust. Flame.* **2009**; 156: 2056-2062

89. Zhang J, Delichatsios M. Further Validation of a Numerical Model for Prediction of Pyrolysis of Polymer Nanocomposites in the Cone Calorimeter. *Fire Technol*. **2010**; 46: 307-319

90. Schartel B. Phosphorus-based flame retardancy mechanisms-old hat or a starting point for future development. *Materials* **2010**; 3: 4710-4745

91. Chigwada G, Wilkie CA. Synergy between conventional phosphorus fire retardants and organically-modified clays can lead to fire retardancy of styrenics. *Polym. Degrad. Stab*. **2003**; 80: 551–557

92. Kroenke WJ. Low-melting sulphate glasses and glass-ceramics, and their untility as fire and smoke retarder additives for poly(vinyl chloride). *J. Mater. Sci.* **1986**; 21: 1123-1133

93. Myers RE, Licursi E. Inorganic glass forming systems as intumescent flame retardants for organic polymers. *J. Fire Sci.***1985**; 3: 415-431

94. Camino G, Costa L, Martinasso G. Intumescent fire-retardant systems. *Polym. Degrad. Stab.* **1989**; 23: 359-376

95. Quinn CJ, Beall GH. Low-temperature glass-polymer blends. In: *Chemical Processing of Advanced Materials*, Hench LL, West JK eds., John Wiley and Sons,Inc, New York, **1992**; pp 799-805

96. Schartel B, Schmaucks G, Roszinsk J. WO/ **2010**/044671

97. Bourbigot S, Le Bras M. Flame retardant plastics. In: *Plastics Flammability Handbooks*, 3rd edition, Troitzsch ed., Carl Hanser Verlag, Munich **2004**; Chap 5: 148-149

98. Quintiere JG. Fire growth: an overview. *Fire Technol*. **1997**; 33: 7-29

99. Lyon RE. Heat release kinetics. *Fire Mater*. **2000**; 24: 179-186

100. Lyon RE. Solid-state thermochemistry of flaming combustion. In: *Fire Retardancy of Polymeric Materials*, A.F. Grand, C.A. Wilkie eds, Marcel Dekker, New York, **2000**; Chap 11

101. Lyon RE. Plastics and rubber. In: *Handbook of Building Materials for Fire Protection.* Harper CA, eds. McGraw-Hill, New York, **2004**; Chap 3

102. Schartel B, Hull TR. Development of fire-retarded materials—Interpretation of cone calorimeter data. *Fire Mater.* **2007**; 31:327–354

103. Hirschler MM. Chemical aspects of thermal decomposition. In: *Fire Retardancy of Polymeric Materials*, Grand AF, Wilkie CA, eds. Marcel Dekker, Inc. **2000**; Chap 2

104. Carrasco F, Pagès. Thermal degradation and stability of epoxy nanocomposites: Influence of montmorillonite content and cure temperature. *Polym. Degrad. Stab.* **2008**; 93: 1000-1007

105. Galimberti M, Giudice S, Cipolletti V, Guerra G. Control of organoclay structure in hydrocarbon polymers. *Polym. Adv. Technol.* **2010**; 21: 679–684

106. Zhang J, Shields TJ, Silcock GWH. Effect of melting behaviour on upward flame spread of thermoplastics. *Fire Mater*. **1997**; 21: 1-6

107. Janssens M. Fundamentals of fire testing and what tests measure. In *Fire Retardancy of Polymeric Materials.* Wilkie CA, Morgan AB, eds. Taylor and Francis Group, LLC **2010**; Chap 14

108. Mowrer FW. Fundamentals of the fire hazards of materials. In: *Handbook of Building Materials for Fire Protection.* Harper CA, eds. McGraw-Hill, New York, **2004**; Chap 1

109. Babrauskas V, Peacock RD. Heat release rate: the single most important variable in fire hazards. *Fire Safety J.* **1992**; **18**: 255-272

110. Cervantes-Uc JM, Cauich-Rodríguez JV, Humberto Vázquez-Torres H, Garfias-Mesías LF, Paul DR. Thermal degradation of commercially available organoclays studied by TGA–FTIR. *Thermochimica Acta*. **2007**; 457: 92–102

111. Camino G, Tartaglione G, Frache A, Manferti C, Costa G. Thermal and combustion behaviour of layered silicate epoxy nanocomposites. *Polym. Degrad. Stab*. **2005**; 90: 354-362

112. Hülsenberg D, Harnisch A, Bismack A. In: *Microstrucuring of Glasses*, Springer Series in Materials Science, Vol. 87, Springer, Berlin Heidelberg **2008**; pp 75

113. Lee SW, Hong KS, Condrate RA, Hapanowicz RP, Speyer RF. Characterization of gas components and deposits in bubbles in silicate glasses prepared with sodium sulphate. *J. Mater. Sci*. **1992**; 27: 4961-4966

114. Levchik SV, Weil ED. Review: thermal decomposition, combustion and flame-retardancy of epoxy resins—a review of the recent literature. *Polym Int* **2004**; 53:1901–1929

115. Wu GM, Schartel B, Kleemeier M, Hartwig A. Fire behaviour of layere silicate epoxy nanocomposite combined with low-melting inorganic Ceepree glass. *Polym. Enginee. Sci.* **2010**; in press. DOI: 10.1002 / pen. 22111

116. Braun U, Knoll U, Schartel B, Hoffmann T, Pospiech D, Artner J, Ciesielski M, Döring M, Perez-Graterol R, Sandler JKW, Altstädt V. Novel phosphorus-containing poly(ether sulfone)s and their blends with an epoxy resin: thermal decomposition and fire retardancy. *Macromol. Chem. Phys.* **2006**; 207: 1501–1514

117. Wu GM, Schartel B, Yu D, Kleemeier M, Hartwig A. Synergistic flame retardancy in layered-silicate epoxy nanocomposite combined with low-melting phenysiloxane glass. *Polymer International*, J. Fire. Sci, submitted in **2011**

118. Yu D, Kleemeier M, Wu GM, Schartel B, Liu WQ, Hartwig A. A low melting organic-inorganic glass and its effect on flame retardancy of clay/epoxy composites. *Polymer,* **2011**; 52: 2120-2131

119. Bishop DP, Smith DA. Combined pyrolysis and radiochemical gas chromatograpy for studying the thermal degradation of epoxy resin and polyimides I: The

degradation of epoxy resins in nitrogen between 400^{o}C and 700^{o}C. *J. Appl. Polym. Sci.* **1970**; 14: 205-223

120. Chen CS, Bulkin BJ, Pearce EM. New epoxy resins III: Application of Fourier transform IR to degradation and interaction studies of epoxy resins and their copolymers. *J. Appl. Polym. Sci.* **1983**; 28: 1077-1091

121. Weil ED. Synergists, adjuvants, and antagonists inflame retardant systems. In *Fire Retardancy of Polymeric Materials*. Grand AF, Wilkie CA, eds. Marcel Dekker, Inc. **2000**; Chap 4:115-145

122. Weil ED. Additivity, synergism and antagonism in flame retardancy. In: *Fire Retardancy of Polymeric Materials*. Kuryla WC, Papa AJ, eds., Marcel Dekker, Inc. **1975**; 3: 185-243

123. Lewin M, Zhang J, Pearce E, Zammarano M. Polyamide 6 treated with pentabromobenzyl acrylate and layered silicate. *Polym. Adv. Technol.* **2010**; DOI: 10.1002/pat 1719

124. Felske JD, Tien CL. Calculation of the Emissivity of Luminous Flames. *Combust. Sci. Technol*. **1973**; 7: 25-31

125. Tsai KC, Drysdale D. Flame Height Correlation and Upward Flame Spread Modeling. *Fire Mater*. **2002**; 26: 279–287

126. Rhodes BT, Quintiere JG. Burning rate and flame heat flux for PMMA in cone calorimeter. *Fire Safety J*. **1996**; 26: 221-240

127. Beaulieu PA, Dembsey NA. Flammability characteristics at applied heat flux levels up to 200 kW m^{-2}. *Fire Mater.* **2008**; 32: 61–86

128. Quintiere JG, Iqbal N. An approximate integral model for the burning rate of a thermoplastic-like material. *Fire Mater.* **1994**; 18: 89-98

129. Henderson JB, Wiebelt JA, Tant MR. A model for the thermal response of polymer composite materials with experimental verification. *J. Comp. Mater.* **1985**; 19: 579

130. Vovelle C, Delfau JL, Reuillon M, Bransier J, Laraqui N. Experimental and numerical study of the thermal degradation of PMMA. *Combust. Sci. Technol*. **1987**; 53: 187–201

131. Hopkins D, Quintiere JG. Material fire properties and predictions for thermoplastics. *Fire Safety J.* **1996**; 26: 241–268

132. Quintiere JG ed. *Fundamentals of Fire Phenomena*. John Wiley & Sons, LTD, Chichester, **2006**; p. 15

133. Staggs JEJ. Heat and mass transport in developing chars. *Polym. Degrad. Stab.* **2003**; 82: 297-307

Appendix: Experimental

- **Material Preparation Methods**

All of the investigated materials in this study were prepared and kindly provided by IFAM (Fraunhofer Institute for Manufacturing and Advanced Materials), Bremen, in cooperation for joint German Research Foundation project (DFG / SCHA 730 / 8-1, 8-2, HA 2420 / 6-1 and 6-2). The materials preparation methods have been published [28, 29]. Materials in this study are listed below:

Epoxy resin (in sections 3.1, 3.2, 3.3.1 and 3.4.1)

The selected polymer material was an epoxy resin system based on a bisphenol A diglycidyl ether (Araldite GY250, Huntsman) with an epoxy equivalent weight of 185 g/eq, which was cured with an equimolar amount of 4-methyl hexahydrophthalic anhydride (MHHPA, Acros Organics). Unless otherwise noted, the curing reaction of the mixture of epoxy resin and anhydride hardener was catalyzed by 1 wt% of 1-methylimidazole (Sigma Aldrich).

Organically modified MMTs

The organically modified layered silicates were produced from a sodium montmorillonite (NaMMT, Nanofil 757, Südchemie, Germany) with a cation exchange capacity of 0.8 meq/g. The unmodified NaMMT had a BET surface of 24 m²/g, as determined by nitrogen adsorption (NOVA-2200, Quantachrome).

Tetraphenylphosphonium montmorillonite (TPPMMT)

A dispersion of 50 g Nanofil 757 (40 mmol exchangeable sodium ions) in 1 L deionised water was prepared and heated to 342 K. A warm solution (16.7 g, 40 mmol) tetraphenylphosphonium bromide (Evonik) in 600 ml deionized water was added slowly while the mixture was vigorously stirred. TPPMMT instantly precipitated in the form of voluminous flakes. The dispersion was diluted with 3 L deionized water and stirred for 1 hour at room temperature before the TPPMMT was filtered off. Through careful rinsing with deionized water, the remaining sodium and halide ions were removed from the products.

The final filter cake, which had a solid content of about 10 wt%, was granulated and deep-frozen with liquid nitrogen. After freeze-drying for 1 week at 0.16 mbar (Alpha 1-4, Christ) TPPMMT was obtained as a light powder with a high specific surface area, typically of 150 m²/g.

2-Phenylimidazolium montmorillonite (2PIMMT)

50 g Nanofil 757 were dispersed in 1 L deionised water and heated to 342 K. The dispersion was adjusted to pH 2 by adding approximately 80 ml of 1 n HCl and was then stirred for 12 h at room temperature. 2-Phenylimidazole (5.77 g, 40 mmol) was dissolved in 10 ml hydrochloric acid (20 wt% in water). The solution was diluted to 600 ml with deionised water before it was slowly added to the NaMMT dispersion. Further sample preparation followed the procedure described for TPPMMT. The dried 2PIMMT had a BET surface area of approx. 50 m²/g.

Further modification of TPPMMT with triphenyl phosphate (for section 3.2)

62.6 g TPPMMT were dispersed in 5 L deionised water and heated to 323 K. Under stirring, a solution of 12.8 g triphenyl phosphate (Aldrich) in 150 ml ethanol was added within 1 h, while the temperature of the mixture was increased to 403 K. After filtering off the modified TPPMMT, it was freeze-dried as described above. The product had a triphenyl phosphate content of 17 wt% and a BET surface of approx. 65 m²/g.

Low-melting glasses (for section 3.3)

Ceepree

Ceepree glass is a commercial product manufactured by Chance&Hunt (UK) and was obtained from Nordmann, Rassmann (Germany). For this work the grade “Ceepree B200U” was used, which has not received an organic coating. An average particle size D50 of 3-8 µm and a maximum particle size of 30 µm are specified by the manufacturer.

Sulphate glass

A sulphate glass with the empirical formula of $NaKZn(SO_4)_2$ was prepared according to the procedure given by Kroenke [Kroenke-1986]. 35.5 g (0.25 mol) sodium sulphate, 43.5 g (0.25 mol) potassium sulphate and 80.5 g (0.5 mol) zinc sulphate (all sulphates purchased in anhydrous form from Fluka, Germany) were ground together and heated to 600 °C in an electric furnace. A clear homogeneous melt with low viscosity was obtained. To vitrify the melt, it was poured drop by drop onto an aluminium plate which was cooled by liquid nitrogen. The sulphate glass was ground in a planetary mill using grinding balls made of zirconia before it was sieved. The resulting fine powder had a maximum particle size of 32 µm. Kroenke specifies a melting point of 420 °C for the sulphate glass.

Phenylsiloxane glass (for section 3.4.2)

Phenylsiloxane glass (G) was prepared by acid catalyzed hydrolysis and polycondensation of phenyltriethoxysilane (ABCR Co. KG) in a water/ethanol/HCl mixture. The intermediate product after evaporating the solvents was thermally treated for 6 h at 250 °C in vacuum in order to obtain the final glass. The glass was then milled and sieved to a maximum particle size of 250 µm. A more detailed description of the synthesis of G [and LS], as well as the preparation of the composites with epoxy resin, is given elsewhere. [Yu-2011]

Preparation of composite samples, general procedure

Unless otherwise noted, layered silicates and glasses were dispersed in the epoxy component of the resin system by using a dissolver equipped with a 60-mm disk (Dispermat CA-40C, VMA Getzmann, Germany). The mixtures were stirred for 1 h at 1500 rpm and room temperature. After mixing with the calculated amounts of hardener and catalyst, the dispersions were cast into pre-heated aluminum molds, which were treated with a release agent (Acmosan 82-6007, Acmos Chemie). The moulds had internal dimensions of 250 x 200 mm² and an internal thickness of 5 mm (specimens for cone test) or 3 mm (specimens for LOI and UL94). Curing was achieved in 1 hour at 393 K in a ventilated air oven.

Modifications of procedure for curing samples in frames with thermocouples

For cone samples with internal thermocouples (internal thickness 25 mm) it is difficult to remove the heat produced by the exothermic curing reaction. In order to avoid overheating, samples were cured according to the following schedule: 1) heating from room temperature to 333 K in 1 h; 2) 3 h at 333 K; 3) 3 h at 423 K.

Modifications of procedure for highly loaded composites of TPPMMT and glass

Preparation of the composite with a mixture of 10 wt% Ceepree / sulphate glass and 5 wt% TPPMMT required a modification of the procedure described above. When both fillers were incorporated in the epoxy resin, the viscosity of the resulting mixture became too high for proper processing. Therefore, only the TPPMMT was dispersed in the epoxy resin. In a separate step, this was mixed with a dispersion of Ceepree / sulphate glass in MHHPA.

Modifications of procedure for composites with TPPMMT and triphenyl phosphate

Composites which contain 5 wt% TPPMMT + 1 wt% triphenyl phosphate were prepared by two distinct routes:

a) Starting from TPPMMT and triphenyl phosphate: Triphenyl phosphate (1 % of total composite weight) was melted at 353 K and dissolved in the epoxy resin, which had been pre-heated to 333 K. In a second step TPPMMT (5 % of total composite weight) was mixed in.

b) Starting from TPPMMT modified with triphenyl phosphate: TPPMMT modified with 17 wt% triphenyl phosphate (6 % of total composite weight) was incorporated the epoxy resin.

For both routes the mixtures were processed by the dissolver for 1 h at 333 K.

Modifications of procedure for composites with TPPMMT and/or polysiloxane glass (G)

Additives G and TPPMMT were dispersed in the epoxy resin by using a dissolver within 2 h at 333 K. MHHPA was used as curing agent. Curing was catalyzed by using 5 wt% of 2,4,6-tris (dimethylaminomethyl) phenol (Ancamine K54, Air Products). Composites and samples of pure resin were cast into aluminium moulds and cured according to the following schedule: 15 h at room temperature, 1 h at 120° and 1 h at 150° C.

- **Differential Scanning Calorimetry (DSC)**

All of the DSC measurements were performed in TA instruments (DSC 2920). All of the investigated samples (about 5 mg powder) were heated twice from 273 K up to 523 K with a heating rate of 10 K min^{-1} under nitrogen with a flow rate of 50 ml min^{-1}.

- **Thermogravimetry connected with Fourier Transform Infrared Spectrometry (TG-FTIR)**

The apparatus used for TG measurements was a TGA/SDTA 851 (Mettler Toledo, Germany). The samples (about 10 mg powder) were heated at a rate of 10 K min^{-1} in alumina pans from room temperature up to about 1200 K in either N_2 or air with a flow rate at 30 ml min^{-1}. The TG was coupled with Fourier transform infrared spectrometry (FTIR Spectrometer Nexus 470 (Nicolet, Germany). The coupling element was a transfer tube with an inner diameter of 1 mm (heated to 473 K) connecting the TG and the infrared cell (heated to 483 K).

- **Limiting Oxygen Index (LOI)**

According to ISO 4589, all of the samples were preconditioned in a standard atmosphere (ISO 219, at 296 K, 50 % relative humidity for 88 hr). The sample size for LOI was 150 x 6.5 (mm) and 3.3 ± 0.1 (mm) thickness.

- **UL 94**

According to the standard UL 94 vertical and horizontal test (IEC 60695-11-10), all of the samples were preconditioned in a standard atmosphere (ISO 219, at 296 K, 50 % relative humidity for 88 hr). The sample size for UL 94 was 125 x 13 (mm) and 3.3 ± 0.1 (mm) thickness.

- **Scanning Electron Microscopy (SEM)**

The fire residues obtained from cone calorimeter under an irradiation of 50 kW m^{-2} were characterized by scanning electron microscopy (SEM), (FEI XL30 ESEM, Eindhoven, the Netherlands). The fire residue samples with a representative structure were selected in the central area of residue formation and investigated for conductivity using a sputtered golden coating surface.

- ## Cone Calorimeter

The fire behaviour was investigated by a cone calorimeter (FTT, UK, shown in Fig 2.5) as a benchscale fire testing according to ISO 5660. Three different irradiations of 35, 50, and 70 kW m^{-2} were applied. The samples were forced to ignited by a spark ignitor. The size of samples was about 100 x 100 (mm^2) surface area and 5.5 ± 0.1 (mm) thick. In sections 3.2 and 3.4.1, the investigated materials were placed into a standard frame sample holder with a irradiated surface area of 88.4 cm^2. The distance between the sample surface and the cone heater was 25 mm. In sections 3.3 and 3.4.2 the investigated materials were placed into an open aluminium tray with an irradiated surface area of 100 cm^2; the distance between the sample surface and the cone heater was 30 mm . All of the measurements were performed in duplicate.

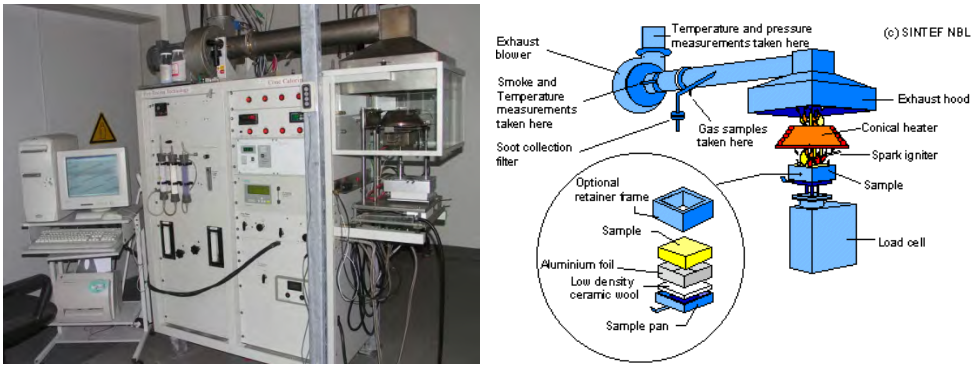

Fig 2.5. *(a) Cone calorimeter apparatus used in BAM, (b) schematic cone calorimeter*

- ## Online heat flux measurements

A slightly modified sample holder was used to insert the heat flux meter (Schmidt-Boelter type) in the centre of the retainer frame as shown in Fig 2.9. The heat flux meter was placed in a metal cylinder (diameter = 13 ± 0.2 mm) about 1 mm higher than the sensing surface of heat flux meter. This barrier prevented boiling material from flowing over the heat flux meter. The sample with a size of 10 x 10 x 5.5 (mm) was placed in the retainer frame. A hole with a diameter of 35 mm was cut in the middle of the specimen, again to prevent material flowing over the heat flux meter, but also to reduce condensation. The heat flux imposed on the centre point of the burning surface was measured during flaming combustion in the cone calorimeter with various irradiations applied.

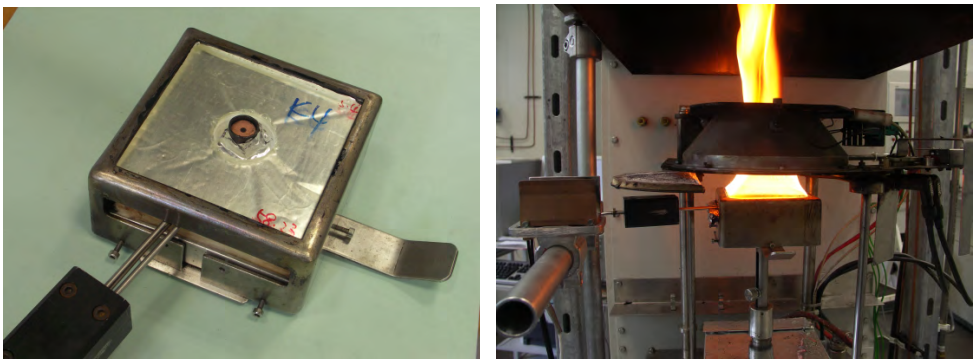

Fig 2.6. *Sample holder with a heat flux meter inserted in the centre of the frame used to measure the heat flux during flaming combustion in the cone calorimeter*

- ## Online temperature measurement

The self-constructed sample holder for temperature measurements is shown in Fig 2.10. It consists of several aluminium parts that were assembled to also function as a mould for the curing of the epoxy resins. The frame can be disassembled to implement the thermocouples and for cleaning. Eleven thermocouples (NiCr-Ni, type K, diameter = 0.5 mm; KTM - D2G, Emerson Process Management) were integrated into the frame before curing the thermosets. The thickness of the beads was about 0.7 mm. Each bead was placed in the centre of the 100 x 100 (mm^2) plane at intervals of 2 mm. The specimen thickness was 25 mm. The thermocouples were fixed by clamps and springs to maintain the position of the wires during burning. The back of the sample was thermally isolated by a ceramic fibre blanket. During fire testing, the thermocouples were monitored by a multichannel temperature scanner. The temperatures measured by thermocouples were scanned every 5 s.

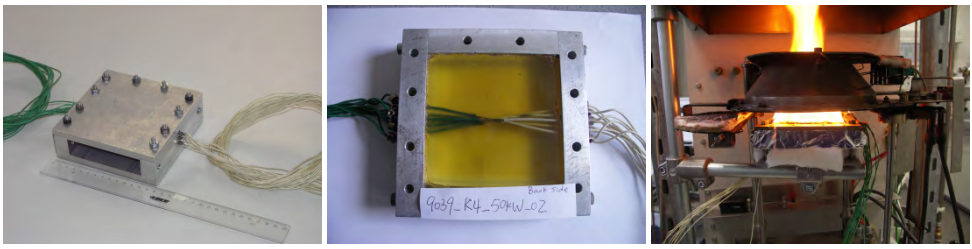

Fig 2.7. *Sample holder with integrated thermocouples used to measure the temperature as a function of depth within the specimens during flaming combustion in cone calorimeter with various external heat fluxes of 35, 50 and 70 kW* m^{-1}

Publications

1. **Wu GM,** Schartel B, Kleemeier M, Hartwig A: Fire behavior of layered silicate epoxy nanocomposites combined with low-melting inorganic Ceepree glass. *Polymer Engineering & Science,* in press. DOI: 10.1002 / pen.22111

2. **Wu GM**, Schartel B, Bahr H, Kleemeier M, Yu D, Hartwig A: Experimental and quantitative assessment of flame retardancy by the shielding effect in layered silicate epoxy nanocomposites. *Combustion and Flame,* revised manuscript submitted in 2010

3. **Wu GM**, Schartel B, Yu D, Kleemeier M, Hartwig A: Synergistic flame retardancy in layered-silicate epoxy nanocomposite combined with low-melting phenysiloxane glass. *Journal of Fire Science*, submitted in 2011

4. Yu D, Kleemeier M, **Wu GM**, Schartel B, Liu WQ, Hartwig A: Phosphorous and silicon containing low-melting organic-inorganic glasses improve flame retardancy of epoxy/clay composites. *Macromolecular Materials and Engineering*, in press 2011, DOI: 10. 1002 / mame. 201100014

5. Yu D, Kleemeier M, **Wu GM**, Schartel B, Liu WQ, Hartwig A: A low melting organic-inorganic glass and its effect on flame retardancy of clay/epoxy composites. *Polymer,* 2011; 52: 2120-2131

6. Yu D, Kleemeier M, **Wu GM**, Schartel B, Liu WQ, Hartwig A: The absence of size-dependency in flame retarded composites containing low-melting organic-inorganic glass and clay: Comparison between micro- and nanocomposites. *Polymer Degradation and Stability,* 2011; Vol. 96, Iss. 9: 1616 -1624

7. **Wu GM**, Schartel B, Kleemeier M, Hartwig A: Flame Retardancy Mechanism of Layered Silicate Epoxy Nanocomposite Combined with Low-melting Inorganic Glass. *12th European Meeting on Fire Retardant Polymers*; p 7

8. **Wu GM**, Schartel B, Bahr H, Kleemeier M, Yu D, Hartwig A: Nanocomposites - Two New Pieces of the Puzzle: Combining Nanocomposite with Low-Melting Glass and Quantitative Experimental Insight on the Shielding Effect. *2010' International Symposium on Flame-Retardant Materials & Technologies*; p 92

Acknowledgements

Firstly, I cannot express enough gratitude to Dr. habil. Bernhard Schartel for accepting me into his working group as a PhD. candidate. His scientific guidance, encouragement, patience and sincerity were tremendous in helping me complete my work and accomplish my goals. I am truly grateful for the experiences I have had under his supervision.

To the members of the flame retardancy group from BAM 6.3.5, I thank you for helping me out whenever I needed it. I have truly enjoyed coming into work every day and working with you. I would like to thank Mr. Henrik Seefeldt, for his kindly support in the measurement of SEM and numerous language translations. I would also like to thank Dr. Emanuela Gallo, Andreas Hörold, and Bettina Dittrich for their great patience with correcting my 'Chinglish'. Sincere thanks to Eliza Wawrzyn, Florian Kempel, Birgit Perret, Sven Brehme, Marie-Claire Despinasse for bringing new ideas and funny stories to our discussions.

I especially thank Mr. Horst Bahr for his expertise and advice regarding experimental work and for the kind friendship I shared with his loving family. I will always remember the happy times we spent together. I also extend special gratitude to Dr. Ulrike Braun, Dr. Heinz Sturm, Dietmar Neubert, Patrick Klack, Erik Dümichen, Michael Schneider, for their kind help offering experimental support and fruitful discussions. I also thank Sabine Kowallik for kindly making my travel and visa arrangements.

I would also like to thank our project partners from the working group of PD. Dr. habil. Andreas Hartwig (IFAM Fraunhofer Institute for Manufacturing Technology and Applied Materials Research, Bremen), and the working group of Prof. R. X. Fischer (University of Bremen, Germany) for its assistance. I could not have completed the work without their support. Funding for this project (SCHA 730/8-1, 8-2, HA 2420/6-1 and 6-2) was provided by the German Research Foundation (DFG).

Finally, I thank my friends who have always been there to support me with their generous help and comforting words. I never walk alone because of you.